UNIVERSTITY OF INSUBRIA

PhD COURSE IN EXPERIMENTAL AND TRANSLATIONAL MEDICINE

XXX CYCLE

THE ROLE OF THE HOMEOBOX GENE FAMILY OTX IN AN ISCHEMIA/REPERFUSION DAMAGE IN THE ENTERIC NERVOUS SYSTEM

Tutor: Prof. Giovanni Porta

PhD STUDENT: Andrea Conti

709337

A.A. 2016/2017

"*Ciò che ho ottenuto in questi anni*

lo devo solo a me stesso: non sono mai arrivato in un posto

grazie a conoscenze pregresse. Questo mondo vive a volte

un paradosso: un ricercatore non è un martire in missione

ma mette in pratica una passione che porta avanti con

grande dignità se ha coscienza e responsabilità. Serve solo

un po' di coraggio e fiducia in sé stessi e dire no a condizioni

di sfruttamento"

Renato Ostuni

SR Tiget, Istituto San Raffaele Telethon per la Terapia Genica

INDEX

INDEX OF FIGURES

INDEX OF TABLES

ABSTRACT

Homeobox genes are a family of genes encoding for transcription factors that play key roles during embryonic morphogenesis, especially in the specification of cellular identity, cellular differentiation and the positioning of body axis during embryo development.

Among the homeobox genes, *Otx* genes encode for an important class of homeodomain proteins that are involved in the induction and morphogenesis of the neuroectoderm, causing the formation of the vertebrate central nervous system (CNS). In the OTX family, *Otx1* and *Otx2* are required for the correct corticogenesis and sense organ development and mutations recurring in these genes are often associated with solid or hematologic malignancies.

In 2013 our laboratory found a correlation between *Otx* genes and p53 family, composed by Tp53-Tp63-Tp73 genes. p53 family plays a key role during the normal cell functioning, responding to a variety of different signals (e.g. hypoxia and DNA damages) and causing the arrest of cell cycle to allow the DNA repair, differentiation, senescence or apoptosis if cells are not able to repair or respond properly to the stresses. Malfunctions of these genes are often associated with the onset of human developmental abnormalities.

Intestinal ischemia is an acute and rarely chronic clinical condition caused by the unbalance between intestinal oxygen supply and the metabolic tissue demand. If ischemia's cause is removed before the developing of irreversible alterations (necrosis and apoptosis), tissue re-oxygenation has a protective role because it promotes aerobic metabolism, toxic compounds removal and restoration of normal cellular functions. Conversely, tissue re-oxygenation causes also a series of biochemical and cellular mechanisms that amplify tissue damage. Cellular and microvascular negative effects caused by intestinal I/R seems to rely on free radicals like ROS produced by XD/XO system and NO. NO is an important physiological mediator and is mainly synthetized by three different nitric oxide synthases: iNOS, nNOS, eNOS. During intestinal I/R, NO can be both cryoprotective and cytotoxic especially when oxidative stress onsets: NO synthetized by constitutive NOS seems to play a protective role acting as vasodilator and anti-inflammatory modulator while an excessive NO production, due to the increased activity of iNOS, is involved in the generation of free cytotoxic radicals that amplify the effects of ischemia.

During this PhD project we have firstly studied, in collaboration with the Laboratory of Pharmacology of the Univeristy of Insubria in Varese headed by Cristina Giaroni, the involvement of the homeobox gene family OTX in a rat model of ischemia/reperfusion obtained through the clamping of the superior mesenteric artery (SMA) for 60 minutes followed by reperfusion. After the validation of the model, we have performed molecular analyses on the OTX genes and the nitrergic pathway on the longitudinal muscle layer with attached myenteric plexus samples (LMMPs). Subsequently we have replicated *in vitro* an I/R damage through the Oxygen and Glucose Deprivation (OGD) procedure on the human neuroblastoma cell line SK-N-

BE(2) previously treated with retinoic acid (ATRA) to induce its differentiation towards a neuronal-like phenotype. Morphological and molecular analyses have been performed at the end of the treatment.

The data presented in this project show, in the rat model of I/R, increased mRNA and protein levels for OTX1 mRNA at 48 hours of reperfusion, concurrently with the increased expression of iNOS, and increased levels of OTX2 at 24 hours in parallel to the increased expression of nNOS. Moreover, we observed that iNOS inhibitor 1400W plays a modulatory effect on OTX1 while nNOS inhibitor NPLA is more active on OTX2 transcription factor. Preliminary results obtained from the *in vitro* induction of an I/R damage strengthen the observations made *in vivo* about the involvement of the homeobox gene family OTX especially during the reperfusion period.

The induction of an I/R damage *in vivo* and *in vitro* resulted in neurodamaging and neuroprotective roles of iNOS and nNOS involving the activation of molecular pathways downstream of OTX1 and OTX2 respectively especially during the reperfusion. These observations suggest for the first time the existence of an interplay between myenteric nitrergic pathways and OTX transcription factors that could sustain the development of motor alterations induced by NO after an I/R injury, with OTX1 and iNOS more related to the effects of I/R on the glial cells while OTX2 and nNOS linked to the consequences on neuronal cells.

LIST OF ABBREVIATIONS

1400W: 3-aminomethylbenzylacetamidine

5-HT: Serotonin

Ac: Acetylation

Ach: Acetylcholine

ACTH: Adrenocorticotropic hormone

AER: Apical ectodermal ridge

AGA: American Gastroenterology Association

AMI: Acute mesenteric ischemia

AML: Acute myeloid leukaemia

ANR: Anterior neural ridge

ANS: Autonomous nervous system

AP-1: Activator protein 1

ATP: Adenosine triphosphate

ATRA: All-trans retinoic acid

AVE: Anterior visceral endoderm

BSA: Bovine serum albumin

cGMP: Cyclic guanosine monophosphate

ChAT: Choline acetyltransferase

CNS: Central nervous system

CO: Carbon oxide

COX-2: Cyclooxigenase-2

Crx: Cone-rod homeobox gene

D.P.C: Days post coitum

DMSO: Dimethyl sulfoxide

DVE: Distal visceral endoderm

ECM: Extracellular matrix

eNOS: Endothelial nitric oxide synthase

ENS: Enteric nervous system

EPANs: Extrinsic primary afferent neurons

Epi: Epiblast

EPSPs: Excitatory post-synaptic potentials

Exe: Extra-embryonic ectoderm

FBS: Fetal bovine serum

FSH: Follicle-stimulating hormone

GAPDH: Glyceraldehyde 3-phosphate dehydrogenase

GH: Growth hormone

GI: Gastrointestinal

H_2O_2: Hydrogen peroxide

HB: Homeobox

HD: Homeodomain

HE: Hematoxylin-eosin

HIF-1α: Hypoxia-inducible factor alpha

HRSs: Histidine-rich regions

HTAB: Hexadecyl trimethylammonium bromide

I/R: Ischemia/reperfusion

IBDs: Inflammatory bowel diseases

IkBα: Inhibitor of kappa B

IKK: IkB kinase

iNOS: Inducible nitric oxide synthase

IPANs: Intrinsic primary afferent neurons

IsO: Isthmic organizer

LH: Luteinizing hormone

LMMPs: External longitudinal muscle layer with attached myenteric plexus

lncRNAs: Long non-coding RNAs

LPS: Lipopolysaccharide

M: Methylation

MDM2: Mouse double-minute 2

miRNAs: micro-RNAs

MPO: Myeloperoxidase

N: Neddylation

NAMI: Non-occlusive mesenteric ischemia

NaN_3: Sodium azide

NES: Nuclear export signal

NF-kB: Nuclear factor-kappa B

NGF: Nerve growth factor

NHS: Normal horse serum

Nkx3.1: NK3 homeobox gene 1

NLS: Nuclear localization signal

NMDA: N-methyl-D-aspartate

nNOS: Neuronal nitric oxide synthase

NO: Nitric oxide

NOS: Nitric oxide synthase

NPLA: N^{ω}-propyl-L-arginine hydrochloride

NUP98: Nuclear pore complex protein 98

O_2^-: Superoxide radical

OGD: Oxygen and glucose deprivation

$OH^{\bullet}$: Hydroxyl radical

$ONOO^-$: Peroxynitrite radical

Otd: Orthodenticle homeobox gene

Otx1: Orthodenticle homeobox gene 1

Otx2: Orthodenticle homeobox 2

P: Phosphorylation

p53REs: p53 responsive elements

p63REs: p63 responsive elements

PIN: Prostatic intraepithelial neoplasia

PRD: Poly-proline rich site

PrE: Primitive ectoderm

PRL: Prolactin

PS: Primitive streak

PSNS: Parasympathetic nervous system

RARs: Retinoic acid receptors

RAREs: Retinoic acid responsive elements

REs: Responsive elements

ROS: Reactive oxygen species

RXRs: Retinoid X receptors

SMA: Superior mesenteric artery

SNS: Sympathetic nervous system

SOD: Superoxide dismutase

SOM: Somatostatin

SU: Sumoylation

TNFα: Tumor necrosis factor alpha

Tp53: Tumor protein 53

Tp63: Tumor protein 63

Tp73: Tumor protein 73

TSH: Thryoid-stimulating hormone

Ub: Ubiquitination

VE: Visceral endoderm

VIP: vasoactive intestinal peptide

XD: Xanthine dehydrogenase

XO: Xanthine oxidase

INTRODUCTION

HOMEOBOX GENES

Homeobox genes are a family of genes that encodes for transcription factors playing key roles during embryonic morphogenesis. They are crucial for the specification of cellular identity, cellular differentiation and the positioning of body axis during embryo development. Homeobox genes have been identified through experiments performed in *Drosophila melanogaster* in which mutations caused the conversion of a part or segment of the body into another of similar identity allowed the identification of homeobox genes. After their discovery, more than 200 homologous homeobox genes have been identified in vertebrates, plants and fungi. In mammals, homeobox genes are crucial in a variety of processes spanning from the development of central nervous system (CNS) and skeleton to limb and digit specification and organogenesis [1]. Several HB genes are also involved in a variety of human diseases and congenital abnormalities [2, 3].

Homeobox genes present a common sequence of 180 nucleotides called “homeobox” (HB) and encode for proteins usually called “homeoproteins” that function as transcriptional factors [4]; however, some homeoproteins don’t exhibit a transcription factor activity since they are implicated in the control mRNA export, translation and protein stability [5]. Homeoprotein present a 60 amino acids domain usually termed “homeodomain” (HD), necessary for the recognition and binding of specific DNA sequences called “responsive elements” (REs) containing a TAAT motif in the promoter of target genes [4, 6]. The HD present a highly evolutionary conserved helix-turn-helix motif composed by two anti-parallel α-helices at the N-terminal (helix 1 and helix 2) and a third α-helix (helix 3) at the C-terminal perpendicular to the axis established by the first two. The third helix is able to interact with the major groove of DNA forming hydrogen bonds (Figure 1) [7]. The specificity and the affinity of the binding between HD proteins and DNA target sequences is related to the different amino acid residues composition and to the interaction with other transcription factors [4, 8]. Additional conserved motifs that are unique across the different homeobox families cooperate to establish transcriptional target selectivity: for examples HOX family presents a motif that mediates interactions with PBX co-factors [9]; PAX proteins possess an additional DNA-binding domain called paired domain [10] while members of the ZEB family contain a zinc-finger domain besides the homeodomain [11]. Many homeoproteins have been shown to function also as regulatory elements capable of activate or repress target genes involved in stem cell differentiation [12].

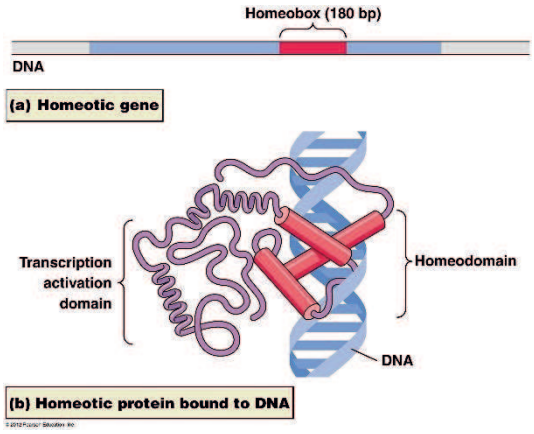

Figure 1: **Homeobox gene and homeoprotein.** HB genes contain a 180 nucleotides sequence called "homeobox" that encodes for a 60 amino acids sequence named "homeodomain" (HD). The homeodomain recognizes and binds specific DNA regions, called responsive elements (REs), located in the promoter of target genes, causing their activation or repression. The structure of the HD is conserved and composed by three α-helices where the third helix, called "recognition helix", is implied in the binding with the DNA in the major groove.

The role of HB genes during embryonic development has been extensively investigated since their initial discovery. As stated by Boncinelli in 1996, the complexity of an organism is related to the re-activation in the adult organism of genes normally active during embryo development. Once re-activated, these genes play different roles [13]. HB genes are involved in biological processes of eukaryotic cells ranging from the control of cellular identity, cellular growth and differentiation, cells-extracellular matrix (ECM) and cell-cell interactions [14]. HB genes are also able to control proliferation and cell cycle: many HB genes are involved in the stimulation of cell cycle and expansion of cellular progenitors before the differentiation while others, like *Gax1* and *HoxA10*, inhibit cell cycle progression and promote cellular differentiation (Figure 2) [15]. Other HB genes are linked to the apoptotic process during cellular remodelling.

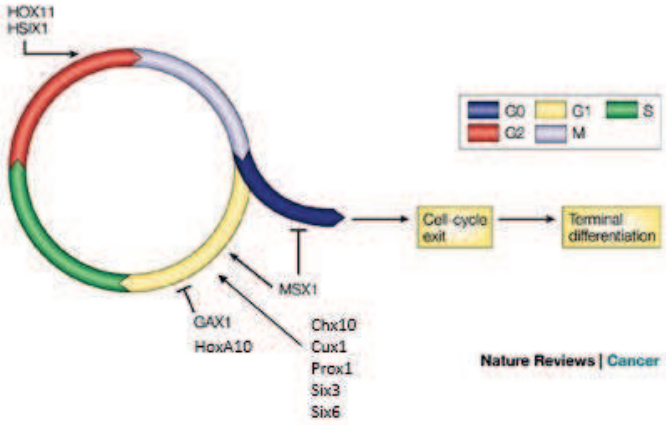

Figure 2: **Effects of HB proteins on cell cycle** (modified from Abate-Shen C. 2002). Hox11 and Six1 perform their activity in the G2-M state and they disrupt the G2 checkpoint resulting in an inappropriate mitosis. MSX1 upregulates cyclin D1 and prevents cells from leaving the cell cycle and undergoing to the differentiation. Gax1 instead upregulates WAF1, a cyclin-dependent kinase inhibitor, and it prevents cell from entering in the S phase.

Cellular vitality and phenotype are regulated by different extracellular signals that includes growth factors, hormones, cytokines, adhesion and ECM molecules: these signals can activate intracellular pathways that result in the expression of HB genes. Alterations in the acetylation state of histone proteins affect the transcriptional activity of specific genes and acetylation/de-acetylation has been proposed as a mechanism able to regulate the transcription of HB genes like *Hox* genes [14].

Given the ability of homeobox genes to regulated cell cycle progression and development, mutations occurring in these genes are usually associated to human congenital, somatic or metabolic defects: as an example, mutations in *HoxA13* genes cause severe manifestations of hand-foot-genital syndrome [16], a rare clinical condition that affects the development of the hands and feet, the urinary tract and the reproductive system.

In addition, homeobox genes are also related cancer, since development and cancer share many common features: both processes in fact present alterations in cellular proliferation and differentiation, death, neo-vascularization, cellular motility and invasion. The relationship between homeobox genes and carcinogenesis can be explained through the evaluation of their expression levels [15]: tissue-specific HB genes normally expressed in tissues undergoing to development can be re-activated in tumors derived from the same tissues (e.g. brain, mammary gland and kidney) [15]; on the other hand homeobox genes expressed in differentiated tissues are usually down-regulated or even lost in tumors [15] (Figure 3).

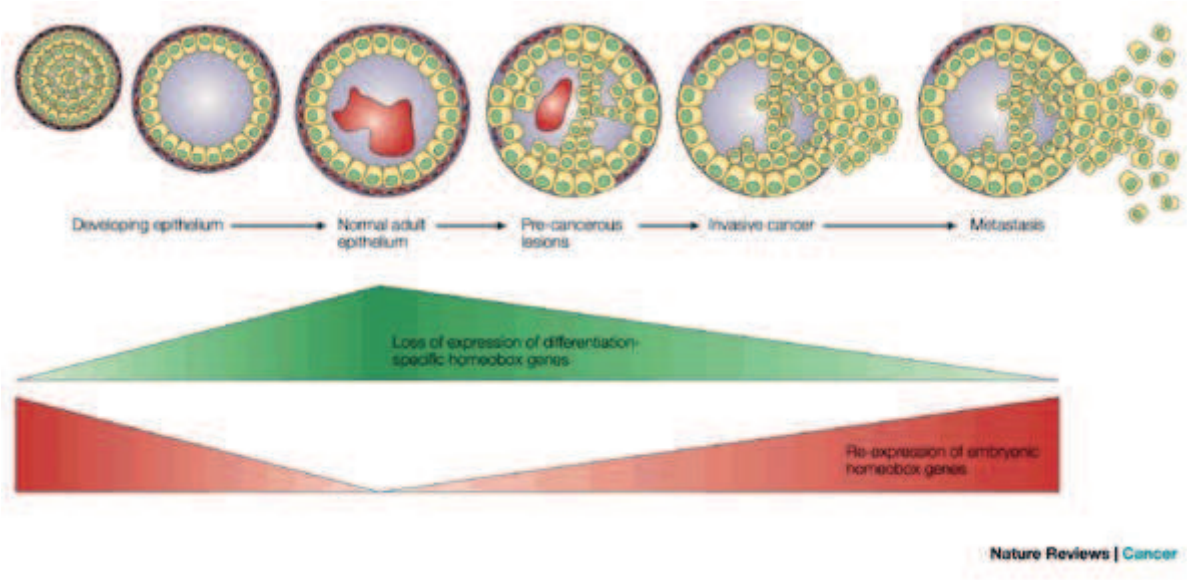

Figure 3: **Relationship between homeobox genes and carcinogenesis** [15]. HB genes usually expressed in tissues during development and down-regulated in differentiated tissues can be re-expressed in tumor; genes expressed in differentiated tissues can be down-regulated or lost during cancer progression.

Over-expression or down-regulation of HB genes has been observed in different human malignancies [8, 15] like leukaemia, lymphoma [17] and solid tumors. One example is the translocation t(7;11) (p15;p15) in acute myeloid leukaemia (AML) that causes the fusion between HOXA9 protein to the N-terminal of the nuclear pore complex protein NUP98 [18]. By contrast, the mechanisms at the basis of the homeobox gene deregulation in solid tumors are yet to be fully discovered but it has been proposed that mechanisms like loss of heterozygosity and gene amplification, DNA methylation and chromatin modification as well as non-coding RNAs could participate to carcinogenesis. For example, NK3 homeobox gene 1 (*Nkx3.1*) on chromosome 8p21 encodes for a transcription factor expressed in the prostate epithelium where is crucial in the maintaining of prostate cell fate and in the suppression of tumour initiation. This region is frequently deleted in the 80% of prostate cancers [19] and undergoes to allelic loss in prostatic intraepithelial neoplasia (PIN) [8, 20]. Both in humans and mouse models it has been seen that *Nkx3.1* expression is frequently lost during prostate cancer initiation [21]. Aberrant methylation of CpG islands often occurs in many solid tumors: methylation of CpG islands within HOX gene clusters are often methylated in lung cancer [22] while hyper-methylated CpG islands associated with homeobox genes are found in early stages of breast cancer [23]. Among non-coding RNAs, long non-coding RNAs (lncRNA) and micro RNAs (miRNAs) are found in the intergenic regions of the HOX clusters and control gene expression through cis- or trans-acting mechanisms [24]: for example, the expression of the lncRNA HOTAIR has been identified as a strong predictor of metastasis and tumor progression in breast cancer [25]; miRNAs instead have been found to either promote or inhibit tumor progression targeting different HB genes: for example, miR-10b is usually found in metastatic breast cancer and it promotes metastasis [26] while miR-185 is down-regulated in breast cancer and inhibits tumor growth [27].

The promotion of tumorigenesis through the gain or loss of HB genes can be the result of their inappropriate effects on the control of growth and differentiation: in fact, the differentiation status of a specific cell type is the consequence of the balance between the expression of specific HB genes and the inhibition of others. Even though these genes are either over-expressed or down-regulated in many tumors, they are not always considered as oncogenes or tumor suppressors: they are indicated as positive or negative tumor modulators and it has been proposed that the oncogenic activity of HB genes is related not to mutant but to wild-type homeoproteins. Thus, the oncogenic capability can be the consequence of an altered spatio-temporal expression rather than the acquisition of new functions.

OTX FAMILY

Otx genes are the vertebrate homologous of the *orthodenticle* (*otd*) homeobox genes of *Drosophila melanogaster* and encode for an important class of HD proteins that are involved in the induction and morphogenesis of the neuroectoderm, causing the formation of the vertebrate CNS. OTX genes belong to PRD homeobox family and are characterized by the presence of a lysine in position 9 of the third α-helix in the homeodomain that gives to OTX proteins a high affinity for TAATCC/T sequences in the promotor of target genes [28]. During vertebrate evolution, this family of homeobox genes underwent to gene duplication that probably caused an increased morphological and functional complexity of the vertebrates. Several OTX-related proteins have been identified during the last years thanks to OTX-HD similarity and homology between OTX proteins can be found especially in the glutamine stretch. The HD is followed by an adjacent $KXRX_{1\text{-}2}KXK$ domain which, in turn, is followed by a highly conserved WSP domain [(S/A) (I/L) WSPA], 45-50 amino acids at the C-terminal of the HD and an imperfect domain of 18-25 amino acids in which is present the highly conserved (D/E) CLDYK (D/E) (Q/P) domain upstream to the C-terminal W (K/R) FQVL motif (Figure 4) [29]. Moreover, based on the sequence homology within the C-terminal, OTX proteins can be classified into three principal groups: OTX1/OTX3, OTX2 and OTX5/CRX. Noteworthy, both OTX1 and OTX2 present three histidine-rich regions (HRSs) between the [(S/A) (I/L) WSPA] and (D/E) CLDYK (D/E) (Q/P) domain [29].

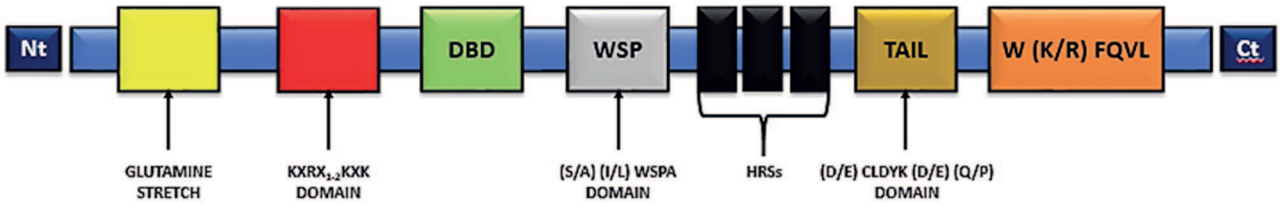

Figure 4: **Primary structure of OTX1 and OTX3 proteins**.

Among the OTX family, *Otx1* located on chromosome 2p15 (http://www.genecards.org/cgi-bin/carddisp.pl?gene=OTX1) (Figure 5A) and *Otx2* on chromosome 14q22.3 (http://www.genecards.org/cgi-bin/carddisp.pl?gene=OTX2) (Figure 5B) play key roles during brain development since they are spatially and temporally regulated resulting in an overlapped expression in many domains [30].

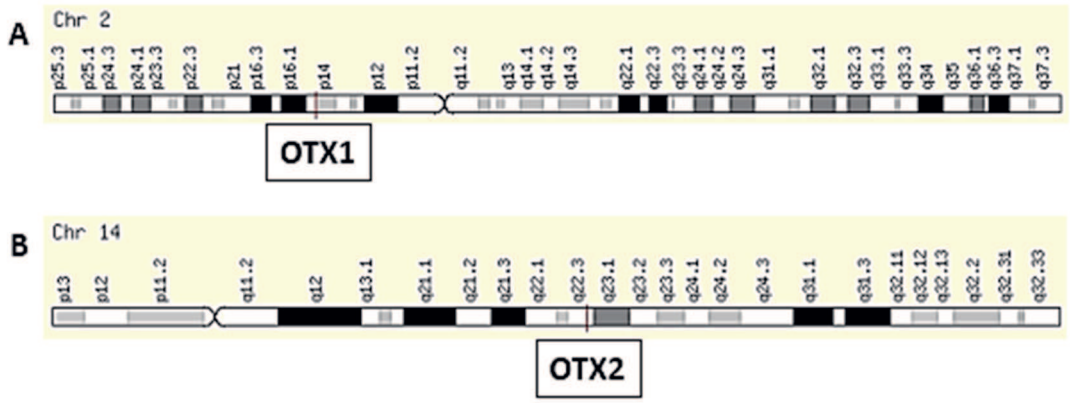

Figure 5: **Chromosome location of OTX1 and OTX2 homeobox genes** (modified from GeneCards).

The development of the CNS in fact is a complex process that requires specific programs and sequential morphogenic events to specify and define the anterior neuroectoderm [31]. The regionalization and specification of the anterior neuroectoderm depends on a range of different signals that originate from non-neural tissues or from cellular populations like the anterior neural ridge (ANR) between the anterior-most neural and non-neural ectoderm or the isthmic organizer (IsO) between hindbrain and midbrain [32]. In a process called “competence”, neuroectoderm is also programmed to respond and to interpret these signals [31].

OTX1

Otx1 (*orthodenticle homeobox 1*) gene has been extensively characterized and studied during the last years and its principal functions are the control of corticogenesis and sense organ development. Most of the studies regarding *Otx1* functions during development have been performed in mice models. *Otx1* expression is detected at 8 d.p.c throughout the neuroepithelium of forebrain and midbrain. *Otx1* is transcribed at first in the entire dorsal telencephalic neuroepithelium and subsequently its expression is restricted in the ventricular zone in relation to the different stages that reflect generations of neurons belonging to deep cortical layers. At the end of the gestation the expression of *Otx1* is found principally in the cortical plate. In the post-natal period *Otx1* expression is detected in a subset of neurons of the V and VI [33].

The development of precise neuronal circuits requires the growth of axons and the formation of precise synaptic connections. The final adult connectivity in the brain is preceded by a time-period in which many exuberant connections are present: for example, the V layer of brain cortex extend axonal connections towards multiple targets and subsequently eliminates a subset of these exuberant connections during early postnatal life. *Otx1* gene is required during this process: during embryonic life OTX1 protein is in the cytoplasm of the progenitor cells in the ventricular zone until neurons start to migrate and differentiate. In the first week of the post-natal life neurons reach the V layer of the cortex, OTX1 protein translocate to the nucleus and controls the synaptic pruning [34, 35].

The prominent role exerted by *Otx1* during the development of neocortex is also demonstrated by some human pathological conditions like focal cortical dysplasia: this pathological state is highly associated to epilepsy and derives from a developmental malformation due to the expression of OTX1 in balloon cells derived from cortical radial glia and not from the ganglionic eminence [30].

In the adult organism *Otx1* is expressed in the choroid plexus of the lateral ventricles, the ventricular zone of the ganglionic eminence, hippocampus and cerebellum. *Otx1* is also expressed in sense organs like the anterior part of the retina, in the olfactory bulb, it's involved in the formation of the ciliary body and in the morphogenesis of the inner ear [30].

The post-natal expression of *Otx1* is also found at low levels in the anterior part of the pituitary gland where it's involved in the triggering of pituitary hormones transcription. The pituitary gland collects signals from the periphery and the brain to control the production and secretion of hormones implicated in growth, reproduction, behaviour and metabolism. The mature pituitary gland is composed by 5 different cellular types that are defined by the production of specific hormones. In the anterior lobe of the gland the principal cell types are thyrotropes, somatotropes, corticotropes, lactotropes and gonadotropes and they produce the thyroid-stimulating hormone (TSH), growth hormone (GH), adrenocorticotropic hormone (ACTH), prolactin (PRL), follicle-stimulating hormone (FSH) and luteinizing hormone (LH). OTX1 binds the promotor of Gh, βFSH and βLH genes stimulating the related hormones [36].

Since the cerebral cortex is the centre of sophisticated perceptive and cognitive functions, many experiments performed in the last years to understand the functions of *Otx1* exploited mice null for this gene. *Otx1*$^{-/-}$ mice survive until the adult age but they present many severe morphological abnormalities that involve eyes, inner ear, pituitary gland and brain which is reduced in weight and dimensions. Furthermore, the dorsal telencephalic cortex shows a significative reduction in the number of cells and thickness at the temporal and perirhinal levels where the layers are also disorganised [37]. The mesencephalon shows an increased volume with swollen superior and inferior colliculi while the telencephalon is reduced; notably, the cerebellum of about the 80% of *Otx1*$^{-/-}$ mice show an extra lobule between *tuber vermis* and *declivus*. From the point of view of the neurological phenotype, these alterations are associated with severe consequences like spontaneous high speed turning behaviour, head bobbing and epileptic crises [37, 38]. As stated before, *Otx1*$^{-/-}$ mice show defects in the inner ear and eyes: in particular they lack of the lachrymal and harderian glands, present a thinner iris and absent ciliary process; the absence of *Otx1* in the inner ear reflect its expression pattern in the lateral canal ampulla, utricle, saccule and cochlea and mice models lack the semi-circular canals.

The null mice show also transient dwarfism and hypogonadism due to the reduction of GH, FSH and LH hormones in the pre-pubescent stage [36]. A gradual recovery is seen in these animal models because at four

months GH, FSH and LH levels are restored as well as growth and gonadal function is rescued. The expression pattern of the related hypothalamic hormones like growth hormone releasing hormone (GnRH) and their pituitary receptors highlight the possibility that Otx1$^{-/-}$ mice have a compromised synthesis of GH, FSH and LH hormones even though hypothalamic and pituitary cells that derive from somatotropic and gonadotropic lineages are unaffected [39].

Beyond neurological alterations *Otx1*$^{-/-}$ mice are also anaemic as reported in the work of Levantini and coworkers [40]. *Otx1* is normally expressed both in hematopoietic pluripotent cells, erythroid progenitor cells and in the mature cells of the erythroid and megakaryocytic pathway in bone marrow, enhancing stem cell differentiation and therefore playing a role during hematopoietic process. Since *Otx1* cooperates with *GATA-1* gene to increase the erythroid differentiation activating the transcription of *Scl* gene, Otx1$^{-/-}$ mice show a reduction in both *Scl* and *GATA-1* gene and hence a reduction of hematopoiesis [40].

OTX2

Otx2 (orthodenticle homeobox 2) is the second member of the OTX family and it encodes for a transcription factor necessary during gastrulation to control the specification of the anterior part of the neural plate [41]. Like *Otx1*, many experiments have been performed in mice models to understand the exact function of *Otx2* gene. In the mouse embryo *Otx2* is expressed and transcribed in the epiblast ($4^{1/2}$ d.p.c) and at the onset of gastrulation ($5^{1/2}$ d.p.c) is required in the visceral endoderm (VE) not only to control and maintain is transcription in the epiblast but also to mediate signals *Otx2*-dependent that come from the VE to the epiblast. From early to late streak stage ($7^{1/2}$ d.p.c) the signal persists in the VE [42]. At the end of gastrulation ($7^{1/2}$ d.p.c) the anterior mesoderm releases a positive signal that promote the transcription of *Otx2* in the neuroectoderm while the posterior mesoderm unleashes a negative signal which plays a role in the positioning of its posterior border [33, 41] (Figure 6 A – C) . The neural plate derives from the neuroectoderm and causes the formation of CNS. From the neural plate neural folds originate, appose and fuse in order to form the neural tube (Figure 6D). The brain originates from the most anterior part of the neural tube and is composed by three principal vesicles: rhombencephalon, mesencephalon and prosencephalon; the forebrain instead is divided into diencephalon and telencephalon. *Otx2* is inhibited in the hindbrain by negative signals that support the demarcation between fore-midbrain and hindbrain itself. *Otx2* expression is found mostly in telencephalon, diencephalon, mesencephalon and archicortex but not in neocortex supporting the possibility to exploit this gene as hippocampal marker in the telencephalon [33]. In the adult organism *Otx2* is principally expressed in choroid plexus and pineal gland [30].

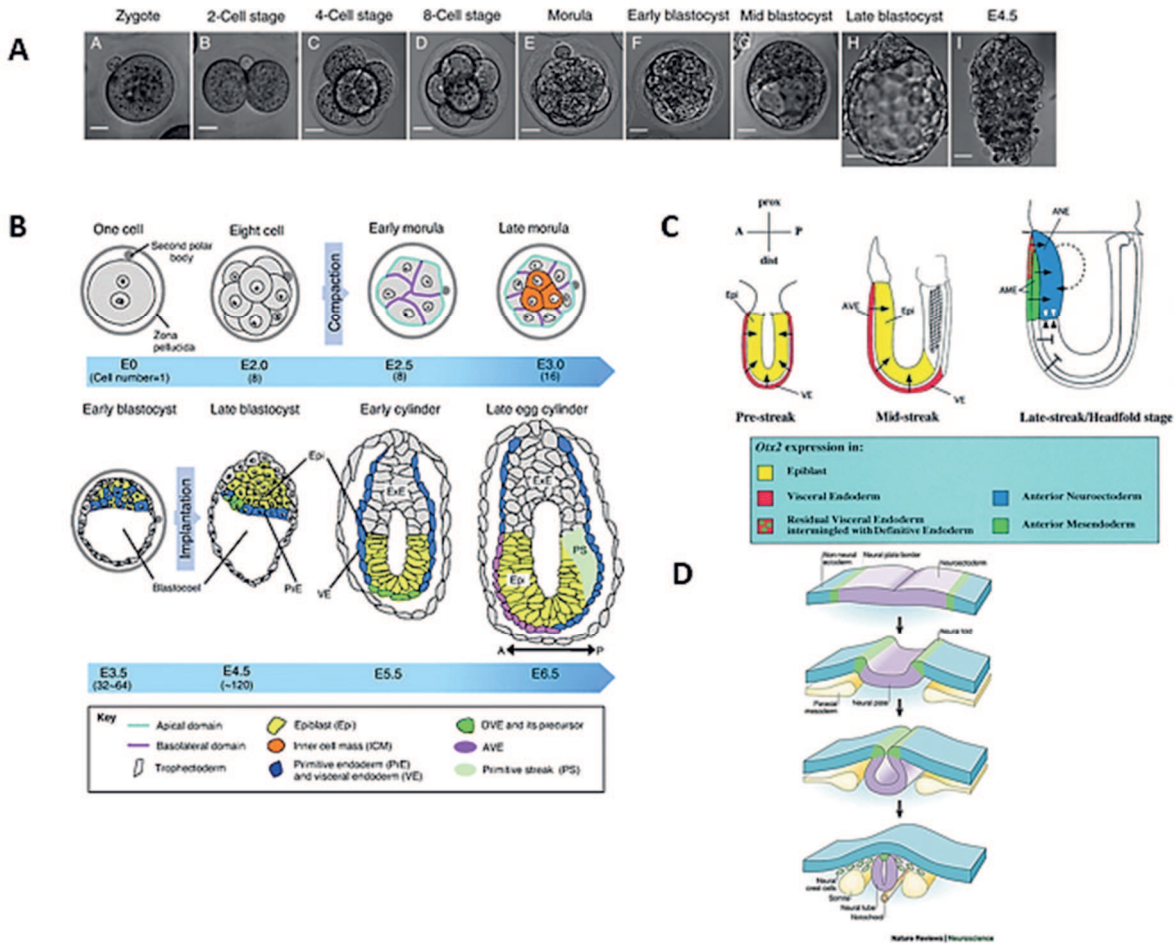

Figure 6: **Embryonic development and involvement of Otx2 homeobox gene.** (A) Images of mouse pre-implantation development from zygote to late blastocyst (modified from Saiz N. et al 2013 [43]). (B) Morphological changes observed in mouse embryo from fertilization to gastrulation (modified from Takaoka K. and Hamada H. 2012 [42]). AVE (anterior visceral endoderm), DVE (distal visceral endoderm), Epi (epiblast), Exe (extra-embryonic ectoderm), PrE (primitive ectoderm), PS (primitive streak), VE (visceral endoderm). (C) *Otx2* expression and possible interactions during murine gastrulation (Simeone A. 1998 [33]). *Otx2* is expressed in the entire visceral endoderm and epiblast in the pre-streak stage; Otx2 expression is then gradually restricted to the anterior third of the embryo and at the headfold stage it involves all the three germ layers. Experiments performed using chimeric or *Otx2*$^{-/-}$ embryos enhanced the possibility that signals emitted from the visceral endoderm could exist and are *Otx2* dependent: these signals are directed to the epiblast and are required also for the early neural plate specification and primitive streak organization. In the late streak/headfold stage a positive signal promote the transcription of *Otx2* in the neuroectoderm while the posterior mesoderm unleashes a negative signal which plays a role in the positioning of its posterior border. After the headfold stage an *Otx2*-autonomous function may be required to maintain the fore-midbrain regional identities. (D) Neural tube formation from the neural plate.

Given the role of *Otx2* during embryo development, mice lacking of *Otx2* (*Otx2*$^{-/-}$) have been generated: these mice die early during embryogenesis and lack of the neuroectoderm committed to become prosencephalon, mesencephalon and rhombencephalon and they also show body plan abnormalities [44].

Otx2 is also a key regulator of the specification of identity, extent, fate of neural progenitor cells and controls the proliferation and differentiation of dopaminergic progenitors: dopaminergic neurons are involved in the control of voluntary movements, cognition and reward processes and are also implicated in the pathogenesis

of Parkinson's disease. *Otx2* also represses GABAergic differentiation controlling identity and fate of glutamatergic progenitors in the thalamus and eventual malfunctioning of this gene is related to the pathogenesis of psychiatric and neurological disorders [30].

Otx2 is also implicated during eye development being expressed in several eye's tissues including neural retina and retinal pigmented epithelium (RPE) [45, 46]. Notably, *Otx2* in neural retina is expressed in post-mitotic neuroblasts destined to become ganglion, bipolar and photoreceptor cells. *Otx2* is able to control photoreceptors differentiation inducing *Crx* (cone-rode homeobox) gene and stimulate Müller cells differentiation towards photoreceptors in presence of retinoic acid [46, 47]. Thus, eventual malfunctions in *Otx2* gene are associated with retinal pathologies [48].

Otx2 has been also indicated as a morphogen able to generate gradients through which other genes are activated or repressed in distinct cells and hence controlling cell proliferation and differentiation [49].

Otx2, like *Otx1*, plays a key role in cancer: in fact, in medulloblastomas with anaplastic histopathologic features this gene is often overexpressed or genetically amplified in a variety of different tumoral subtypes [50, 51] and the administration of retinoic acid is reported to repress *Otx2*.

p53 FAMILY

The tumour suppressor *p53* gene, located on chromosome 17p13.1 (http://www.genecards.org/cgi-bin/carddisp.pl?gene=TP53, Figure 7A) is the centre of a molecular network playing a key role during cell proliferation and death in response different type of stresses. Two *p53* related genes have been discovered in 1997-1998 on two different chromosomes: *p63* on chromosome 3q28 (http://www.genecards.org/cgi-bin/carddisp.pl?gene=TP63, Figure 7B) and *p73* on chromosome 1p36.32 (http://www.genecards.org/cgi-bin/carddisp.pl?gene=TP73, Figure 7C) [52, 53]. These two genes are part of the same network and undergo to at least the same modifications and interactions that provide signals to *p53*, actively contributing to cellular responses [54]. Each gene of the family encodes for transcription factors that share high level of similarity especially in the DNA binding domain (Figure 8) [55] allowing *p63* and *p73* to transactivate p53-responsive genes and hence causing cell cycle arrest and eventually apoptosis. In addition, *p53* family members express multiple splicing variants that encode for proteins containing different domain and expressed in different tissues [56].

Since p53 family play a key role during the normal cell functioning, malfunctions of this family are often associated with the onset of human developmental abnormalities. Mutations in *p53* lead to Li-Fraumeni syndrome and cancer; *p63* mutations causes various combinations of limb malformations, orofacial clefting and ectodermal dysplasia [57]. Eventually, p73-associated syndromes are likely to exist but they have been

not identified yet: in fact, *p73* gene is almost never mutated in human tumor that generally develop because of the inhibition in the tumour suppressor activity of *p73* [58].

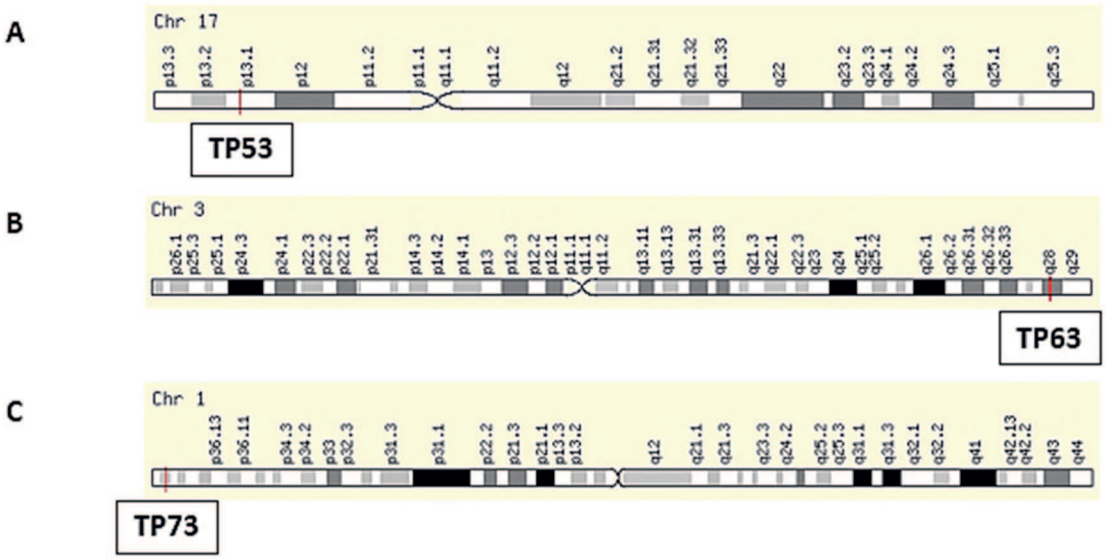

Figure 7: **Chromosome position of p53 family members** (modified from GeneCards).

Figure 8: **Percentages of similarity between p53 family members.**

p53 family members are able to interact to induce the expression of common target genes and can also regulate each other's expression: p53, TAp63 and TAp73 bind the P2 promoter inducing the transcription of ΔN isoforms that inhibit TA variants creating a negative feed-back loop.

During the normal development the ratio of the different isoforms is an important factor to regulate proliferation, survival and differentiation while each alteration is involved in tumorigenesis [59].

p53

Tp53 gene consists of 11 exons (Figure 9A) spanning over 19 Kb and encodes for a 57 kDa protein divided into six domains with specific functions even though different isoforms could exist (Figure 9B). The N-terminal contains the transactivation domain divided into two sub-domains (TA1 and TA2): TA1, that contains also the binding site for the regulator mouse double-minute 2 (MDM2), allows the transactivation while TA2 selects the specific target. A poly-proline-rich site (PRD) follows the transactivation domain and possesses complex roles in the regulation of apoptosis. The DNA binding domain is in the central part of the protein and about the 90% of the p53 mutations found in human cancers occurs in this domain. This region is followed by the oligomerization domain (4D), that contains also a nuclear export signal (NES), composed by a β-strand and an α-helix necessary for the tetramerization of p53. The C-terminal of the protein present three nuclear localization signals (NLS) and a non-specific DBD necessary for the binding of the damaged DNA and for the down-regulation of the central DBD (Figure 9C) [60].

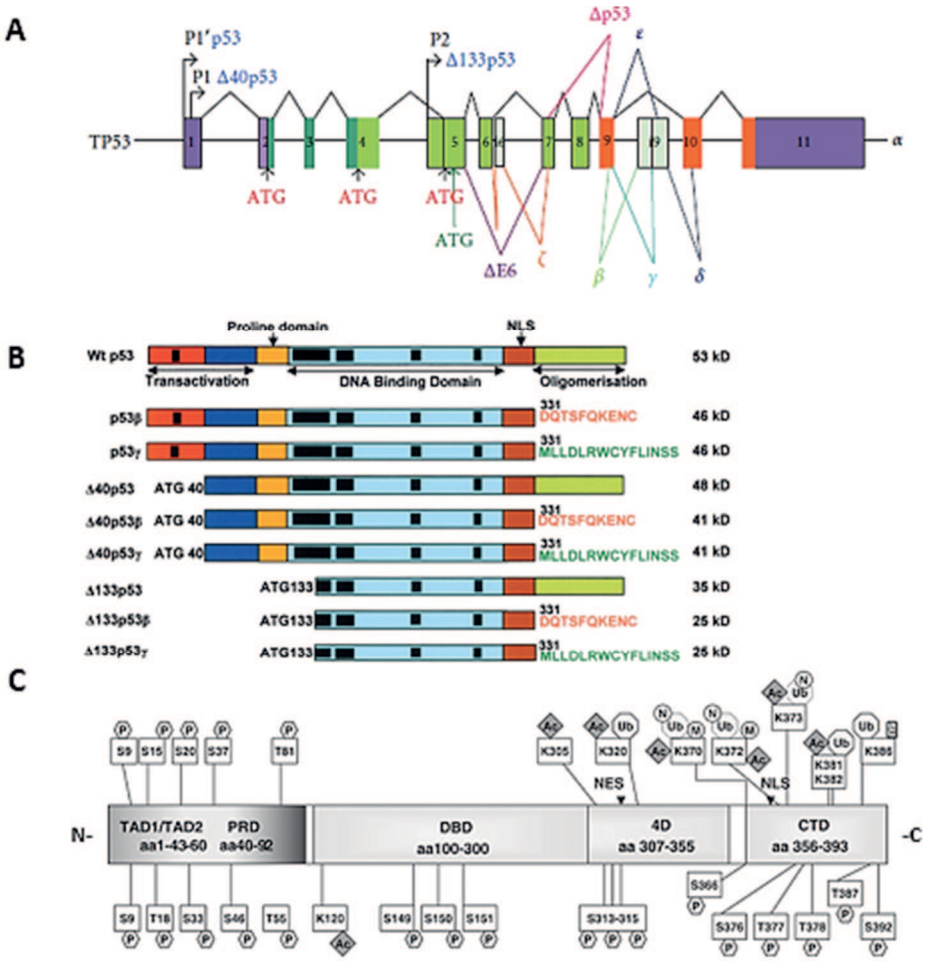

Figure 9: **The human Tp53 gene and protein.** (A) *Tp53* gene is divided into 11 exons spanning 19 Kb and presents two promoters: the P1 produces the full-length protein with complete transactivation (TA) capability while the P2 promoter produces TAD-deficient proteins (generally indicated as ΔN) that play a role as dominant-negative proteins. The transcription of p53 starts two distinct sites indicated as P1 and P1' [61]. (B) p53 splicing variants encoded by the human p53 gene. (C) The p53 protein consists of six major

domains: TAD1 and 2 (amino-acid residues 1–43 and 44–60), the PRD (residues 40–92), the DBD (residues 100–300) the 4D (residues 307–355) and the CTD (residues 356–393). NLS (nuclear localization signal) NES (nuclear export signal). Post-translational modifications are depicted in the individual domains of p53: P (phosphorylation), Ac (acetylation), Ub (ubiquitination), M (methylation), N (neddylation) and SU (sumoylation)

Many studies have been performed to elucidate the mechanisms that control the effects of *p53* during development. In mouse, *p53* is expressed ubiquitously until 10.5 days and during advanced stages is mainly expressed during the differentiation of specific tissues like brain, thymus, liver, lung, kidney and intestine [57]. *Tp53* is also expressed in post-mitotic but not terminally differentiated cells and the expression of p53 in undifferentiated cells is able to induce their differentiation; on the other hand, the reduction of p53 expression in human stem cells prevents the spontaneous apoptosis and differentiation [62]. *Tp53*$^{-/-}$ models are characterized by hyperplasic regions the brain's sub-ventricular zone since the proliferation is not suppressed [63]; the same effect can be seen in hematopoietic stem cells and progenitors cells whose number is increased in *Tp53*$^{-/-}$ mice than in the wild-type [64]. Mice and zebrafish (*Danio rerio*) *Tp53*$^{-/-}$ models can sometimes develop without morphological defects probably for the other p53 family members that compensate p53 loss. However, death before birth is seen in about the 25% of the mice embryos *Tp53*$^{-/-}$: these embryos are characterized by an over-growth of the neural tissue in the midbrain as consequence of the impaired neural tube closure and they also suffer of craniofacial and limb malformations. Conversely, *Tp53* overexpression leads to embryonic death: mice deficient for MDM2, the principal regulator of p53 activity, die earlier during the development while those lacking in both MDM2 and p53 are viable [57].

The half-life of p53 protein in unstressed cells varies from 6 to 20 minutes since p53 interacts with MDM2, COP1, PIRH2 or JNK and is degraded through the ubiquitin-proteasome pathway [65]. p53 protein is activated by different stress signals like telomere shortening, hypoxia, mitotic spindle damage, heat or cold shock, unfolded protein, etc. and when activated form a tetramer increasing its half-life from 6-20 minutes to hours [65]. Different stress signals can also induce post-translational modifications in p53 like phosphorylation, acetylation, ubiquitination, methylation, neddylation and sumoylation (Figure 9C). The active p53 tetramer binds specific regions in the promotor of target genes called p53 responsive elements (p53REs) mediating their activation or repression [65]. The final consequences of p53 activation are cell cycle arrest, DNA repair, differentiation, senescence or apoptosis if cells are not able to repair or respond properly to the stresses.

As stated before, *Tp53* is the most commonly mutated gene in human cancer [66]. Frameshift or nonsense mutations lead to p53 protein loss but the more frequent tumour alterations in p53 results in missense mutations in the DNA binding domain, with six hotspots of mutation identified. Since p53 acts as a tetramer, mutant proteins may act as dominant negative inhibitors towards wild-type p53 [67]. In addition, also p53 isoforms are implicated in human cancer even if their precise role is not understood yet. For example, the Δ133p53 isoform could have an oncogenic role while the overexpression in mice of the Δ122p53 isoform (the

homologous of the human Δ133p53 isoform) results in increased cellular proliferation, reduced apoptosis and onset of a wide spectrum of aggressive tumor like lymphomas, osteosarcomas and other malignant or benign tumor [61]. These mice display also increased multi-organ inflammation and blood cytokines levels. The Δ133p53 variant has been found in a variety of human cancers like breast cancer, renal cell carcinomas, colon adenoma and in melanoma associated to the increased expression of the Δ40p53 variant [61].

p63

The human *Tp63* gene consists of 14 exons spanning over 270 Kb. Structurally, *Tp63* gene consists of a promoter upstream to the first exon (generally indicated as P1) and a second promoter in the third intron (called P2). The human *Tp63* gene generates six different mRNA variants from which derive six protein isoforms as result of alternative splicing: three transactivating isoforms (TAp63α, TAp63β, TAp63γ) are generated from the P1 promoter while the N-truncated isoforms (ΔNp63α, ΔNp63β, ΔNp63γ) are generated from the P2 promoter [56] (Figure 10A – B).

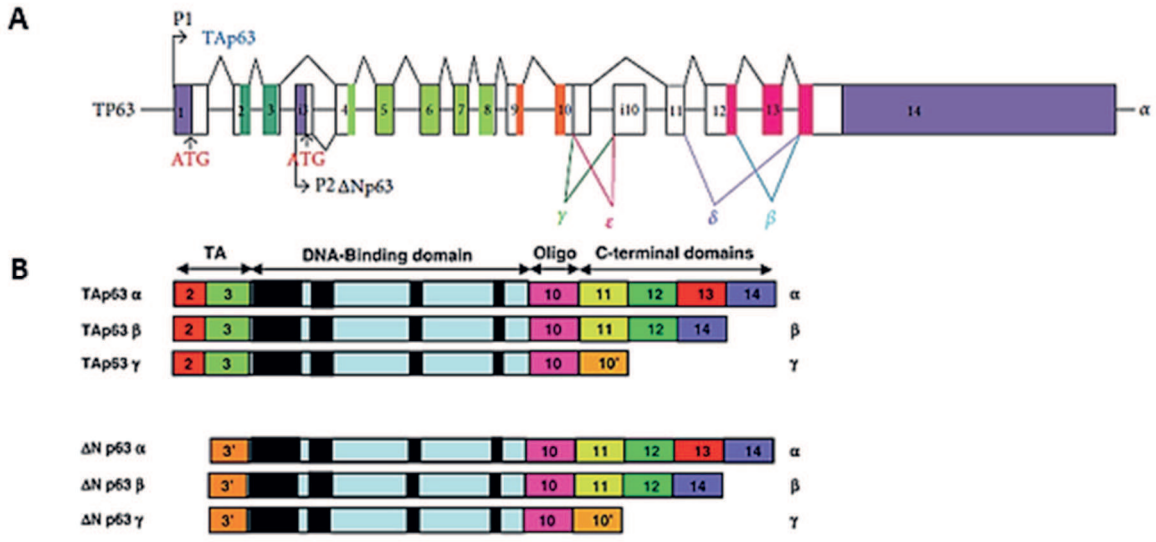

Figure 10: **The human *Tp63* gene and protein.** (A) Structure of the human *Tp63* gene. (B) TA and ΔN protein isoforms generated from the human *Tp63* gene.

TAp63 isoforms can bind DNA target sequences and activate the transcription of target genes through p53REs even though studies performed during the last years have highlighted the existence of p63 responsive elements (p63REs) that confer specificity for p63 but not for p53. Af for p53, the activation of p63 results in the arrest of the cell cycle or in the induction of apoptosis [56]. On the other hand, ΔNp63 isoforms can bind and activate target genes that are not activated by TAp63 isoforms because of the presence of 14 amino acid residues that contribute to the formation of an alternative transactivation domain (usually called TA2).

During development, T*p63* deficiency has severe effects: the absence of *Tp63* in mice model results in alterations of squamous epithelia and of all their derivates (including skin, hair, teeth, etc.) that are usually

lacking; limb formation, thymic morphology and cellularity is unbalanced in these mice that die early before birth. In *Tp63*$^{-/-}$ mice models the complementation of ΔNp63 alone or the double complementation of TAp63/ΔNp63 can rescue the observed alterations indicating that ΔNp63 is involved in the control of epithelial cells expansion from their progenitors while TAp63 regulates differentiation [57, 68]. ΔNp63α is expressed in the ectoderm before the stratification while in the adult organism its expression is limited to the basal layer and marks keratinocyte stem cells. ΔNp63 expression has been found also in mammary, prostate and lung stem cells [57, 69]. ΔNp63 controls also the formation of epithelial derivates that requires the interaction of WNT, FGF, Hedgehog, Notch and TNF pathways [57]: their formation starts with the budding of the epithelium into the mesenchyme before the following growth and folding in specific patterns. ΔNp63 is expressed in a region called apical ectodermal ridge (AER) at the tip of the limb bud that interacts with the underlying mesenchyme to promote limb formation. In the AER, ΔNp63 co-ordinates the expression of target genes.

TAp63 isoforms are also important since they are pro-apoptotic factors in developing neurons and oocytes. During neuronal development nerve growth factor (NGF) is necessary to neurons to survive; NGF absence causes TAp63 activation and hence apoptosis that can be promoted by TAp63 alone or in combination with p53. Ovaries present high expression of TAp63 and especially TAp63α: its expression progressively increases in developing oocytes that go through non-reductive DNA replication and homologous chromosome recombination and ends in the prophase of meiosis. Opposed to what has been seen in neurons, TAp63 is not required for ovarian development but is able to control germ line accuracy and, in cases of stresses or damaged DNA, it activates apoptosis independently from p53 [57, 70].

Mutations occurring in *Tp63* gene are often rare in human tumor. Mice models that lack of p63 (*Tp63*$^{-/-}$) show severe developmental defects while heterozygous mice (*Tp63*$^{+/-}$) models are susceptible to tumour development, even though conflictual data are present in literature. Several works reported the action of ΔNp63 as onco-suppressor: ΔNp63α, for example, represses oncogene-induced senescence and co-operates with Ras to promote tumour-initiating stem-like proliferation [71]. Since ΔNp63 is the predominant isoforms in epithelial cells, its overexpression is linked to nasopharyngeal, head and neck, urinary, lung and ovarian tumor generally associated to a poor outcome. TAp63 isoforms instead inhibit cellular proliferation and induce senescence: reduced expression of TAp63 is associated to an increased proliferation and oncogenesis in many Ras-mediated tumor [61].

p73

The human *Tp73* gene consists of 14 exons spanning over 80 Kb. Like *Tp53* and *Tp63* different isoforms derive from the *Tp73* gene: the TAp73 isoforms are generated from the first promoter (P1) located upstream of the first exon while the ΔNp73 isoforms derive from an alternative promoter (P2) in the third intron. In total,

Tp73 gene expresses at least 35 different mRNA variants from which derive 29 different p73 proteins but, in contrast to what observed for p63, p73 isoforms can be expressed from a different ATG codon and present different parts of the N-terminal, highlighting the hypothesis that they could develop not only different interactions possibilities but also different activities (Figure 11) [56].

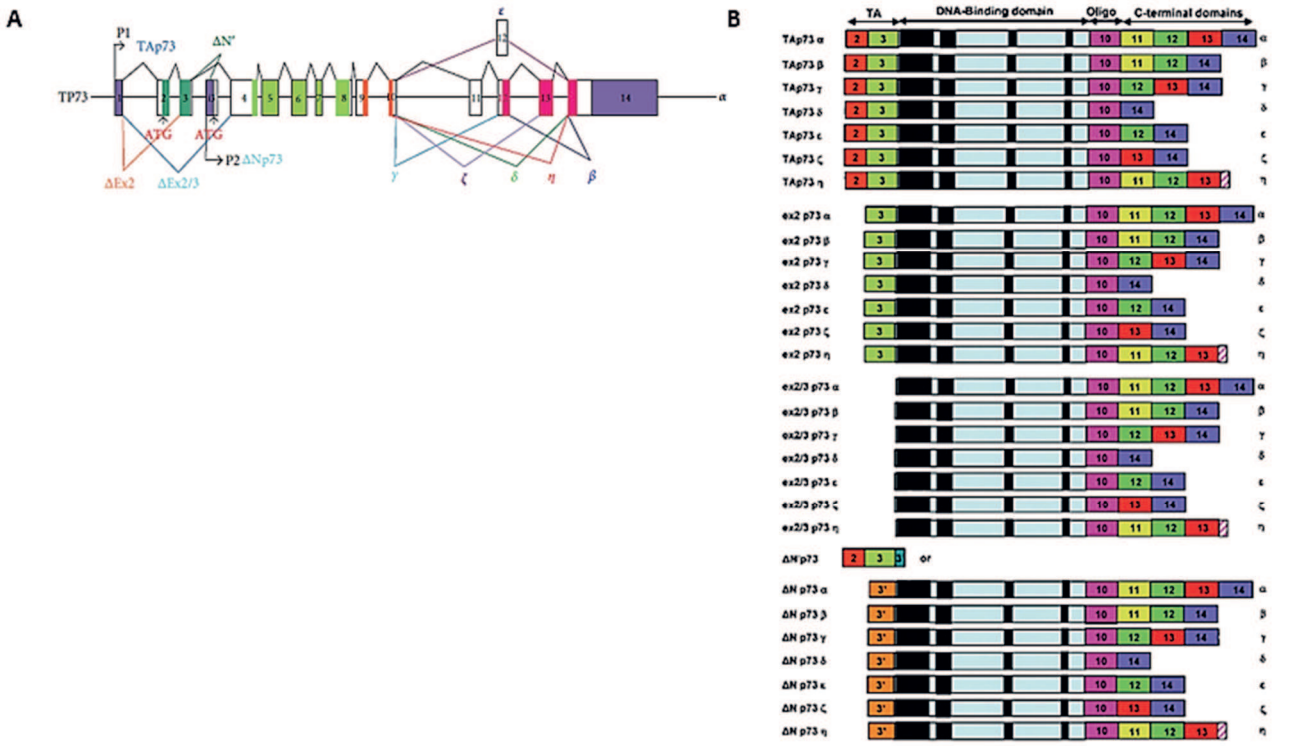

Figure 11: **The human *Tp73* gene and protein.** (A) Structure of the human *Tp73* gene. (B) TA and ΔN protein isoforms generated from the human *Tp73* gene.

TAp73 isoforms bind and activate the transcription of target genes involved in cell cycle arrest and apoptosis through p53REs; in response to genotoxic stresses TAp73 isoforms bind the P2 promoter and allow the transcription of the ΔNp73 variants. ΔNp73 variants in turn bind DNA through p53REs and exert a dominant-negative effect on p53, TAp63 and TAp73 isoforms. Moreover, ΔNp73 is the principal variant in developing mouse brain and the only one expressed in the neonatal brain and sympathetic ganglia since carries out an anti-apoptotic effect during development [72]. TAp73 isoforms instead are essential mediators of apoptosis especially after a chemotherapy-induced DNA damage.

Mice deficient for *Tp73* gene are more viable than *Tp63*$^{-/-}$ animals, they can survive for about two months and nearly the 25% of them reaches the adult age. These mice show hippocampal dysgenesis, hydrocephalus, loss of pheromone recognition, chronic infections and inflammation [57]. Apart from these severe neurological malformations, *Tp73*$^{-/-}$ mice show also a generalized pan-mucositis and, consequently, microbiological infections characterized by massive neutrophil infiltration.

In the case of tumor, the role exerted by p73 is still on debate: contrary to what observed for *Tp53* and *Tp63*, *Tp73* is rarely mutated and frequently over-expressed in tumor. Mice with isoform-specific knock-outs have been generated and the phenotype shown reflects the differences between the distinct variants. TAp73 null mice are prone to the onset of tumor while ΔNp73 knock-outs are more susceptible to DNA damage and apoptosis mediated by p53. Moreover, ΔNp73 isoforms play an oncogenic role and are upregulated in many liver, ovarian, breast, etc. tumor [61, 72]; several studies performed during the last years have shown that the upregulation of ΔNp73 is often associated with metastases, failure of chemotherapy and poor prognosis [61, 73]. Along with ΔNp73 also TAp73 has been found in tumor although its specific role is still unclear.

ENTERIC NERVOUS SYSTEM (ENS).

Neuronal control of digestive functions occurs at different levels: in the central nervous system (CNS), spinal cord, pre-vertebral sympathetic ganglions and in the enteric nervous system (ENS) that is one of the three branches of the autonomous nervous system along with the ortho-sympathetic nervous system and the parasympathetic nervous system [74]. Neurons and glial cells of the ENS originates from multipotent precursor cells deriving from the vagal segment of the neural crest. During the migration, neural crest cells are indistinguishable from mesenchymal cells and do not express any neuronal or glial phenotype. During and following the colonization of the gut, many different types of enteric neurons derive from massive proliferation of neural crest derived cells and this process is regulated by homeobox genes encoding for transcription factors like PHOX2A and PHOX2B [75].

Enteric neurons are organised into two different plexuses

- the MYENTERIC PLEXUS, also known as Auerback's plexus, between the outer longitudinal layer and the circular internal layer of the muscular tunica
- the SUB-MUCOSAL PLEXUS, or Meissner's plexus, localized in the sub-mucosal tunica

The neuronal network of the ENS controls both motor and secretive functions and is located in the internal wall of the oesophagus, stomach, small and large intestine, gallbladder, salivary glands and pancreas [76].

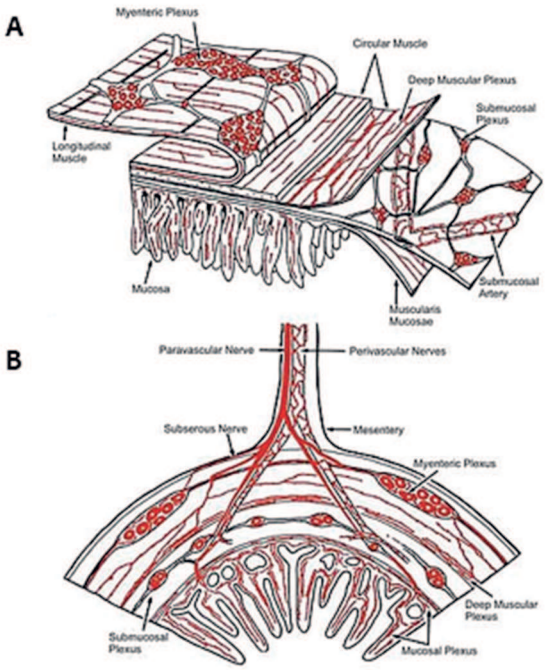

Figure 12: **Small intestine representation.** (A) Schematic representation of the different small intestine layers; (B) Transversal section of the small intestine (B).

Myenteric and sub-mucosal plexuses are interconnected and extent around the circumference and length of the gastrointestinal (GI) tract. Both plexuses are composed by ganglionic structures containing neurons' cellular body from which many nervous fibres depart: these fibres innervate circular and longitudinal musculature, vessels, mucosa, mucosal gland and villi [74].

Enteric glial cells, derived from the neural crest, are the equivalent of astrocytes and microglia in the SNC and are a fundamental component along with neurons in the ENS. Their laminar extensions cover the majority of neural bodies' surface creating synaptic contacts with vesicle-containing nerve varicosities [77]. Glial cells perform not only a nutritive or supporting role but they also contribute to the basal physiological functions of processes and neuronal cell bodies; they synthetize interleukins and express MHC II antigens in response to cytokines' stimulations, suggesting a modulatory role during intestinal inflammation [78]. Glial cells express also receptors for neurotransmitters, contribute to their reuptake and degradation and hence are involved in neurotransmission. These cells are also fundamental in the maintaining of the integrity of mucosal wall and are implicated in different aspects of the intestinal homeostasis [77].

Enteric neurons can be classified into four principal categories basing on their morphological, electrical, neurochemical and functional properties [76].

According the morphological classification, based on the Dogiel's criteria (Dogiel A. S. 1899), neurons are divided into three classes

- DOGIEL I neurons present a flat cellular body with one axon and many short dendrites; they receive afferent informations and show immunoreactivity to the Ca^{2+}-binding protein calretinin.
- DOGIEL II neurons possess a large round or oval cell body, an irregular surface, different axonal prolongations and show immunoreactivity to the Ca^{2+}-binding protein calbindin.
- DOGIEL III neurons are similar to Dogiel II class neurons but present more processes generally shorter than that observed in the previous class.

Enteric neurons present a rest membrane potential of about -40/-70 mV and can be divided into two classes

- S-TYPE (SYNAPTIC) neurons are similar to Dogiel I class neurons, are inter- or motoneurons and show multiple and rapid excitatory post-synaptic potentials (EPSPs) in response to synaptic stimulation.
- AH-TYPE (AFTER HYPERPOLARISATION) cells are similar to Dogiel II or III class of neurons, are sensory neurons and show early and late hyperpolarising potentials. They communicate between each other through slow EPSPs and with inter- and motoneurons with both slow and rapid EPSPs.

From the neurochemical point of view, enteric neurons express different combinations of neurotransmitters (a process called *chemical coding*) that depends on the type of neuron, animal species and intestinal segment. The strict relationship between chemical coding and neuronal function confers to enteric neurons a great adaptive capacity in different physio-pathological conditions, like in inflammatory processes, gastric ulcer or in cases of atrophy [79]. About 30 different neurotransmitters have been identified in the ENS and include both small molecules (e.g. serotonin and norepinephrine) and large peptides and gas like nitric and carbon oxides (NO and CO). The principal neurotransmitter is acetylcholine that is released by both intrinsic neurons and extra-mural fibres [76] and that mediates fast EPSPs on nicotinic receptors.

The last classification of enteric neurons relies on their functional properties and three types of neurons can be distinguished.

- SENSORY NEURONS: these neurons are divided into two categories
    - Intrinsic primary afferent neurons (IPANs) belong to AH-type, present an oval or rounded soma and their prolongations contact different neurons in the mucosal and sub-mucosal plexus. Their activation after mechanical or chemical stimuli applied to the intestinal mucosa allow the ENS to generate appropriate reflex responses. Chemosensitive IPANs respond to chemical stimuli applied on the luminal surface of the small intestine's mucosa while mechanoreceptor myenteric IPANs react to intestinal wall musculature's contraction through mechanosensitive ion channels [80]. Sub-mucosal IPANs instead response indirectly to mucosal distortions through enterochromaffin cells that release serotonin after a mechanical stimulus.

- Extrinsic primary afferent neurons (EPANs) can be vagal or spinal afferents where the first are involved in physiological events while the second primary respond to physio-pathological stimuli.

Sensory neurons can be also nociceptors because their activation after a nociceptive stimulus evokes protective responses [74].

- INTERNEURONS: usually these neurons belong to Dogiel II class and could be S- or AH-type. In guinea pig, four types of interneurons constitute chains extended along the intestine: one ascendant interneuron is cholinergic and is the conduct for the ascendant path that compose the projectile reflexes. Three descendant interneurons have a complex chemical distinction and studies performed on the connections established by these neurons revealed that each type perform different actions.
  - ChAT (choline acetyltransferase)/NOS (nitric oxide synthase)/VIP (vasoactive intestinal peptide) interneurons are involved in local motor reflexes [81].
  - ChAT/SOM (somatostatin) interneurons play a key role in the conduction of migrating myoelectric complexes in the small intestine [81].
  - ChAT/5-HT (serotonin) interneurons are associated in secreto-motor but not directly in motor reflexes [81].
- MOTONEURONS: these neurons belong to Dogiel I class and are S-type [76].
  - Muscular motoneurons innervate the muscularis mucosae, longitudinal and circular musculature of the entire digestive tract. They mediate cholinergic and tachichinergic excitatory stimulation but also inhibitory arousal [76].
  - Secretomotor and vasomotor neurons control secretion and blood flow and are directly regulated by IPANs through the release of Ach (acetylcholine) and VIP. The soma of the majority of secretomotor and vasomotor neurons is in the sub-mucosal plexus and some of these neurons project in the myenteric plexus while other in the muscularis mucosae. These neurons can be either cholinergic or non-cholinergic: Ach released by cholinergic neurons acts on muscarinic receptors in the mucosal epithelium, VIP instead is released by non-cholinergic neurons as transmitter [76]. Sympathetic afferents modulate local reflexes loops that regulate secretion and blood flow [76].

INTESTINAL ISCHEMIA AND ISCHEMIA/REPERFUSION SYNDROME

Intestinal ischemia is an acute and rarely chronic clinical condition caused by the unbalance between oxygen perfusion to the entire or part of the intestine and the metabolic tissue demand. Two theories have been proposed to explain the importance of intestinal ischemia [82, 83].

- The METABOLIC THEORY assumes that the disequilibrium between oxygen support and tissue demand causes an increased concentration in local metabolites responsible for vasodilatation and hyperaemia, two intrinsic control mechanisms accountable for instant variations of hematic flow in the splanchnic district.
- The MYOGENIC THEORY suggests that an unexpected decrease in perfusion's pressure is compensated by a reduction of blood vessels' wall through arteriolar tension receptors hence causing the maintaining of splanchnic flow.

In case of an important blood flow reduction, intestine undergoes to ischemic tissue damage [84] caused by vasculopathies like artery's occlusion due to blood clots or emboli or, more frequently, by non-occlusive processes like small blood flow or artery's vasospasm or a reduction of blood volume. Generally, the most affected vessels originate from the abdominal aorta and are the coeliac tripod (left gastric artery, common hepatic artery and splenic artery), the superior and inferior mesenteric arteries with their branches (Figure 13). In addition to artery's occlusions, also veins obstructions could happen and they cause similar severe effects even if they are rare.

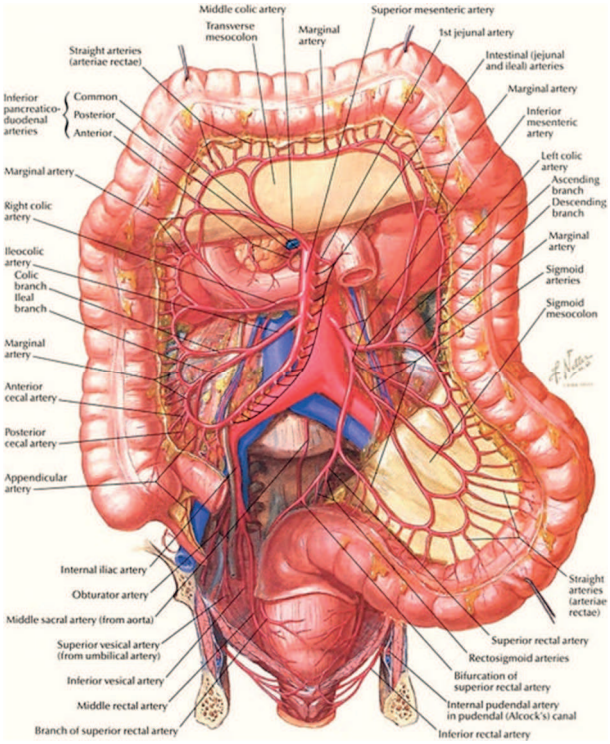

Figure 13: **Organisation of human abdominal arteries** (Netter's Atlas of Human Anatomy 4^ Edition).

Multifocal intestinal strokes are often seen in inflammatory intestinal disease (IBD, inflammatory bowel diseases) like Chron's disease and ulcerative colitis [85].

The American Gastroenterology Association (AGA) promotes a classification of intestinal ischemia basing on its clinical aspects [86]: different severe conditions have been identified like acute mesenteric ischemia (AMI) and the more lethal non-occlusive mesenteric ischemia (NOMI), arterial embolism, arterial thrombosis, venous mesenteric thrombosis, chronic mesenteric ischemia and colon ischemia.

Because the 70% of hematic mesenteric flow distributes in the mucosal and sub-mucosal tunics while the other 30% is directed to muscular and serous layers, the enteric mucosa is the first structure that presents morphological alterations following hypoxic or hypoglycaemic conditions. All the biomolecular events following these stresses overlaps to that observed in central nervous system: when the mesenteric hematic perfusion reduces, tissue oxygen availability and perfused capillary density increase. This contributes to two opposite effects: firstly, intestinal tolerance to ischemia is improved and oxygen consumption is constant but, secondly, fluid loss from intra-vascular spaces causes an in increase in local haemoconcentration and hence capillary obstruction [87]. O_2 levels progressively decrease reaching a threshold where the compensation abilities are exceeded and the principal consequence is the alteration of cellular respiration due to the deprivation of fundamental substrates necessary for the ATP synthesis. Anaerobic glycolysis bypasses ATP synthesis producing lactic acid that in turn causes acidosis. Ionic ATP-dependent pumps are altered during the interruption or slowdown of the hematic flow causing increasing Na^+ levels and osmotic swelling. $2Na^+/Ca^{2+}$ exchangers compensate the increase of Na^+ levels exchanging Ca^{2+} from intracellular stores and simultaneously Ca^{2+} re-uptake is reduced. Enteric dying neurons release glutamate that activates NMDA receptors hence increasing Ca^{2+} influx and potentiating damaging mechanisms. Contextually, the imbalance in glial re-uptake mechanisms results in an increase of K^+ levels that cause an enhanced consumption of O_2 and glucose hence worsening neuronal energetic supply. The alteration of normal ionic currents causes a massive Ca^{2+}input that activates many Ca^{2+}-dependent processes involved in oxidative stress [88], inflammation [87] and apoptosis.

If ischemia's cause is removed before the developing of irreversible alterations (necrosis and apoptosis), tissue re-oxygenation performs a protective role because it promotes aerobic metabolism, toxic compounds removal and the restoration of normal cellular functions: in this phase intestinal reperfusion is fundamental for the recovery of the ischemic tissue. Conversely, O_2 return in tissues causes a series of biochemical and cellular mechanisms that amplify tissue damage in a process called oxygen paradox [89]. Ischemia/reperfusion (I/S) syndrome plays a key role in the physiopathology of many clinical-surgical conditions like that developed after small intestine transplant. The negative effects of intestinal I/R, like cellular and microvascular damages [90], seems to rely on free radicals like ROS produced by XD (xanthine dehydrogenase)/XO (xanthine oxidase) system [87] and NO (nitric oxide). Endothelium is considered the

initiator of the intestinal lesions after re-oxygenation because its presents the highest XO concentrations and, during the ischemic insult, synthetises in abnormal way NO [86]: the combination of NO, provided by endothelial cells during ischemia, with superoxide (O_2^-) radical, generated during the conversion of hypoxanthine to uric acid mediated by xanthine oxidase, produces peroxynitrite radical ($ONOO^-$) that damages phospholipids, nitrosylates proteins acting on tyrosine residues, causes DNA breaks and deoxyribose oxidation (Figure 14) [91].

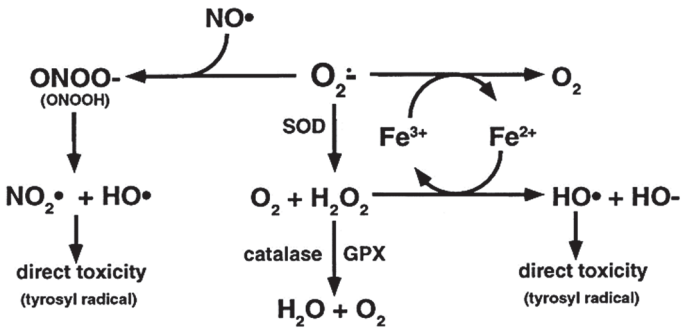

Figure 14: **Mechanism of action of O_2^- radical on NO.** O_2^- radical is produced during the conversion of xanthine to uric acid mediated by xanthine oxidase. Superoxide dismutase (SOD) mediates the transformation of O_2^- into hydrogen peroxide (H_2O_2) which is subsequently converted into H_2O and O_2 by catalase or glutathione peroxidase (GPX). Fe^{2+} increase promotes the interaction between O_2^- anion and water that undergo to Fenton's reaction followed by Haber-Weiss's reaction with production of the instable OH^- radical. O_2^- is also able to combine with nitric oxide (NO) producing the highly reactive peroxynitrite ($ONOO^-$) radical.

Experiments performed in the rat after the induction of an hypoxic and hypoglycaemic damage *in vitro*, showed an evident mucosal damage with important histological features; interestingly, if the damage was followed by 24 hours of reperfusion the injury was transient because of the complete regeneration of the mucosa [92].

During reperfusion following ischemic insults, mucosal lesions stimulate the release of chemotactic substances and the expression of adhesion molecules (CAM, e.g. integrins and selectins). These molecules promote leukocyte infiltration through adhesion of the inflammatory cells to post-capillary venular endothelia, their rolling on the endothelial surface and their migration through diapedesis within the interstitial space.

Tissues involved in ischemia followed by reperfusion activate also a protein-kinase family that convey on specific transcription factors like activator protein 1 (AP-1) and nuclear factor-kappa B (NF-kB) which, in turn, regulate the expression of pro-inflammatory genes [93]. Activation of NF-kB pathway by different stimuli leads to phosphorylation of inhibitor of kappa B (IkBα) by IkB kinase (IKK) which separates the NF-kB dimers (p50 and p65) and leads to the degradation of IkBα. The free NF-kB translocates from the cytoplasm into the nucleus and acts as transcription factor. In the nucleus, NF-kB dimers combine with target DNA elements to activate transcription of genes encoding for inducible enzymes like cyclooxygenase-2 (COX-2)and inducible

nitric oxide synthase (iNOS), cytokines such as tumor necrosis factor-α (TNF-α) and interleukin-6 (IL-6) and adhesion molecules like P-selectin and E-selectin [94]. NF-kB has a dual role since is able to promote or inhibit intestinal I/R damages preventing systemic increase of TNF-α levels or inducing apoptosis to the reperfused mucosa [95]. The complement system is activated after I/R as demonstrated by experiments performed on rat's intestine: the activation of the classical pathway results in the increased transcription of iNOS [96] with the sequent increase of NO levels. In such conditions, O_2^- synthesis could be increased by both neutrophils activation and platelet recall and SOD levels reduction. In the ileal mucosa of rats exposed to hypoxic damages hypoxia inducible factor-1 alpha (HIF-1α) levels increase and this factor seems to be implied also in the subsequent re-oxygenation of the intestine since its high levels in this phase. This persistence might be mediated by intestinal bacteria and/or by their products like lipopolysaccharide [97]. HIF-1α partial deficiency in the small intestine of the mouse attenuates the I/R induced damage: HIF-1α activation is in fact associated to a loss of function of the mucosal wall, pronounced villi damage, marked inflammatory response and caspase-3 activation. In the light of the role exerted by hypoxia in the propagation of local and systemic inflammatory response after I/R, O_2 inhalation experiments performed in rats model showed a decreased intestinal damage, accelerated turnover of the enterocytes and ameliorated intestinal rehabilitation [98].

As described for the CNS, also the ENS show a significative immediate or retarded neuronal death after I/R [99, 100]: during reperfusion in the ileum of rat in fact the total number of myenteric neurons decreases and the survived neurons show evidences of damage for some weeks. Neuronal damage seems to be also selective and depends on the type of molecule expressed in neurons: the expression of iNOS is related to cellular swelling and deformation, while no alterations are seen if calretinin is expressed [101]. A gradual reduction in the number of neurons both in sub-mucosal and myenteric plexus has been also seen in human pathologies like neonatal necrotizing enterocolitis. Other data suggest that if the ischemic insult is transitory the enteric micro-environment damage is reversible because neither the total number of neurons in the ganglions of the myenteric plexus nor intestinal motility are affected [90].

Information regarding the effect of I/R on intestinal musculature of the GI tract are scarce: intestinal motility and secretive processes depends on enteric neurons and their loss could result in an altered release of neurotransmitters and hence in intestinal disfunction [90]. Recent works on mice demonstrate that I/R causes a damage on the longitudinal musculature and it has been assumed that damage and inflammation resulting from I/R may contribute to long-term loss of function of the intestinal motility [102].

NITRIC OXIDE (NO): ROLE IN THE ENS AND IN ISCHEMIA/REPERFUSION.

Nitric oxide (NO) is an important physiological mediator involved in the regulation of vascular tone and in biological functions. In biological tissues NO causes physical-chemical alterations of molecules like heme-containing proteins, oxygen, superoxide anion, ozone, amines and tyrosine. During hypoxia and acidosis, NO

is rapidly oxidized into nitrite (NO_2^-) and converted into nitrate (NO_3^-) in presence of oxyhemeproteins, xanthine oxidoreductase, polyphenols, protons and ascorbic acid since the reduced partial O_2 pressure causes an impaired NO synthesis [103].

NO biosynthesis is principally mediated by nitric oxide synthases (NOS) that catalyze the oxidation of L-arginine into L-citrulline in a two-passages reaction: in the first L-arginine is oxidized into N-hydroxi-L-arginine using 1 equivalent of NADPH and O_2; in the second N-hydroxy-L-arginine is concerted into NO and L-citrulline using 0.5 equivalents of NADPH and 1 molecule of O_2 (Figure 15).

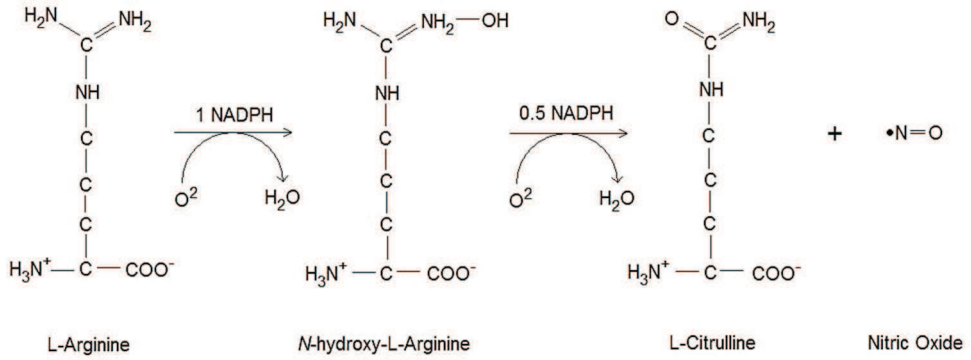

Figure 15: **Synthesis of nitric oxide (NO) from L-arginine in mammals.**

NO is synthetized by three different structurally and functionally correlated NOS isoforms [104], encoded from genes located on different chromosomes and, probably, derived from a common ancestral progenitor.

- NEURONAL NITRIC OXIDE SYNTHASE (nNOS): nNOS is encoded by *NOS1* gene located on chromosome 12q24.22 (http://www.genecards.org/cgi-bin/carddisp.pl?gene=NOS1) and has been identified in rat's and pig's cerebellum. nNOS is expressed also in different SNC areas like spinal cord and sympathetic ganglions, olfactory bulb and hippocampus; its expression is found even in adrenal glands, nitrergic peripheral nerves, epithelial cells, pancreatic islands and smooth vessels' musculature. Different types of stimuli like neuronal damage, pharmacological therapy, hypoxia or stress can up- or downregulate its expression [105-108]. nNOS activity is mediated by Ca^{2+}-activated calmodulin.
- INDUCIBLE NITRIC OXIDE SYNTHASE (iNOS): iNOS is encoded by *NOS2* gene on chromosome 17q11.2 (http://www.genecards.org/cgi-bin/carddisp.pl?gene=NOS2), has been isolated from activated mouse macrophages and its expression is induced by pro-inflammatory cytokines (e.g. interleukin-2, interleukin-18, interleukin-12, interferon-α), endotoxins and viruses [104]. iNOS is typically present in microglia and astrocytes, endothelia, smooth and cardiac muscle, keratinocytes, hepatocytes and mastocytes. When expressed, iNOS is constantly activated and is not influenced by intracellular Ca^{2+} levels [109]. Excessive concentrations of nitric oxide synthetized by iNOS result harmful for the

healthy cells of the organism and they play a key role during septic shock, a condition characterized by a massive arteriolar vasodilatation, hypotension and microvascular damages.

- ENDOTHELIAL NITRIC OXIDE SYNTHASE (eNOS): eNOS is encoded by *NOS3* gene on chromosome 7q36.1 (http://www.genecards.org/cgi-bin/carddisp.pl?gene=NOS3) and, in addition to the endothelium, is expressed in T and B lymphocytes, hepatocytes, certain cerebral neurons, cardiac myocytes, platelets, syncytiothrophoblast of the human placenta and renal epithelial tubular cells [109]. It's a typical membrane enzyme since only the 5% of eNOS is found in the cytoplasm and, similarly to nNOS, its activity is regulated by Ca^{2+}-activated calmodulin. Conditions like metabolic deficiency, hypoxia, ischemia, cold exposition and physical exercise increase eNOS expression in the endothelium, cardiac muscles, hepatocytes and brown adipose tissue. NO produced by eNOS is the most important endogenous vasodilator [110] and *NOS3* deletions causes an increase in blood pressure [111]. Moreover, nitric oxide synthetized by eNOS inhibits platelet aggregation and adhesion to vascular bed.

nNOS, iNOS and eNOS present also a high homology degree in their catalytic site and this domain is also homologous to that of cytochrome P450 reductase, the terminal enzymatic complex of the mitochondrial transport chain to which the O_2 used during cellular respiration binds [112].

Nitric oxide is considered an important neurotransmitter mediating nitrergic neurotransmission not only in the CNS but also in the GI tract. Being lipophilic NO is not released through endocytosis but comes out the nerve endings through diffusion acting both in the synthesis site and in the extra-cellular space. NO influences all the nearby structures and hence is considered also as a potent neuromodulator in the CNS through the promotion of cyclic guanosine monophosphate (cGMP) and S-nitrosylation [113].

Nitrergic neurons represent the 34% of the total enteric neurons number and, in the normal human colon, nNOS immunoreactivity is evident both in sub-mucosal and myenteric plexuses. The principal function of nitrergic paths in the ENS consists in the mediation of smooth musculature relaxation: nNOS lack in fact is associated with an unbalanced NO production that may be responsible for the muscular relaxation failure [114]. NO is fundamental for the peristaltic reflex consisting of two principal phases in the small intestine: ascendant ACh-mediated contraction and descendant NO-dependent relaxation (Figure 16).

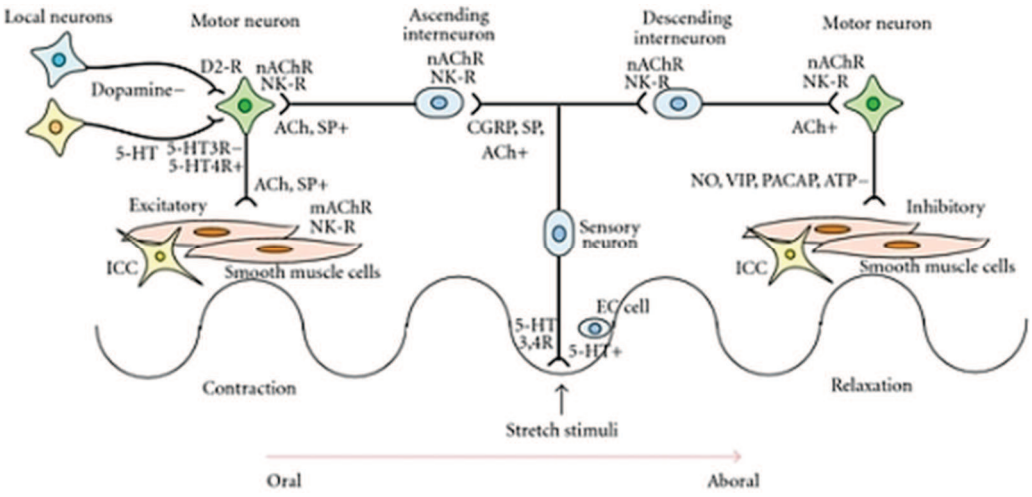

Figure 16: **Enteric neural circuitry relevant for peristaltic reflex** (from Sakakibara R et al 2011). [115]

Several studies have demonstrated the inhibitory effects of NO on intestinal motility and animal models reproducing a slow-down of intestinal transit show its normalization upon administration of NOS inhibitors in combination with adrenergic drugs [116].

Differently from the great amount of information regarding the effects of the ischemic damage in the CNS, little is known about neurotransmission in the ENS after the same insult. In focal cerebral ischemia, nNOS and iNOS-mediated NO synthesis causes neurotoxicity, while eNOS-dependent synthesis results in a protective effect on brain tissue. Moreover, several evidences show that nNOS-mediated NO synthesis is the principal source of neuronal neurotoxicity: animal models of focal ischemia demonstrate that nNOS activation is related to neuronal damage, while mice lacking *NOS1* gene display a reduced infarct-related effects [117, 118]; primary cortical neurons cultures lacking nNOS are resistant to NMDA-mediated excitotoxicity [119], similar cultures derived from *NOS1*$^{-/-}$ mice show resistance to oxygen and glucose deprivation (OGD) while neuronal cultures subjected to ischemia and treated with NOS inhibitors are not affected by the ischemic insult [120].

iNOS and its catalytic activity are detectable after 12 hours of focal ischemia and present a peak at 48 hours returning to basal levels after 7 days [120]. The administration of relatively non-selective iNOS inhibitors 24 hours after the ischemic attack causes a reduction of the infarcted area; moreover, *NOS2*$^{-/-}$ mice display a smaller infarcted area than wild-type animals [120] hence suggesting that iNOS is implied in late neuronal damage following cerebral ischemia.

During intestinal I/R, NO can be both cytoprotective and cytotoxic especially when oxidative stress onsets [121]: NO synthetized by constitutive NOS seems to play a protective role acting as vasodilator and anti-inflammatory modulator, inhibiting neutrophils adhesion and platelets aggregation that contribute to I/R damage [84]; on the contrary, an excessive NO production due to the increased activity of iNOS is involved

in the generation of free cytotoxic radicals that amplify the effects of ischemia [122]. Several evidences support the role of iNOS during I/R events: in rats, the inflammation following mesenteric reperfusion is characterized by an enhanced NO production correlated to increased iNOS expression [123]; in rats' ileum affected by a severe I/R damage the increased iNOS expression correlates to a decreased intestinal transit [124] while, in mice models, iNOS selective inhibition during post-ischemic reperfusion protects the intestine from motility alterations, increased vascular permeability and leucocytes recruitment [125].

AIM OF THE PROJECT

During the last years the research carried out in our laboratory focused on the investigation of the role of the homeobox gene family OTX in different physiological and pathological conditions both in animals and human.

In 2011 we demonstrated that in breast cancer p53 is able to regulate OTX1 gene expression [126]. Using SaOs2 cell line (p53 Tet-On) which didn't express endogenous p53 and whose expression was induced by doxycyclin, we idientified an increased expression of OTX1 using Real Time PCR and Western blot analyses. To confirm the result an *in-silico* analysis of the promoter of OTX1 gene was performed to identify responsive elements regulated by p53. We discovered two putative elements regulated by p53 called respectively p53RE-5' and p53RE-3'. To understand which of these two sites represented the effective binding region of p53, chromatin immunoprecipitation analysis on SaOs2 p53 Tet-On cell line in presence or absence of doxycyclin was performed; two regions of abouat 160-170 bp sorrounding the two responsive elements were amplfied through PCR and only p53RE-3' gave positive signal indicating as this region was implicated in the interaction between p53 and OTX1. Using luciferase assay performed after cloning p53RE-3' and cotransfecting different amounts of p53, we observed that this region was able to activate luciferase transcription directly proportional to the increased expression of p53. The same effect developed by p53 was also discoverd for the other two members of its family TA/ΔNp63-73. To evaluate the molecular interaction between p53 and OTX1 during cellular differentiation, we studied LA7 cancer stem cells (CSCs) either control or differentiated with DMSO. We observed and increased expression for both p53 and OTX1 implying a role for these genes during asimmetric division of CSCs. OTX1 was also detected at high levels during laction process in mice both in presence and absence of p53 indicating that p53 in not involved in the physiological remodeling of breast tissue during lactation.

On the basis of this work our research proceeded and in 2013 our laboratory found the expression of VEGFα, OTX and p53 family genes in Proliferative Vitreoretinopathy (PVR), a complication connected to retinal detachment and characterized by a severe inflammatory status [127]. We observed basal expression levels for all the genes in the control samples; retinae affected by PVR showed little or absent expression of OTX1, reflecting an indifferentiate status of retinal tissue, and a variable expression of VEGFα, OTX2, OTX3, p53 and p63. We suggested the existence of two possible pathways with an opposite trend of expression and which are capable of influencing the course of the pathology: the first pathway involved VEGFα-OTX2-p53-p63 while the second OTX1-OTX3. Immunoistochemical analyses identified also the expression of OTX protein in the internal field of photoreceptors, horizontal cells, bipolar cells and neuronal cells. It was hypotesized that OTX2 could have a role in the maintenance of cellular identity and in the survival of adult differentiated retinal cells. Its high expression in PVR samples could correlate with the rientry of differentiated cells in cell cycle and staminal status, suggesting a role for this gene in the proliferation of retinal staminal cells as replacement for dead cells.

In a recent work produced by our research group in collaboration with the Department of Pathological Anatomy of the Ospedale di Circolo in Varese, OTX1 and OTX2 were proposed as possible molecular markers of sinonasal tumors and olfactory neuroblastomas [128]. Real Time PCR and immunoistochemical analyses performed on formalin-fixed paraffin-embedded (FFPE) sections of normal sinonanasal mucosae, inverted papillomas (IPs), sinonasal intestinal-type adenocarcinomas (ITACs), non-intestinal type adenocarcinomas (NITACs), adenoid cystic carcinomas (ACCs), pleomorphic adenomas (APs), olfactory neuroblastomas (ONs), poorly-differentiated neuroendocrine carcinomas (PDNECs) and neuroendocrine tumors (NETs) revealed expression of both genes in normal sinonasal mucosa and a variable expression and immunoreactivity in the studied tumors. We found nuclear expression for OTX1 in all NITACs samples while little or absent immunoreactivity was highlighted in ITACs. Intense immunoreactivity was present in all ONs; among PDNECs, OTX expression varied in intensity and percentage of positive cells. Real Time PCR analyses confirmed the expression of both OTX1 and OTX2 genes in control samples; OTX1 but not OTX2 was expressed in NITACs samples and both genes were completely downregulated in ITACs. In ONs samples we found only the expression of OTX2 gene while OTX1 was downregulated and among the PDNECs samples the expression of both genes varied. We hypothesized that activation or inactivation of OTX homeobox genes is a relevant event in the pathogenesis of different sinonasal tumors and these factors could also be useful diagnostic, prognostic and therapeutic targets.

Tumors and inflammatory conditions could share many different features, and, among these, hypoxic/ischemic events are often correlated with impaired clinical outcomes. Ischemic events cause the lack of oxygen and nutrients in cells and tissues. If ischemia is prolonged for long time the first alteration is the reduction of available ATP which is subsequently degraded and converted up to hypoxanthine. During ischemic suffering, also Ca^{2+} metabolism is alterated: in physiological conditions Ca^{2+} is pumped out from the cells while the lack of ATP causes the inability of cellular pumps to transport Ca^{2+} outside hence resulting in its accumulation inside. The increase in Ca^{2+} levels allows the activation of proteases which convert xanthine dehydrogenase into xanthine oxidase. Xanthine oxidase converts hypoxanthine to uric acid using oxygen as substrate and produces free oxygen radicals (e.g. O^{2-}) which destroy cellular membranes through phospholipids oxidation. Inflammatory processes are the result of reperfusion after ischemic stress. To evaluate the involvement of *Otx* genes and p53 family during inflammation processes we used zebrafish (*Danio rerio*) as animal model and a soy-based diet to feed the animals since it's reported to generate intestinal inflammation similar to the one observed in Inflammatory Bowel Diseases (IBDs, e.g. Chron disease and ulcerative colitis) [129]. Both *Otx* genes and p53 family members were upregulated during the treatment and their expression was related to pro-inflammatory cytokines expression trend. These results were also confirmed by analyses performed on CaCo-2 cell line treated with IL-22 and U937 cell line exposed to PMA (data not shown). Inflammatory states are a hallmark of cancer and are also triggered by the activation of inducible factor alpha (HIF-1α) during an hypoxic event. HIF-1α is able to stimulate the transcription of VEGFα

to induce the creation of new blood vessels necessary to supply the tumor with oxygen and nutrients. We have already observed a connection between VEGFα, OTX genes and p53 family members [127] but little is known about the involvement of OTX genes in hypoxic/ischemic conditions. Previous studies in our laboratory performed on MIO-M1 cell line exposed to either 1% oxygen or to Cobalt(II) Chloride (data not shown) revealed an influence of HIF-1α on OTX genes and p53 family members and we proposed a model in which OTX1 could be a potential target of HIF1α during early hypoxic events.

During this PhD project we have firstly studied, in collaboration with the Laboratory of Pharmacology of the Univeristy of Insubria in Varese headed by Cristina Giaroni, the involvement of the homeobox gene family OTX in rat model of ischemia/reperfusion. Male Wistar rats were subjected to laparotomy procedure to expose a loop of the small intestine supplied by a single branch of the superior mesenteric artery (SMA). SMA was temporarly occluded for 60 minutes, the abdominal wall sutured and animals returned to their cage to recover for 24 and 48 hours (ischemia/reperfusion group). At the same time, another experimental group consisted of animals subjected only to the laparotomy procedure without the clamping of the SMA and a following recovery of 24 and 48 hours (sham-operated group). To validate the model, we have evaluated histological changes, inflammatory infiltration degree and upper GI transit efficiency after 60 minutes of ischemia followed by 24-48-72 hours of reperfusion. I/R and sham-operated group of animals were also treated IP with the iNOS inhibitor 1400W and nNOS inhibitor NPLA. Real-Time PCR, Western blot and immunohistochemical analyses were then performed on longitudinal muscle layer with attached myenteric plexus preparations (LMMPs).

The use of cell lines to replicate *in vitro* observations made *in vivo* is a powerful tool in the field of translational medicine since it allows the identification and the elucidation of molecular mechanisms at the basis of pathological conditions. In the second part of this PhD project we decided to replicate *in vitro* an ischemia/reperfusion damage using the human neuroblastoma SK-N-BE(2) cell line as cellular model. Firstly we developed an experimental protocol in which SK-N-BE(2) cell line was treated with all-trans retinoic acid (ATRA) for 12 days in order to differentiate the cells towards a neuronal-like phenotype as reported in several literature works. To replicate an ischemic/hypoxic condition cells were subjected to Oxygen and Glucose Deprivation (OGD) procedure using sodium azide at the end of the treatment: this compound was chosen among others because it provokes the block of the electron transport chain and the production of ATP as observed during hypoxic/ischemic events. The reperfusion was replicated changing the medium used for OGD with the standard culture medium. For every condition considered, morphological analyses were performed to evaluate the differentiation status of SK-N-BE(2) cells during the treatment; samples collected at the end of the treatment with ATRA, OGD and recovery were studied through Real-Time PCR, Western blot and immunofluorescence analyses.

The results obtained from the analyses performed in vivo and in vitro have been collected and studied to understand and elucidate the involvement of the homeobox gene family OTX and the nitrergic pathway during an ischemia/reperfusion damage in the enteric nervous system.

MATERIALS AND METHODS

ANIMALS

Male Wistar rats (Harlan Italy, Correzzana, Monza, Italy) were enclosured in groups of four animals under controlled environmental conditions (temperature: 22 ± 2 °C; relative humidity: 60 – 70%; light/dark cycle: 12-12 hours) and free access to standard diet and water. All the experiments were previously approved by the animal welfare board of the University of Insubria in compliance with national and international laws.

ISCHEMIA/REPERFUSION

Pentobarbital was diluted in sterile phosphate-buffered-saline (PBS) and anaesthesia was performed intraperitoneally (IP) administering the drug at the final concentration of 50 mg/kg. Animals were subjected to laparotomy procedure to expose a loop of the small intestine supplied by a single branch of the superior mesenteric artery (SMA) and the artery was temporarily occluded for 60 minutes with an atraumatic micro-vascular clamp. The clip was removed, the abdominal wall sutured and the animals returned to cages after recovery from anaesthesia. To validate the model, histological changes, inflammatory infiltration degree and upper GI transit efficiency were evaluated after 60 minutes of ischemia followed by 24-48-72 hours of reperfusion. Other experimental groups (sham-operated animals) included rats subjected to the same surgical manipulation without SMA occlusion and control un-operated animals. Because major histological and functional changes were observed after 24 and 48 hours of reperfusion (see the results section), the subsequent analyses were performed only in these I/R, sham-operated and control animal groups. 20 minutes before ischemia or sham-operation, 4-8 animals from each group were also treated IP with the following drugs diluted in PBS at a final concentration chosen on the basis of literature data indicating the efficacy and the absence of toxicity

- nNOS SELECTIVE INHIBITOR: N^{ω}-propyl-L-arginine hydrochloride (NPLA, Tocris, Bristol, UK), 10 mg/kg [130-132].
- iNOS SELECTIVE INHIBITOR: 3-aminomethylbenzylacetamidine dihydrochloride (1400W, Tocris, Bristol, UK), 5 mg/kg [131, 133].

At the end of the reperfusion periods animals were sacrified by decapitation and segments of about 6-8 cm of the small intestine were excised and rinsed with a physiological ice-cold Tyrode's solution (137 mM NaCl, 2.68 mM KCl, 1.8 mM $CaCl_2.2H_2O$, 2 mM $MgCl_2$, 0.47 mM NaH_2PO_4, 11.9 mM $NaHCO_3$, 5.6 mM glucose). Whole wall intestine segments were fixed and stored for the immunohistochemistry experiments. Real-Time PCR and Western blot assays were performed on external longitudinal muscle layer with attached myenteric plexus (LMMP) preparations: samples used for Real-Time PCR were stored in RNA Later solution (Ambion Life

Technologies Italia, Monza, Italy) at -20 °C while LMMP samples used for Western blot were maintained at -80 °C until their further use. Myeloperoxidase activity (MPO) experiments were performed on intestinal segments deprived of mucosa and stored at -80 °C.

GASTROINTESTINAL TRANSIT

GI transit measures were performed modifying the protocol established by Puig and coworkers in 2000 [134]. Rats were fasted for 20 hours before the experiments and had free access to water. Small intestinal motility was evaluated measuring the distance covered by a charcoal meal (0.25 mL of a mixture of 10% vegetable charcoal and 5% arabic gum in saline) administered by oral gavage to each animal 30 minutes before death. The abdominal cavity was subsequently opened the small intestine removed after the ligation of pylorus and ileocecal junction. The distance covered by the black marker across the small intestine was measured through a premeasured template and expressed as percentage of the small intestine length from pylorus to cecum.

MYELOPEROXIDASE (MPO) ACTIVITY

MPO analyses were conducted with modifications with respect to the protocol of Bradley and collaborators in 1982 [135]. Briefly, intestinal samples deprived of mucosa were homogenized (50 mg/mL) in ice-cold 50 mM potassium phosphate buffer pH 6.0 containing 0.5% hexadecyl trimethylammonium bromide (HTAB) and the homogenate was centrifuged at 13.000 r.p.m for 20 minutes at 4 °C. An aliquot of 34 µL from the supernatant fraction was added to 986 µL of the same buffer with the addition of 0.167 mg/mL O-dianisidine dihydrochloride and 0.0005% H_2O_2. Absorbance was measured at 460 nm and the results were expressed as units per milligrams of wet tissue weight where one unit (U) of MPO is defined as the amount of enzyme able to degrade 1 µmol/min of H_2O_2 at 25 °C.

HISTOLOGY

Full-thickness small intestine samples were placed in histology cassette, fixed with 4% formaldehyde and 0.05 M acetate buffer for 24 – 48 hours and embedded in paraffin. Sections of 3 µm were stained with hematoxylin-eosin (HE) to perform a morphological evaluation. Additional sections were mounted on poly-L-lysine coated slides and analyzed through immunohistochemistry using the avidin-biotin-peroxidase method and a polyclonal antibody anti-MPO (760-2659, Ventana Medical System, Tucson, AZ). Endogenous peroxidase activity was blocked incubating sections for 10 minutes in 3% H_2O_2 solution. Sections were then incubated with primary antibody overnight at 4 °C; specific biotinylated secondary antibody and avidin-biotin-peroxidase complexes were added each for 1 hour at room temperature. The immunohistochemical reaction was developed using diaminobenzidine-hydrogen peroxide reaction and the section were counterstained with hematoxylin. Neutrophil infiltration was measured counting MPO^+ cells in four high-

power fields (x400, 0.55 mm diameter) for each mucosal, sub-mucosal, muscular, serosal and sub-serosal layer. MPO levels were expressed as the amount of MPO^+ cells for field in each layer.

REAL-TIME QUANTITATIVE RT-PCR

Total RNA extracted from LMMPs was processed with TRIzol (Invitrogen) and DNase I (DNase free, Ambion) to remove DNA's traces. cDNA was obtained retrotranscribing 2 µg of total RNA using High Capacity cDNA synthesis kit (Applied Biosystems, Life Technologies, Grand Island, NY) according the manufacturer protocol. Real-Time PCR analyses were performed on ABI Prism 7000 apparatus with Power Sybr Green Universal PCR Master Mix (Applied Biosystems) and primers were designed using Primer Express software (Applied Biosystems) using deposited sequences in public databases (Table 1): each primer presented similar amplicon size and similar amplification efficiency as required for the $2^{\wedge-\Delta\Delta Ct}$ method used to compare gene expression [136]; each primer was used at a final concentration of 500 nM and β-actin was chosen as housekeeping gene to normalize gene expression in the $2^{\wedge-\Delta\Delta Ct}$ method. For each different preparation Real-Time PCR analyses were performed from four to eight times and the effect of drug tested on the different experimental groups was evaluated comparing $2^{\wedge-\Delta\Delta Ct}$ values.

GENE	FORWARD PRIMER	REVERSE PRIMER
β-ACTIN	5'-AGGCCCCTCTGAACC-3'	5'-GGGGTGTTGAAGGTC-3'
iNOS	5'-CACTTTGACGACTCA-3'	5'-AGCGAACAAATAGA-3'
nNOS	5'-ACAGTCATCAGACAC-3'	5'-GGGCAGCAACGGAT-3'
OTX1	5'-GCGAGGAGGTGGCTCTCA-3'	5'-GGCTCGGCGGTTCTTGA-3'
OTX2	5'-CCCAATTTGGGCCGACTT-3'	5'-GCGTAAGGCGGTTGCTTTAG-3'
VEGFα	5'-GCTGTGTGTGTGAGTGGCTTA-3'	5'-CCCATTGCTCTGTACCTTGG-3'
HIF-1α	5'-AAGCACTAGACAAAGCTCACCTG-3'	5'-TTGACCATATCGCTGTCCAC-3'

Table 1: **Sets of primers used for Real-Time PCR analyses on LMMPs sections.**

WHOLE MOUNTS IMMUNOHISTOCHEMISTRY

Segments of the rat's small intestine were fixed for 4 hours at room temperature in 0.2 M PBS (0.14 M NaCl, 0.003 KCl, 0.015 M Na_2HPO_4, pH 7.4, 4% formaldehyde, 0.2% picric acid). After the removal of the fixative solution, preparations were stored at 4 °C in PBS added of 0.05% thimerosal. Whole mounts experiments on LMMP samples were performed as described by Giaroni et al in 2011 [137]. Samples were incubated with blocking solution composed of 1% Triton X-100 and 10% normal horse serum (NHS, Euroclone; Celbio, Milan, Italy) in PBS for 1 hour at room temperature. Optimal diluted primary antibodies were then added (Table 2, section A). Double-labeling was performed incubating section with the primary antibody overnight at 4 °C followed by incubation with the secondary antibody for 2 hours at room temperature; whole mounts were

then incubated with the second primary antibody overnight at 4 °C and with the appropriate secondary antibody for 2 hours at room temperature. DAPI (Vectashield; Vector Laboratories, Burlingame, CA) was used to counterstain nuclei and mount glass slides. OTX, iNOS and nNOS expression in myenteric neurons was determined counting firstly the number of neurons positive for the pan-neuronal marker HUC/D (HUC/D$^+$) in a ganglion and secondly the number of neurons positive for the second antibody labeled with a different fluorophore. The cohort size consisted of 10 – 15 ganglia and data were obtained from preparations derived from at least 3 animals for each experimental group. Morphological changes in nNOS$^+$ neurons were determined measuring the total area of the neuronal profile as described by Rivera et al in 2009 [101]. The cohort size was 20 neurons and data were collected from the whole mounts obtained from at least 3 animals for each experimental group. Negative controls consisted of preparations lacking the primary or secondary antibody or incubating the sections with a non-immune serum and no signal was obtained in these preparations. Leica TCS SP5 confocal microscopy and confocal laser scanning system (Leica Microsystems, Wetzlar, germany) was used to analyze the sections processing pictures using Adobe-Photoshop CS2.0 software.

WESTERN BLOT

Protein level analyses of OTX1, OTX2, iNOS and nNOS was performed on LMMPs sections as described in Giaroni et al 2009 [138]. Purified membrane fractions and supernatants were diluted with Laemmli sample buffer, boiled for 2 minutes and electrophoresed through SDS-PAGE and transferred to nitrocellulose membranes. Membranes were incubated with optimally diluted primary and secondary horseradish peroxidase-conjugated (HRP) antibodies (Table 2, section B). OTX1, OTX2 and iNOS were evaluated in the supernatant while nNOS protein levels were determined in the membrane fraction. Moreover, to confirm the specificity of each antibody iNOS and nNOS were also evaluated respectively in RAW 264.7 macrophages cells and rat hippocampus while OTX1 and OTX2 in the Müller cell line MIO-M1 [139] and in the rat hippocampus [140] (data not shown). Omission of the primary antibody was also carried out as a control of specificity. Immunoblots were developed using an enhanced chemiluminescence technique (ECL advance Amersham Pharmacia Biotech, Cologno Monzese, Italy) and signal intensity was analysed through ImageJ National Institutes of Health Software (downloadable at http://imagej.nih.gov/). β-actin was used as protein loading control. For each preparation experiments were performed from four to seven times and the effects of I/R on protein levels were determined comparing the percentage variation to values obtained from control un-operated animals.

SECTION A: IMMUNOHISTOCHEMISTRY			
PRIMARY ANTIBODY	**DILUTION (HC)**	**HOST SPECIES**	**SOURCE**
iNOS	1:50	RABBIT	Santa Cruz Biotechnology
iNOS	1:50	MOUSE	AbCam
nNOS	1:200	SHEEP	Millipore
nNOS	1:50	RABBIT	Santa Cruz Biotechnology
OTX1/2	1:100	GOAT	Santa Cruz Biotechnology
OTX1	1:50	RABBIT	Santa Cruz Biotechnology
OTX2	1:50	GOAT	Santa Cruz Biotechnology
HUC/D	1:100	MOUSE	Molecular Probes
S-100	1:200	RABBIT	Dako
SECONDARY ANTIBODY	**DILUTION (HC)**	**HOST SPECIES**	**SOURCE**
Anti-rabbit Alexa Fluor 488	1:200	DONKEY	Molecular Probes
Anti-goat Cy3	1:500	DONKEY	Jackson ImmunoResearch
Cy3-conjugated streptavidin	1:500		Amersham
FITC-conjugated streptavidin	1:200		Molecular Probes
F(ab')2 anti-mouse IgG (H+L) biotin	1:300	GOAT	Caltag Laboratories
F(ab')2 anti-rabbit IgG (H+L) biotin	1:300	GOAT	Caltag Laboratories
SECTION B: WESTERN BLOT			
PRIMARY ANTIBODY	**DILUTION (WB)**	**HOST SPECIES**	**SOURCE**
iNOS	1:300	RABBIT	Santa Cruz Biotechnology
nNOS	1:200	RABBIT	Santa Cruz Biotechnology
OTX1	1:200	RABBIT	Santa Cruz Biotechnology
OTX2	1:200	GOAT	Santa Cruz Biotechnology
β-ACTIN	1:1000	MOUSE	Cell Signal Technology
SECONDARY ANTIBODY	**DILUTION (WB)**	**HOST SPECIES**	**SOURCE**
Anti-rabbit IgG HRP-conjugated	1:10.000	GOAT	Santa Cruz Biotechnology
Anti-goat IgG HRP-conjugated	1:7500	DONKEY	Santa Cruz Biotechnology
Anti-mouse IgG HRP-conjugated	1:1000		Cell Signal Technology

Table 2: **Primary and secondary antibodies and their relative dilutions used for immunohistochemistry and Western blot experiments.**

CELL CULTURES

Human neuroblastoma SK-N-BE(2) cell line was obtained from the Department of Experimental Medicine and Surgery of the University of Tor Vergata (Rome, Italy) and cultured in RPMI-1640 medium supplemented with 10% FBS (Euroclone S.P.A), 1% L-Glutamine (Euroclone S.P.A) and 1% Penicillin/Streptomycin (Euroclone S.P.A) in S@afeGrow 188 CO_2 incubator (Euroclone S.P.A) at 37 °C.

DIFFERENTIATION OF SK-N-BE(2) CELL LINE

Retinoic acid (ATRA) is reported to induce differentiation from neuroblastoma cell type to neuron-like phenotype. SK-N-BE(2) cells were seeded in T25 flasks at a density of 150.000 cells in 4 mL of RPMI-1640 medium supplemented with 1% FBS, 1% L-Glutamine and 1% Penicillin/Streptomycin for 24 hours to synchronize cell cycle. After medium replacement, cells were treated with ATRA at the final concentration of 10 µM for 12 days in RPMI-1640 medium supplemented with 5% FBS, 1% L-Glutamine and 1% Penicillin/Streptomycin. Control cells were exposed to DMSO, the vehicle used to dissolve ATRA. Fresh

medium and ATRA was added every three days. After 12 days cells were collected and every sample was divided for RNA and protein extraction (Figure 17).

OXYGEN AND GLUCOSE DEPRIVATION PROCEDURE

SK-N-BE(2) cells treated with ATRA were subjected to ischemia/reperfusion *in vitro* through the inhibition of the respiratory chain performed with Oxygen and Glucose Deprivation (OGD) procedure. Briefly, cells were exposed to NaN_3 at the final concentration of 10 mM added in DMEM no glucose (Thermo Fisher Scientific) supplemented with 5% FBS, 1% L-Glutamine and 1% Penicillin/Streptomycin for 5 minutes at 37 °C. The medium used for the OGD procedure was then replaced by the medium used for the normal culture and cells were maintained in this condition for 24 hours (Figure 17). Cells have been collected and the samples divided to perform RNA and protein extraction.

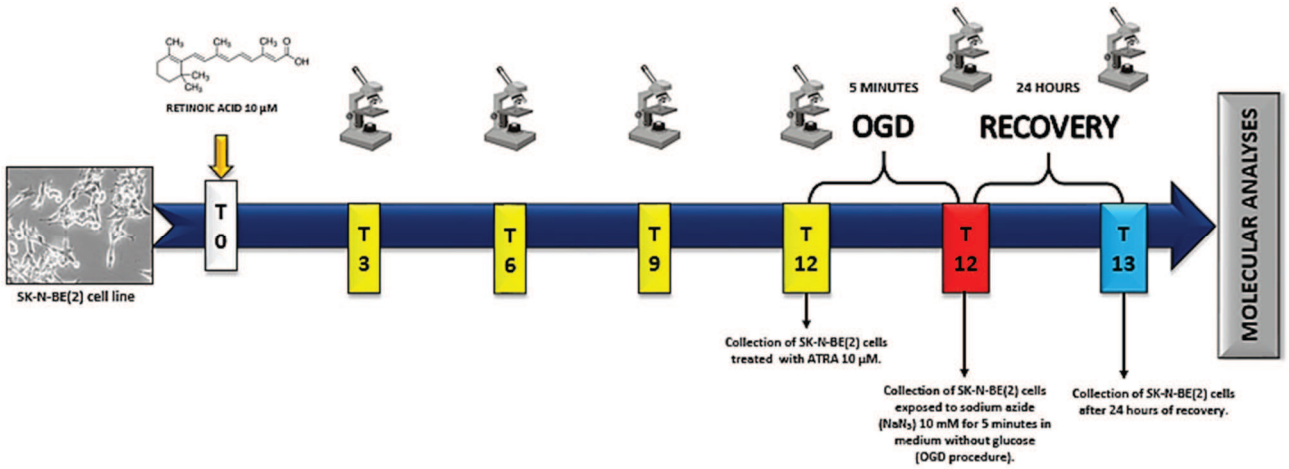

Figure 17: **Flow-chart of the treatment performed on SK-N-BE(2) cell line.** SK-N-BE(2) cell line was seeded in 1% FBS medium for 24 hours to induce quiescence. After 24 hours retinoic acid (ATRA) was added at the final concentration of 10 µM and medium was changed every 3 days; contrast-phase images of the cells were acquired through Olympus IX51S8F-3 microscope (Olympus Corporation, Tokyo, Japan) during the course of the treatment. At the end of the treatment (T12) cells were collected for Real Time PCR and Western Blot experiments. Cells treated with ATRA were subjected to the OGD procedure consisting of the addition of sodium azide (NaN_3) at the final concentration of 10 mM in medium without glucose for 5 minutes. After the OGD procedure SK-N-BE(2) cells were collected for Real Time PCR and Western blot experiments. Cells exposed to sodium azide underwent to a recovery phase of 24 hours in standard medium and, after the recovery, samples were collected for Real Time PCR and Western blot experiments.

REAL-TIME QUANTITATIVE RT-PCR

Total RNA was extracted with Eurogold Total RNA Kit (Euroclone S.P.A) according to the manufacturer protocol and 1 µg of total RNA was retrotranscribed using High Capacity cDNA kit (Applied Biosystems, Foster City, CA, USA) according to the protocol. Real Time PCR assays were performed on the ABI Prism 7000 apparatus (Applied Biosystems, Carsbad, California, USA). All the PCR reactions were carried out in triplicate and every mix contained 12.5 µL of iTaq Universal Sybr® Green Supermix (Bio-Rad Laboratories S.R.L), X µL

of primers at a specific concentration (Table 3), 30 ng of cDNA for each well and X µL of nuclease-free water. Every couple of primer used for Real Time PCR assays was previously designed and validated with Primer Blast (http://www.ncbi.nlm.nih.gov/tools/primer-blast/) and OlygoAnalyzer 3.1 software (https://eu.idtdna.com/calc/analyzer). Human Glyceraldehyde 3-phosphate dehydrogenase (GAPDH) was used as housekeeping gene to normalize gene expression levels in the relative quantitative analysis using the $2^{-\Delta\Delta Ct}$ method.

GENE	FORWARD PRIMER	REVERSE PRIMER
GAPDH	5'-AGAGACCCTCACTGCTGGGGAG-3'	5'-CCTAGGCCCCTCCCCTCTTCAA-3'
OTX1	5'-TTGTTGAAATGTAAGGCAGTCC-3'	5'-TTTGCATTTATTTTCGGGAAG-3'
OTX2	5'-GGTACCCAGACATCTTCATGC-3'	5'-ACTTAGCTCTTCGATTCTTAAACCA-3'
TP53	5'-TCTTCTGTCCCTTCCCAGAA-3'	5'-AGAATGCAAGAAGCCCAGAC-3'
TAp73	5'-AACCAGACAGCACCTACTTCG-3'	5'-CGCCCACCACCTCATTATT-3'
NeuN	5'-TTCTATGCAGTGACGGGGTT-3'	5'-TCCATCCTGATACACGACCG-3'
MAP2	5'-GGTGAAGGCCAAGACTCTCT-3'	5'-AGTGTGTTGGAACCTCGGAA-3'
PSD95	5'-TCGCCCCATCATCATCCTTG-3'	5'-CGTGTCGTATGGGGAACACA-3'
SOX2	5'-GGGGGAATGGACCTTGTATAG- 3'	5'-GCAAAGCTCCTACCGTACCA-3'

Table 3: **Set of primers used for Real Time PCR assays on SK-N-BE(2) cell line.** Every couple was designed and validated using Primer Blast and OlygoAnalyzer 3.1 softwares. The length of the product amplified varied from 70 to 120 base pairs (bp).

SDS-PAGE AND WESTERN BLOT

OTX1 protein level analysis was carried out from total protein lysates. 200 µg of total proteins were denatured using 5X Laemmli buffer (Tris-HCl 0.5 M pH 6.8, 5% SDS, Glycerol, 0.25% Bromophenol Blue) supplemented with 20% of 2-mercaptoethanol (Sigma-Aldrich S.R.L); every sample was boiled for 10 minutes at 100 °C, separated by SDS-PAGE and transferred to nitrocellulose membranes (Amersham™ Protran™ Premium 0.45µm NC, GE Healthcare Life Sciences). To check the success of the transfer, membranes were incubated with Ponceau S solution (Euroclone S.P.A) for 5 minutes at R.T while gels were stained with Bio-Safe™ Coomassie G-250 (Bio-Rad Laboratories S.R.L). Membranes were probed with the specific primary antibody rabbit anti-OTX1 (Santa Cruz Biotechnology) diluted 1:300 overnight at 4 °C. After 3 washes in Tris-buffered saline added of 0.1% Tween-20 (Euroclone S.P.A), membranes were incubated goat anti-rabbit IgG HRP-conjugated secondary antibody (Santa Cruz Biotechnology) diluted 1:3500 for 90 minutes at real temperature. Every antibody was previously tested to confirm its specificity and to identify the appropriate concentration.

Immunocomplexes were detected by enhanced chemiluminescence using Clarity Max™ Western ECL Substrate (Bio-Rad Laboratories S.R.L) according to the manufacturer instructions. Signal intensity was quantified by densitometric analysis using ImageJ National Institutes of Health image software

(downloadable at http://imagej.nih.gov/). In each membrane β-actin was monitored and used as protein loading control.

IMMUNOFLUORESCENCE ASSAYS

Immunofluorescence assays were performed on SK-N-BE(2) cells seeded in a 12 multiwell plate in triplicate at a density of 20.000 cells on coverslips coated with Poly-D-Lysine. Cells treated with retinoic acid were fixed using 4% paraformaldehyde in PBS pH 7.4 for 10 min at room temperature. Permeabilization was achieved using sterile PBS added of 0.1% Tryton X-100 (Thermo Scientific) and 10% FBS (Euroclone S.P.A) for 30 minutes at R.T. Cells were then incubated with the specific primary antibody mouse anti-S100 (CST Technology) diluted 1:400 in permeabilization buffer overnight at 4 °C in a humified chamber. After 3 washes in PBS, cells were incubated with F(ab')2 anti-mouse IgG(H+L) Alexa Fluor 488 (CST Technology) fluorescent secondary antibody for 90 minutes at R.T in a humified. Coverslips were mounted using DAPI (Vectashield; Vector Laboratories, Burlingame, CA, USA) and images were acquired through Leica TCS SP5 confocal microscopy and confocal laser scanning system (Leica Microsystems, Wetzlar, Germany).

STATISTICAL ANALYSES

Statistical analyses were performed with Graph Pad 5.3 software (PRISM, San Diego, CA, USA). Data were analysed by ONE-way ANOVA followed, when significant, by Tuckey's multiple comparisons post hoc test. Differences were considered significant when $p \leq 0.05$

RESULTS

HISTOLOGICAL OBSERVATIONS

The intestinal segment involved in SMA occlusion varied in colour changing from pink to purple; during reperfusion, the restoration of blood flow resulted in a further colour change and tissue returned to pink. Animals recovered easily from anaesthesia and didn't show signs of distress, eating normally and being active. A macroscopic evaluation of the regions engaged by I/R didn't reveal any abnormality with respect to sham-operated and control animals. From the microscopic point of view, intestinal sections showed cellular distress both in muscular and neuronal cells. In the myenteric and sub-mucosal plexuses at 24 and 48 hours after reperfusion many neurons were swollen and showed cytoplasmic vacuolisations in addition to an unclearly defined cellular membrane with respect to control animals (Figure 18 A – B). Nuclear inclusions were sometimes present but cytoplasmic vacuolisations and spaces between muscular cells were the main histologically-defined degenerative changes in certain areas of the lamina propria mucosae. No evident changes have been observed in mucosal and serosal epithelia and cellular distress was rarely identified in neurons or muscle cells of sham-operated animals.

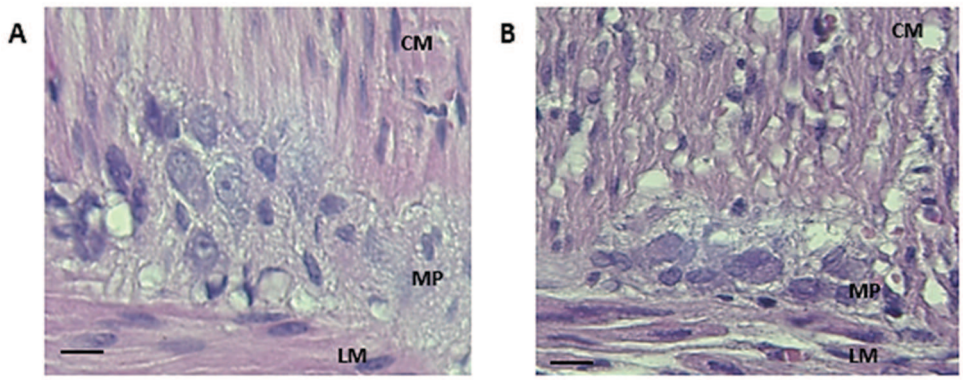

Figure 18: **Histological analysis of rat's intestine.** (A) Muscular cells in circular (CM) and longitudinal (LM) layers and myenteric plexus (MP) in the small intestine of control animals (HE; original magnification X600, bar 0.01 mm); (B) Muscular cells in the CM, LM and MP of rats after 60 minutes of ischemia and 24 hours of reperfusion. Neurons show signs of cellular distress with an irregular and unclearly-defined membrane while cytoplasmic vacuolisations and spaces between muscular cells are present in muscle tissue (HE, original magnification X600, bar 0.01 mm).

NEUTROPHIL INFILTRATION AND MYELOPEROXIDASE (MPO) ACTIVITY

MPO activity was measured to evaluate the number of infiltrated neutrophils in three different compartments: mucosa, sub-mucosa and lamina muscularis propria (Figure 19 A – D). No significant variation was visible in mucosa (Figure 19A) for the number of MPO^+ cells per field after both I/R and sham-operation with respect to control animals. In the sub-mucosal layer (Figure 19B), a significant increase in the number of infiltrated neutrophils was observed at 24 hours of reperfusion ($P < 0.05$) and in the relative 24 and 48 hours sham-operated ($P < 0.01$ and $P < 0.05$ respectively). In the muscularis propria lamina (Figure 19C), a significant increase in MPO^+ cells ($P < 0.01$) was detected after 24 hours of reperfusion.

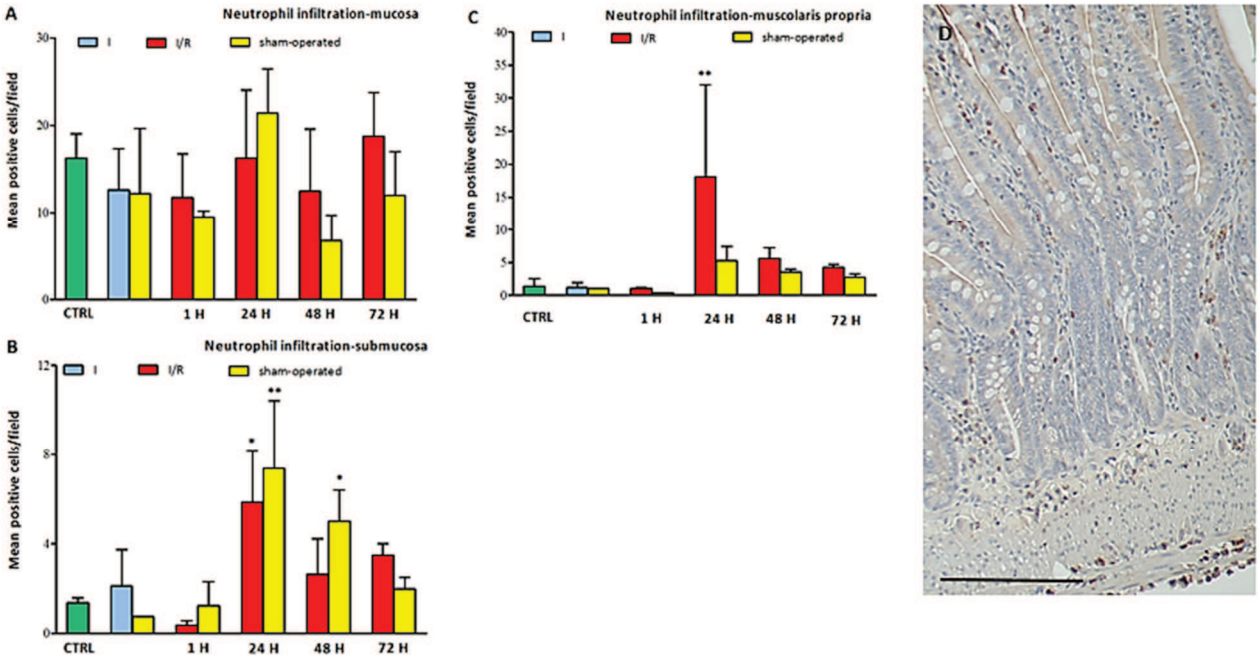

Figure 19: **Evaluation of neutrophil infiltrate in the intestinal wall after I/R damage.** Neutrophil infiltration is expressed as the number of neutrophils in the intestinal mucosa (A), sub-mucosa (B) and muscularis propria (C) of normal control animals (green bars) after 60 minutes of *in vivo* ischemia (light-blue bars), at different time-points after the induction of *in vivo* I/R (red bars) and in animals subjected to sham-operation (yellow bars). Values are expressed as mean ± SD of the neutrophils counted in 4 – 5 experiments. Statistical analysis was performed with one-way ANOVA followed by Tuckey's post-hoc test. *$P < 0.05$, ** $P < 0.01$ vs control animals. (D) MPO staining of the whole intestinal wall obtained after 60 minutes of in vivo ischemia followed by 24 hours of reperfusion: neutrophils are marked in brown and are visible in all the layers hence simplifying their count.

MPO activity significantly increased in mucosa-deprived rat small intestine segment after 60 minutes and 24-48 hours of reperfusion ($P < 0.05$ and $P < 0.01$) when compared to control animals (Figure 20A). The same increase was also observed in sham-operated animals in which MPO activity significantly increased ($P < 0.05$) after 24 and 48 hours of reperfusion respectively. After 72 hours of reperfusion MPO values returned to control levels in both I/R and sham-operated animals (Figure 20A).

NPLA and 1400W administration did not alter MPO activity in control animals. In animals subjected to 60 minutes of ischemia followed by 24 and 48 hours of reperfusion both drugs caused a significant reduction ($P< 0.001$ and $P < 0.01$ respectively) of the I/R-induced MPO activity. In sham-operated animals the treatment with NPLA and 1400W resulted in a significant reduction ($P < 0.05$) of the laparotomy-induced MPO activity at both 24 and 48 hours after the surgery (Figure 20B)

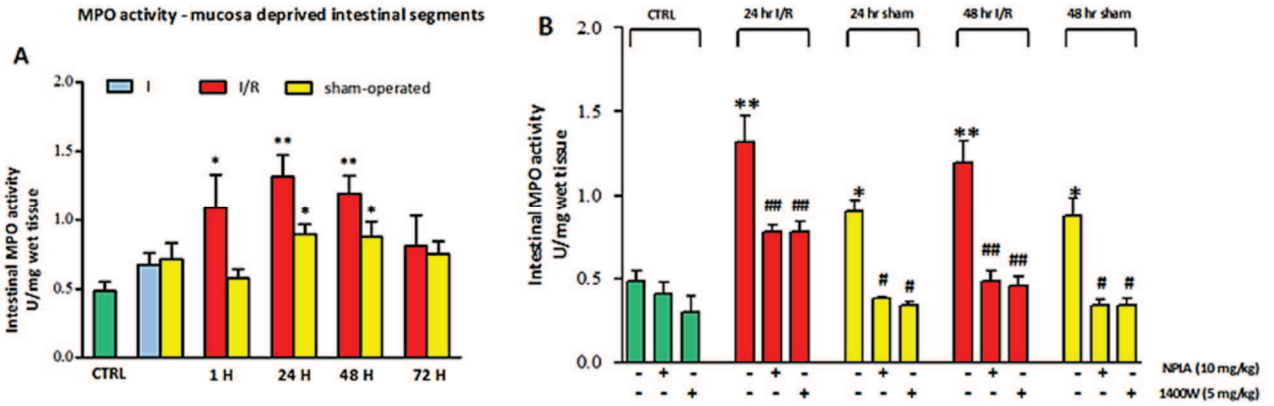

Figure 20**: MPO activity in samples of mucosa-deprived intestinal samples and the effects of NPLA and 1400W NOS inhibitors.** (A) MPO activity in control animals (green bar), after 60 minutes of ischemia (light-blue bar), at different time-points of reperfusion (red bars) and in sham-operated animals (yellow bars). (B) Effects of NPLA and 1400W (specified below the graph) on MPO activity in control animal (green bars), after 60 minutes of ischemia followed by 24 and 48 hours of reperfusion (red bars) and the respective sham-operated animals (yellow bars). Values are expressed as mean ± SE of MPO activity measured in 4 – 9 experiments and statistical analysis is performed through one-way ANOVA followed by Tuckey's post-hoc test; *$P < 0.05$, **$P < 0.01$ respect to values obtained in controls, #$P < 0.05$, ##$P < 0.01$ respect to values in the respective I/R or sham-operated animals.

EVALUATION OF GASTROINTESTINAL TRANSIT

In vivo ischemia caused a significant reduction of the upper GI transit that decreased 60 minutes after ischemia ($P < 0.05$) and returned to control levels 60 minutes after reperfusion (Figure 21A). At 24 hours and much more at 48 hours a significant delay of transit was observed ($P < 0.01$) while little but not statistically significant difference between control and I/R animals was highlighted at 72 hours of reperfusion. The same situation was observed in sham-operated animals where the transit was reduced with respect to controls but not significantly.

NPLA administration determined a significant decrease of transit in controls, in 48 hours reperfused animals ($P < 0.001$) and in 48 hours sham-operated group ($P < 0.05$) (Figure 21B).

The treatment with 1400W didn't modify gastrointestinal transit in controls and 48 hours sham-operated group and the reduction of transit observed at 48 hours of reperfusion was completely restored after the administration of iNOS inhibitor.

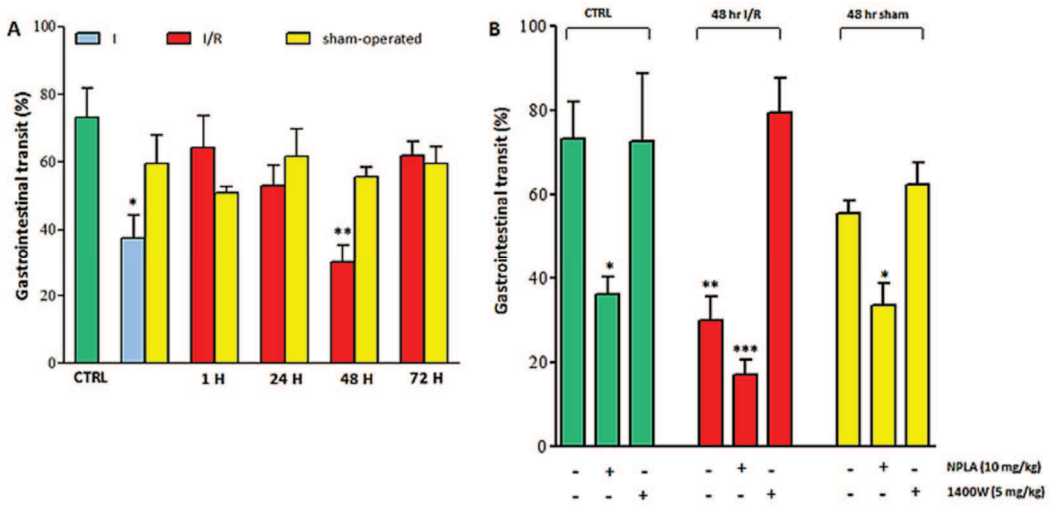

Figure 21: **Evaluation of intestinal transit during I/R and effects of the treatment with NPLA and 1400W.** (A) GI transit in control animals (green bar), after 60 minutes of ischemia (light-blue bar), at different time-points after the induction of I/R (red bars) and the respective sham-operated animals (yellow bars); (B) Effects of the treatment with iNOS and nNOS inhibitors (1400W and NPLA respectively, treatment specification below the graph) on GI transit in controls (green bars), after 60 minutes of ischemia followed by 48 hours of reperfusion (red bars) and in the relative sham-operated group of animals (yellow bars). Values are expressed as mean ± SE of 4 – 8 experiments analysed through one-way ANOVA followed by Tuckey's post-hoc test (*P < 0.05, **P < 0.01 and ***P < 0.001).

REAL TIME PCR ANALYSES ON LMMPs SAMPLES

Hypoxia-inducible factor alpha (HIF-1α) and vascular endothelial growth factor (VEGFα) were assessed in LMMPs samples obtained from animals subjected to 60 minutes of *in vivo* ischemia followed by 24 and 48 hours of reperfusion and in the related sham-operated groups (Figure 22 A – B).

mRNA levels of HIF-1α were significantly upregulated after 24 hours of reperfusion and in the relative sham-operated animals (P < 0.001 and P < 0.05 respectively) with respect to control animals. After 48 hours of reperfusion HIF-1α levels returned to control values in both the I/R and sham-operated groups.

VEGFα mRNA levels were significantly upregulated (P < 0.001) at 24 hours of reperfusion following ischemia but not in the sham-operated animals; after 48 hours of reperfusion and in the relative sham-operated group VEGFα expression levels were similar to controls.

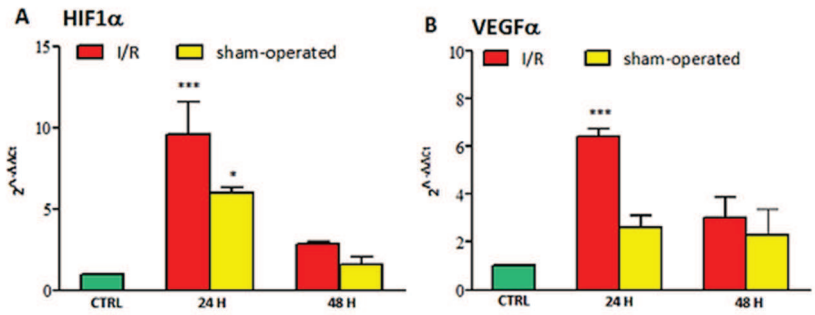

Figure 22: **qRT-PCR analyses of the gene expression levels of hypoxia-inducible factor alpha (HIF-1α) and vascular endothelial growth factor (VEGFα) in LMMPs samples.** (A) mRNA levels of HIF-1α in controls (green bar), at 24 and 48 hours of reperfusion following in vivo ischemia (red bars) and in the relative sham-operated groups (yellow bars); (B) mRNA levels of VEGFα in controls (green bar), at 24 and 48 hours of reperfusion following in vivo ischemia (red bars) and in the relative sham-operated groups (yellow bars). Values obtained from 4 – 5 experiments represent the variation in gene expression levels with respect to control animals and are expressed as mean ± SE. *P < 0.05, ***P < 0.001 through one-way ANOVA followed my Tuckey's multiple comparison test. β-actin was used as housekeeping gene to normalize the expression levels of the target genes.

iNOS and nNOS gene expression levels were measured in LMMPs samples and are shown in figure 23 A – B. Real-Time PCR analyses showed that at 24 and 48 hours of reperfusion and in sham-operated group, nNOS mRNA levels (Figure 23A) were not influenced in comparison with control animals; notably, the administration of NPLA and 1400W didn't alter its expression levels in all the experimental groups.

On the other hand, iNOS mRNA levels (Figure 23B) were significantly upregulated at 24 and 48 hours of reperfusion with respect to control (P < 0.001) and sham-operated animals (P < 0.001 and P < 0.05). The increase of iNOS gene expression levels was found also in sham-operated groups but it was not statistically significant. The administration of NPLA and 1400W in sham-operated animals didn't influence gene expression levels; instead, the treatment with 1400W caused a non-significant reduction of the I/R-induced enhancement of mRNA levels for iNOS while NPLA didn't show any effect both at 24 and 48 hours of reperfusion.

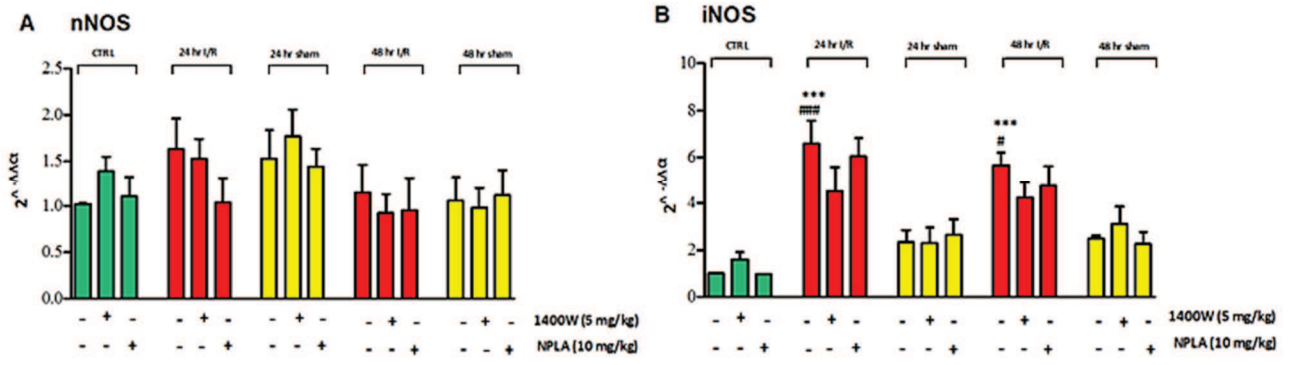

Figure 23: **qRT-PCR analyses of nNOS and iNOS mRNA levels in LMMPs samples.** (A) nNOS mRNA levels in controls (green bars), at 24 and 48 hours of reperfusion following in vivo ischemia (red bars) and in the relative sham-operated groups (yellow bars); (B) mRNA levels of iNOS in controls (green bar), at 24 and 48 hours of reperfusion following in vivo ischemia (red bars) and in the relative sham-operated groups (yellow bars). Treatment details are reported below the graphs. Values obtained from 4 – 8 experiments represent the variation in gene expression levels with respect to control animals and are expressed as mean ± SE. ***P < 0.001 vs control animals, #P < 0.05 and ###P < 0.001 vs relative sham-operated groups through one-way ANOVA followed my Tuckey's multiple comparison test. β-actin was used as housekeeping gene to normalize the expression levels of the target genes.

In LMMPs samples, qRT-PCR analyses revealed a significative upregulation of OTX1 gene expression levels (P < 0.001) both at 24 and 48 hours of reperfusion after in vivo ischemia while in sham-operated animals its levels were upregulated but not significantly with respect to control animals.

Both in control and sham-operated group, the treatment with NPLA or 1400W didn't change OTX1 gene expression levels; on the contrary, NPLA and 1400W caused a downregulation of the transcript at both 24 and 48 hours of reperfusion ($P < 0.05$ and $P < 0.001$ for NPLA, $P < 0.01$ and $P < 0.001$ for 1400W) (Figure 24A).

mRNA levels for OTX2 gene significantly increased at 24 ($P < 0.001$) and returned to control levels at 48 hours of reperfusion. In sham-operated group of animals OTX2 gene was significantly upregulated 24 hours after the surgery ($P < 0.05$) but they were unchanged from control levels at 48 hours (Figure 24B)

The treatment with NOS inhibitors caused a significative downregulation of OTX2 levels at 24 hours of reperfusion ($P < 0.001$) but not in the other experimental conditions studied (Figure 24B)

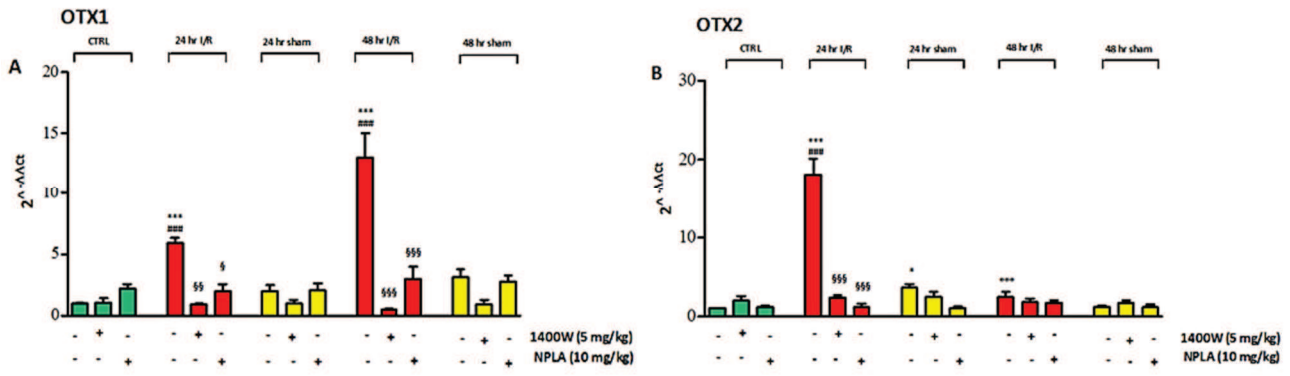

Figure 24: **qRT-PCR analyses of OTX1 and OTX2 mRNA levels in LMMPs samples.** (A) OTX1 mRNA levels in controls (green bars), at 24 and 48 hours of reperfusion following in vivo ischemia (red bars) and in the relative sham-operated groups (yellow bars); (B) mRNA levels of OTX2 in controls (green bar), at 24 and 48 hours of reperfusion following in vivo ischemia (red bars) and in the relative sham-operated groups (yellow bars). Treatment details are reported below the graphs. Values obtained from 4 – 8 experiments represent the variation in gene expression levels with respect to control animals and are expressed as mean ± SE. ***P < 0.001 vs control animals, °°°P < 0.001 vs 24 hours of I/R group of animals, ###P < 0.001 vs relative sham-operated groups, §§P < 0.01 and §§§P < 0.001 vs relative I/R or sham-operated group through one-way ANOVA followed my Tuckey's multiple comparison test. β-actin was used as housekeeping gene to normalize the expression levels of the target genes.

WESTERN BLOT ANALYSES ON LMMPs SAMPLES

iNOS and nNOS protein levels were measured in LMMPs preparations and results of Western blot analyses are shown in figure 25 A – B. nNOS specific antibody reveals one band at 155 kDa (Figure 25A): during I/R and sham-operation, nNOS protein levels were not different with respect to control animals and NOS inhibitors didn't change nNOS protein levels in any experimental group studied.

iNOS specific antibody identifies a band at 125 kDa (Figure 25B): at 24 hours of reperfusion iNOS protein levels were significantly upregulated ($P < 0.01$) with respect to controls and the upregulation further increased at 48 hours of reperfusion. In this condition iNOS protein levels were also significantly higher than the observed levels in sham-operated animals ($P < 0.001$). iNOS levels in sham-operated groups were not different with respect to controls.

NPLA administration didn't alter iNOS levels in all the experimental groups while 1400W caused a significative reduction of I/R-induced enhancement of inducible nitric oxide synthase both at 24 and 48 hours of reperfusion ($P < 0.05$ and $P < 0.001$ respectively).

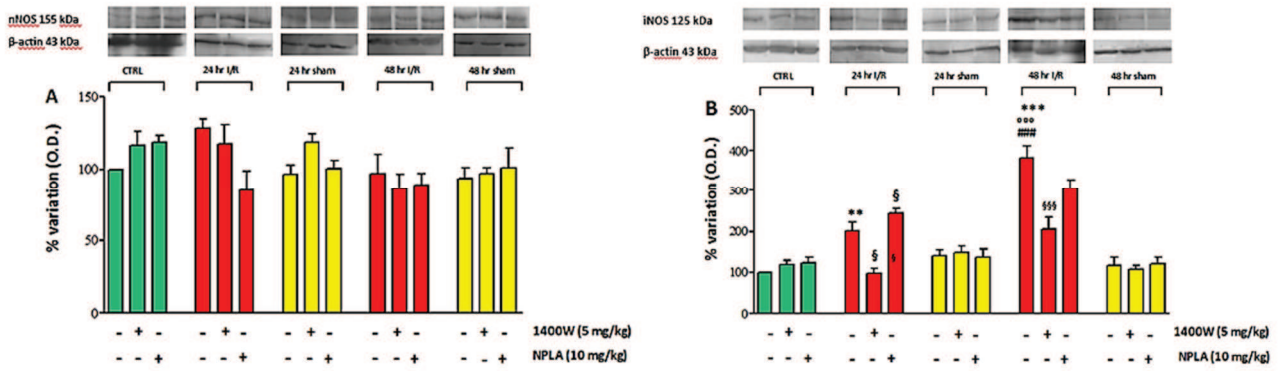

Figure 25: **Western blot analyses of iNOS and nNOS protein levels**. Protein expression levels for nNOS (A) and iNOS (B) were measured in the membrane and supernatant fractions of LMMPs respectively in controls (green bars), at 24 and 48 hours of reperfusion (red bars) and in the relative sham-operated animals (yellow bars). At the top of the graphs are reported the immunoblots of iNOS, nNOS and β-actin with their molecular weights in the different experimental conditions. 100 µg of samples were separated through SDS-page in 10% polyacrylamide gels and the details of treatments with NPLA and 1400W are reported below the graphs. Values are expressed as mean ± SE of 4 – 7 experiments of the percentage variation of the optical density (O. D.) with respect to values obtained in control animals. **P < 0.05 and ***P < 0.001 vs controls, °°°P < 0.001 vs 24 hours of reperfusion, ###P < 0.001 vs sham-operated animals, §P < 0.05 and §§§P < 0.001 vs the related I/R group by one-way ANOVA followed by Tuckey's post-hoc test.

Because OTX1 mRNA showed a significative increase at 48 hours of reperfusion, the analysis of its protein levels was performed in LMMPs samples at this time point and in the relative sham-operated group. OTX1 protein levels (Figure 26A), revealed as a single band by the specific antibody at 37 kDa, showed a significant increase at 48 hours of reperfusion ($P < 0.01$) and no variation was observed in sham-operated animals. The administration of NOS inhibitors determined no alterations of OTX1 protein both in controls and sham-operated group while 1400W and NPLA caused a significative downregulation of protein levels at 48 hours of reperfusion ($P < 0.001$ and $P < 0.05$ respectively).

OTX2 specific antibody revealed a single band at 32 kDa and because mRNA levels were increased at 24 hours of reperfusion, the analysis of protein levels were performed at this time-point and in the related sham-operated group (Figure 26B). OTX2 expression significantly increased at 24 hours of reperfusion ($P < 0.001$) while its levels were unchanged in sham-operated animals with respect to controls. The administration of NPLA caused a significant reduction of protein levels at 24 hours of reperfusion and in sham-operated animals ($P < 0.001$ and $P < 0.01$). 1400W didn't modify OTX2 protein levels in both control and sham-operated animals but significantly reduced OTX2 protein expression at 24 hours of reperfusion ($P < 0.05$).

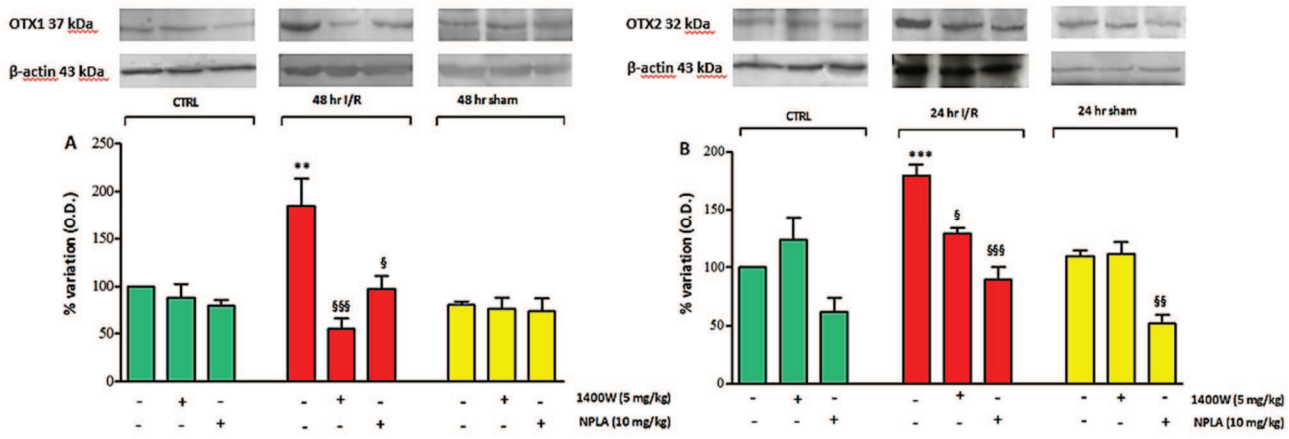

Figure 26: **Western blot analyses of OTX1 and OTX2 protein levels**. Protein expression levels for OTX1 (A) and OTX2 (B) were measured in supernatant fractions of LMMPs in controls (green bars), at 24 and 48 hours of reperfusion (red bars) and in the relative sham-operated animals (yellow bars). At the top of the graphs are reported the immunoblots of OTX1, OTX2 and β-actin with their molecular weights in the different experimental conditions. 100 µg of samples were separated through SDS-page in 10% polyacrylamide gels and the details of treatments with NPLA and 1400W are reported below the graphs. Values are expressed as mean ± SE of 4 – 7 experiments of the percentage variation of the optical density (O. D.) with respect to values obtained in control animals. **P < 0.05 and ***P < 0.001 vs controls, §P < 0.05, §§P < 0.01 and §§§P < 0.001 vs the related I/R group by one-way ANOVA followed by Tuckey's post-hoc test.

EVALUATION OF iNOS, nNOS, OTX1 AND OTX2 IN LMMPs WHOLE MOUNTS.

nNOS immunoreactivity was found mainly in the cytoplasm of the myenteric neurons in all the preparations obtained from the different experimental groups. nNOS^{+} neurons showed different morphologies: some neurons presented a large cells body and numerous dendrites while others were smaller with an ovoidal shape and no visible dendrites. Positive immunoreactivity for nNOS was also evidenced in neuronal fibers within the ganglions, along the interconnecting strands and in the secondary/tertiary fibre tracts as visible in Figure 27. nNOS^{+} neurons were 21.8 ± 2.8% (n = 4) in control animals and the number was not significantly different from the number obtained at 24 and 48 hours of reperfusion or in the related sham-operated group (Figure 30A). nNOS^{+} neurons at both time points (24 and 48 hours of reperfusion) showed a significative total cell area and ratio between the total area and the cell soma compared to controls and sham-operated animals (P < 0.001 and P < 0.05 respectively, Figure 31A-B); as index of the damage, significative nuclear eccentricity was also observed in nNOS^{+} myenteric neurons compared to control and sham-operated animals (P < 0.001 and P < 0.05 respectively) (Figure 31C). 24 and 48 hours of reperfusion didn't alter the parameters indicated above in controls and sham-operated animals in which no difference was found (Figure 31 A – C).

iNOS staining was found in myenteric neurons characterized by an ovoidal shape and no visible dendrites (Figure 27). In control animals the percentage of iNOS^{+} neurons was 5.2 ± 0.6% (n = 6) and percentage further significantly increased to 11.6 ± 1.3% (n = 5, P < 0.001) at 24 and 11.7 ± 0.8% (n = 6, P < 0.001) at 48 hours of reperfusion. In sham-operated animals the percentage of iNOS^{+} neurons was similar to controls (Figure 30B).

Moreover, the double staining with S100 showed immunoreactivity for iNOS also in the enteric glial cells both in the myenteric ganglions and muscular layer (Figure 27).

Pan-immunoreactivity for OTX (Pan-OTX$^+$) was observed in cytoplasm and nucleus of myenteric neurons and in the prolongations surrounding neuronal membranes. Some neurons presented a large cell body while others were smaller with an ovoidal shape and localized in the periphery of the ganglion (Figure 28). Pan-OTX$^+$ neurons in control animals were 5.7 ± 0.4% (n = 6) and the percentage significantly increased at 24 and 48 hours of reperfusion reaching 17.0 ± 1.6% (n = 6, $P < 0.001$) and 17.3 ± 0.8% (n = 6, $P < 0.001$) respectively (Figure 30C). In sham-operated animals, the percentage of pan-OTX$^+$ neurons was significantly higher than control animals at 24 (10.0 ± 1.4%, n = 4, $P < 0.05$) and 48 (11.0 ± 0.6%, n = 4, $P < 0.01$) hours after the surgery (Figure 30C). The double staining of OTX1 and OTX2 specific antibodies with S100 showed OTX1$^+$ neurons in the enteric glial network while no immunoreactivity was seen at this level for OTX2 (Figure 28); double staining of OTX1 and OTX2 specific antibodies with HUC/D displayed neuronal immunoreactivity for OTX2 (Figure 28) and few neurons were OTX1$^+$. Moreover, OTX1 immunoreactivity colocalized with iNOS labelling and no myenteric neurons were positive for the double staining OTX1-nNOS (Figure 29); conversely, OTX2$^+$ neurons were also immunoreactive for nNOS and no there was no evidence for the colocalization between OTX2 and iNOS (Figure 29).

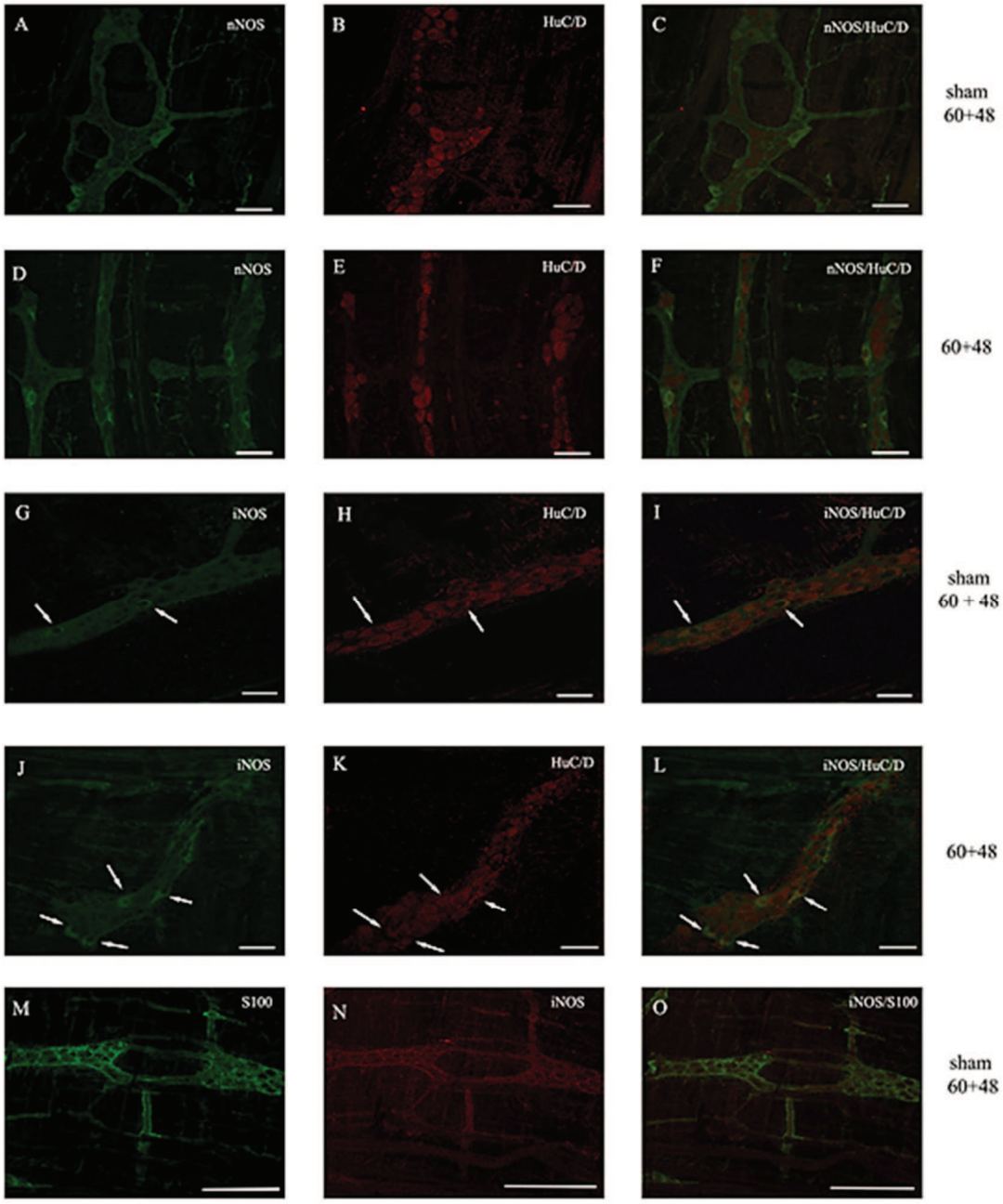

Figure 27: **Immunohistochemical localization of nNOS and iNOS in whole mounts of LMMP samples from animals subjected to 60 minutes of *in vivo* ischemia followed by 48 hours of reperfusion and in the relative sham-operated group.** (A – F) Colocalization of nNOS with the neuronal marker HUC/D; (G – L) Colocalization of iNOS with HUC/D; (M – O) Colocalization of iNOS with the glial marker S100. HUC/D neuronal markers stained the somata of myenteric neurons (B, E, H, K). Arrows indicate $iNOS^+$ and HUC/D^+ myenteric neurons (G – L). Bars = 50 µm.

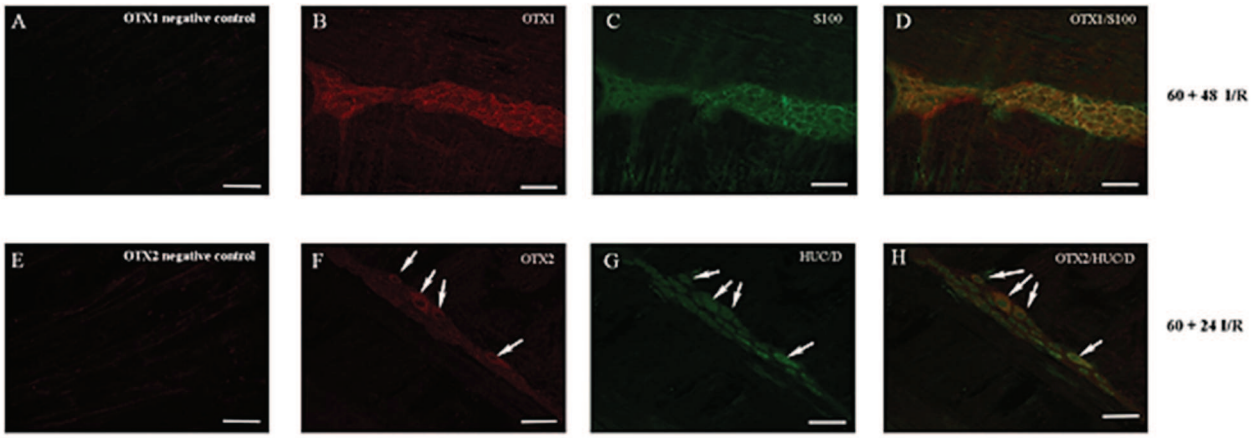

Figure 28: **Immunohistochemical localization of OTX1 and OTX2 in whole mounts of LMMP samples obtained after 60 minutes of *in vivo* ischemia and followed by 24 and 48 hours of reperfusion.** (A – D) Colocalization of OTX1 with the glial marker S100; (E – H) Colocalization of OTX2 with the neuronal marker HUC/D. OTX1 and OTX2 negative controls are represented by sections incubated with non-immune rabbit and goat serum respectively. Arrows indicate $OTX2^{+}$ and HUC/D^{+} myenteric neurons (F – H). Bars = 50 µm.

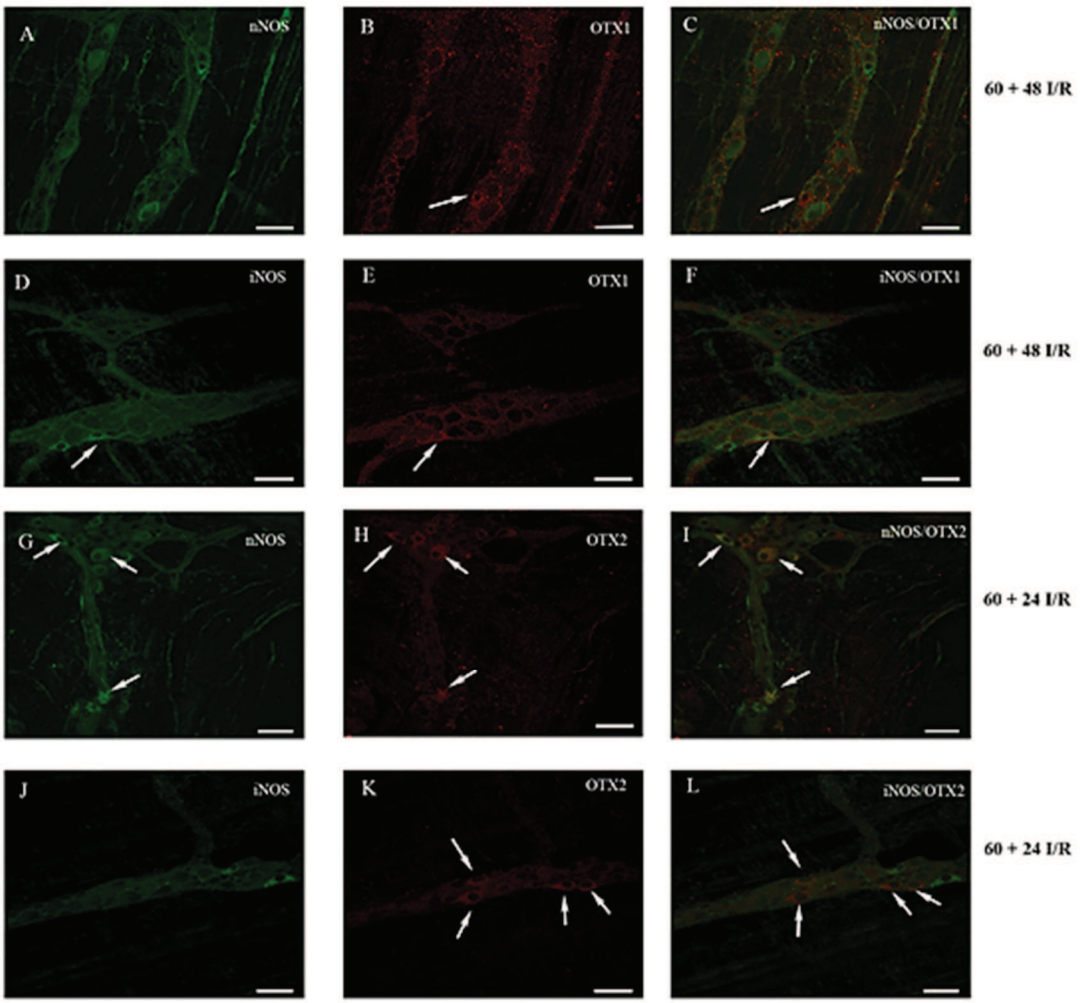

Figure 29: **Immunohistochemical colocalization of OTX1 and OTX2 with nNOS and iNOS in whole mounts of LMMP samples at 24 and 48 hours of reperfusion after 60 minutes of *in vivo* ischemia.** (A – F) Colocalization of OTX1 with nNOS and iNOS at 48 hours of reperfusion after 60 minutes of *in vivo* ischemia; (G – L) Colocalization of OTX2 with nNOS and iNOS at 24 hours of reperfusion after

60 minutes of *in vivo* ischemia. (B – C) OTX1$^+$ and nNOS$^-$ neurons; (D – F) OTX1$^+$ and iNOS$^+$ neurons; (G – I) OTX$^+$ and nNOS$^+$ neurons; (K – L) OTX2$^+$ and iNOS$^-$. Bars = 50 µm.

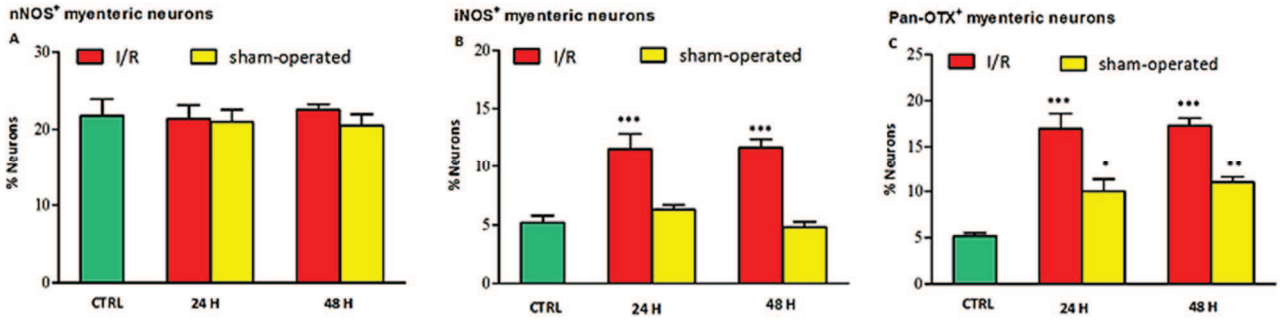

Figure 30: **Percentage of nNOS$^+$, iNOS$^+$ and pan-OTX$^+$ myenteric neurons in LMMP samples.** (A – C) Percentage of myenteric neurons per mm^2 staining for HUC/D and immunoreactive for nNOS (A, nNOS$^+$), iNOS (B, iNOS$^+$) and OTX (C, pan-OTX$^+$) in controls (green bars), at 24 and 48 hours of reperfusion (red bars) and in the related sham-operated animals (yellow bars). Values are expressed as mean ± SE of 4 experiments. *P < 0.05, **P < 0.01 and ***P < 0.001 through one-way ANOVA followed by Tuckey's post-hoc test.

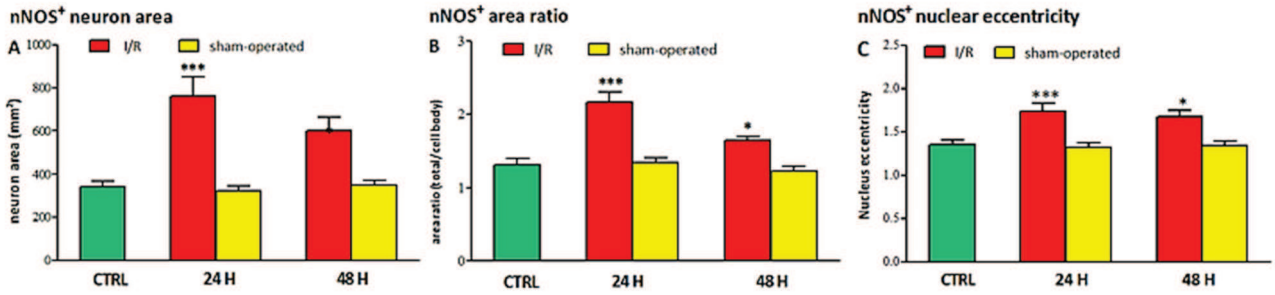

Figure 31: **Morphological analysis of nNOS$^+$ neurons in LMMP samples after *in vivo* I/R.** (A) nNOS cell profile area including dendrites, (B) ratios of total cell areas, including dendrites, to cell body areas, (C) nuclear eccentricity (ratio between the major and minor diameters) in controls (green bar), at 24 and 48 hours of reperfusion (red bars) and in the relative sham-operated animals (yellow bars). Values are expressed as mean ± SE of 4 – 6 experiments. *P < 0.05 and ***P < 0.001 by one-way ANOVA followed by Tuckey's multiple comparison test.

MIMICKING AN ISCHEMIA/REPERFUSION DAMAGE *IN VITRO*

Phase-contrast microscopic evaluations were performed during the entire course of the treatment. No evident morphological changes were visible between normal untreated cells and cells exposed to DMSO (Figure 32 A – B). The administration of retinoic acid resulted in gradual phenotypic changes from 6 to 12 days of treatment: neurite-like processes started forming creating a network of contacts between neighbour cells and the process appeared complete at the end of the treatment (12 days) (Figure 32 C – F). At the end of the treatment some cells appeared like neurons or glial cells while other were larger, resembling epithelial cells. Contextually, cells reduced their soma and the growth rate, not reaching the confluence at the end of the treatment (Figure 32F). The exposition to sodium azide caused an evident cellular suffering (Figure 32G): SK-N-NE(2) cells acquired a round shape, became poorly adherent to the substrated creating floating aggregates and pyknotic nuclei were visible. In the next recovery phase (Figure 32H), the remained cells presented a dual morphology: some cells maintained their neuronal- and/or glial-like morphology while others were larger and flattened.

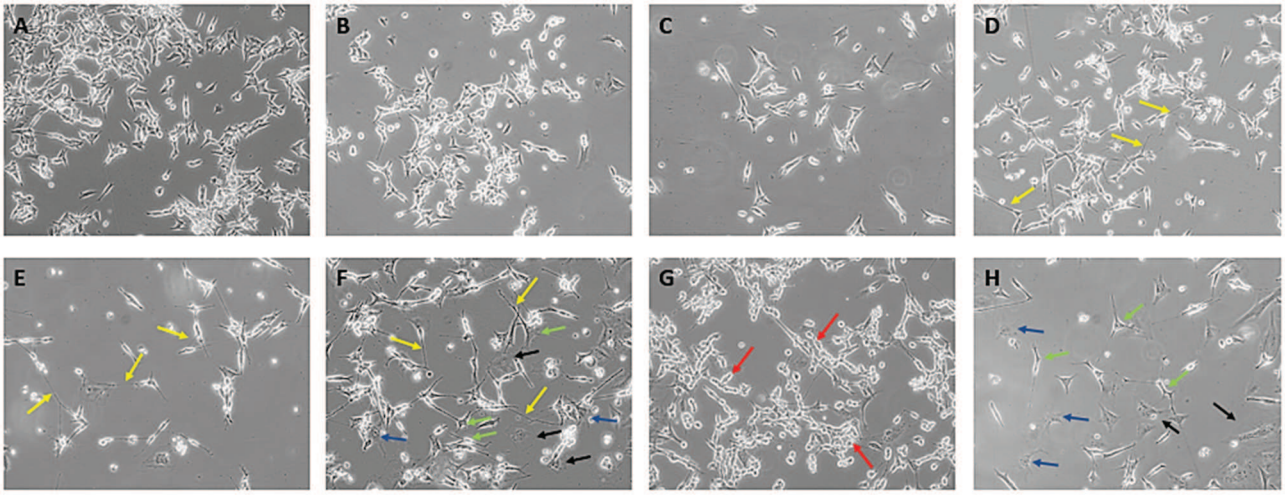

Figure 32: **Effects of the treatment with ATRA and *in vitro* induction of I/R damage.** Contrast-phase microscopic analyses on (A) untreated SK-N-BE(2) cells, (B) SK-N-BE(2) cells exposed to DMSO, (C – F) SK-N-BE(2) cells at 3-6-9-12 days of treatment with 10 µM ATRA, (G) SK-N-BE(2) cells after the induction of an hypoxic stimulation with 10 mM sodium azide for 5 minutes, (H) SK-N-BE(2) cells at 24 hours of recovery after the induction of hypoxia. Neuritic-like processes (yellow arrows), neuron-like cells (green arrows), suffering cells (red arrow), epithelial/fibroblast-like cells (black arrows), microglial-like activated cells (light blue arrows).

REAL TIME PCR ANALYSES ON SK-N-BE(2) CELL LINE

qRT-PCR analyses revealed no difference in gene expression levels between normal untreated cells and cells exposed to DMSO for all the target genes analysed (data not shown). The analyses performed at the end of the treatment revealed that ATRA administration caused a significant reduction of mRNA expression levels of *MAP2* ($P < 0.001$) while *NeuN* mRNA levels were slightly but significantly upregulated ($P < 0.001$) with respect to cells exposed only to DMSO (Figure 33 A, C). The treatment with retinoic acid caused also a

significant upregulation of the mRNA levels for *PSD95* ($P < 0.001$) and SOX2 homeobox gene ($P < 0.001$) (Figure 33 E, G). During the induction of hypoxia, the analyses of mRNA levels for the genes mentioned above showed a significant downregulation of *MAP2* ($P < 0.01$), no significant changes for the mRNA levels of *NeuN* (Figure 33 B, D) while significant downregulation for *PSD95* and *SOX2* levels with respect to cells exposed to ATRA ($P < 0.05$ and $P < 0.001$ respectively) (Figure 33 F, H). In the recovery phase the mRNA levels of *MAP2* were significantly downregulated ($P < 0.001$), *NeuN* levels were unchanged from cells treated with retinoic acid, *PSD95* levels were significantly upregulated ($P < 0.001$) while *SOX2* levels showed a significant downregulation ($P < 0.01$) with respect to ATRA-treated cells (Figure 33 B, D, F, H).

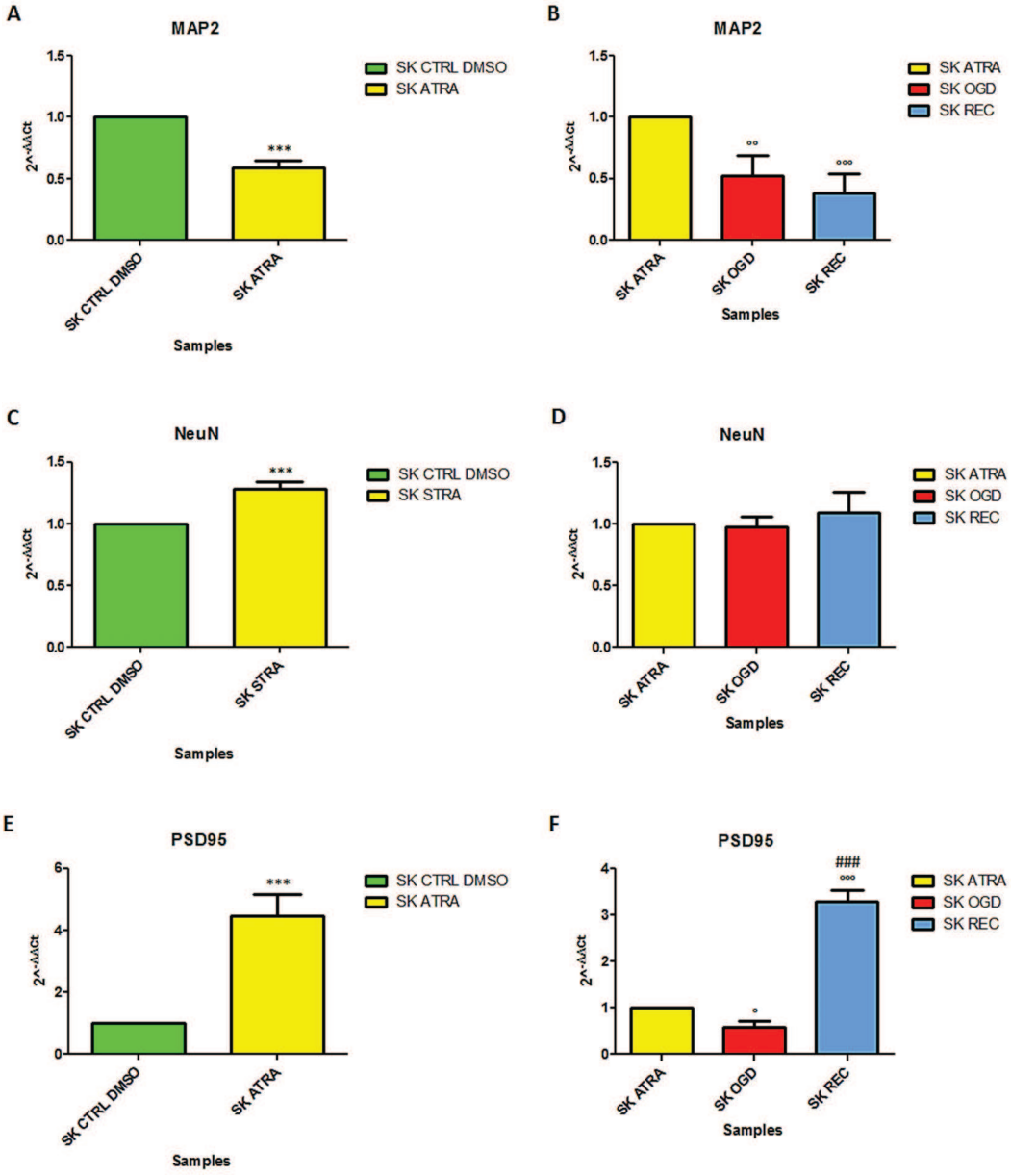

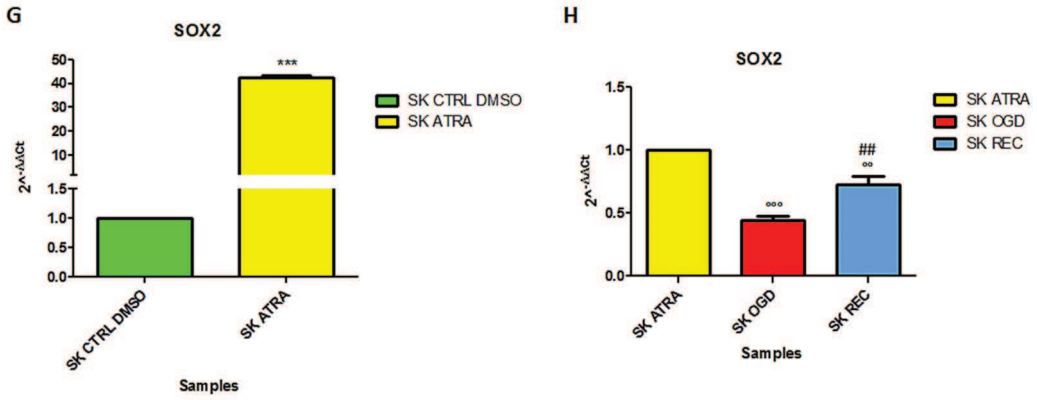

Figure 33: **qRT-PCR analyses on neuronal and glial markers during the treatment with retinoic acid and the induction of an in vitro I/R damage.** (A – B) MAP2 mRNA levels, (C – D) NeuN mRNA levels, (E – F) PSD95 mRNA levels, (G – H) SOX2 mRNA levels in control cells (green bars), cells exposed to ATRA for 12 days (yellow bars), cells exposed to sodium azide for 5 minutes (red bars) and in cells after 24 hours of recovery (light blue bars). Cells exposed to DMSO were used to evaluate the effects of the treatment with retinoic acid (graphs on the left) while cells treated with ATRA were used as controls to determine the effects of the in vitro I/R damage. Values are expressed as mean ± SE of 3 independent experiments. ***P < 0.001 vs cells exposed to DMSO; °P < 0.05, °°P < 0.01 and °°°P < 0.001 vs cells treated with ATRA; ##P < 0.01 and ###P < 0.001 vs cells subjected to OGD procedure by one-way ANOVA followed by Tuckey's test.

HIF-1α and VEGFα mRNA levels were measured in our experimental model and both genes were significantly upregulated by retinoic acid (P < 0.001) (Figure 34 A, C). OGD procedure caused a significant downregulation for HIF-1α while a slight significant decrease was observed for VEGFα levels with respect to cells exposed to ATRA (P < 0.05 and P < 0.001 respectively). In the recovery phase HIF-1α mRNA levels were significantly upregulated (P < 0.05) while VEGFα levels were downregulated if compared to cells treated with retinoic acid (Figure 34 B, D).

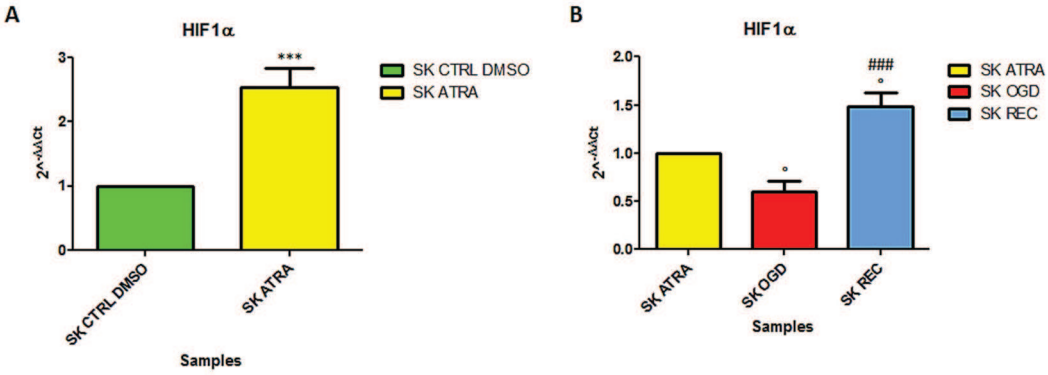

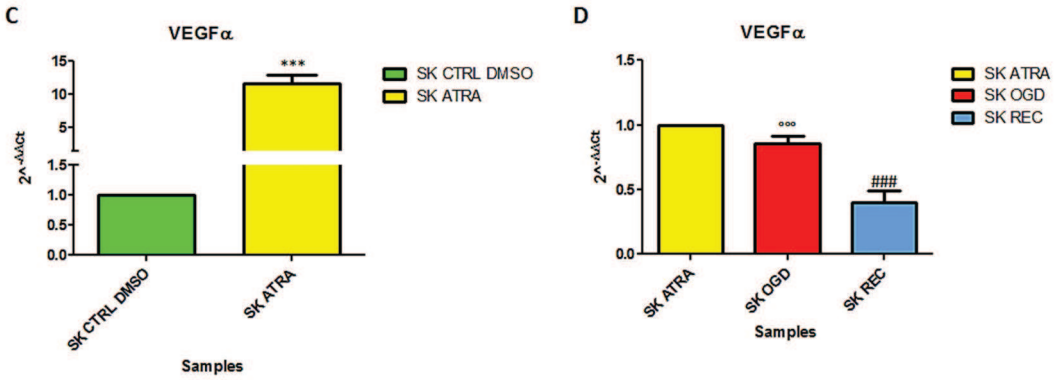

Figure 34: **qRT-PCR analyses on HIF-1α and VEGFα during the treatment with retinoic acid and the induction of an in vitro I/R damage.** (A – B) HIF-1α mRNA levels, (C – D) VEGFα mRNA levels in control cells (green bars), cells exposed to ATRA for 12 days (yellow bars), cells exposed to sodium azide for 5 minutes (red bars) and in cells after 24 hours of recovery (light blue bars). Cells exposed to DMSO were used to evaluate the effects of the treatment with retinoic acid (graphs on the left) while cells treated with ATRA were used as controls to determine the effects of the in vitro I/R damage. Values are expressed as mean ± SE of 3 independent experiments. ***P < 0.001 vs control cells; °P < 0.05 and °°°P < 0.001 vs cells treated with ATRA; ###P < 0.001 vs cells exposed to OGD procedure by one-way ANOVA followed by Tuckey's test.

Real-Time PCR analyses revealed that retinoic acid had no effects on OTX1 expression levels, OTX2 mRNA levels were significantly upregulated (P < 0.01) while TAp73 was slightly significant upregulated (P < 0.05) with respect to control cells exposed to DMSO (Figure 35 A, C, E). OGD procedure resulted in generalized significant downregulation for each gene (P < 0.05 for OTX1 and TAp73, P < 0.01 for OTX2) with respect to cells exposed to ATRA (Figure 35 B, D, F). In the recovery phase instead, each gene's expression levels was rescued reaching control levels, as observed for OTX2, or being upregulated as in the case of OTX1 and TAp73 (P < 0.05) (Figure 35 B, D, F).

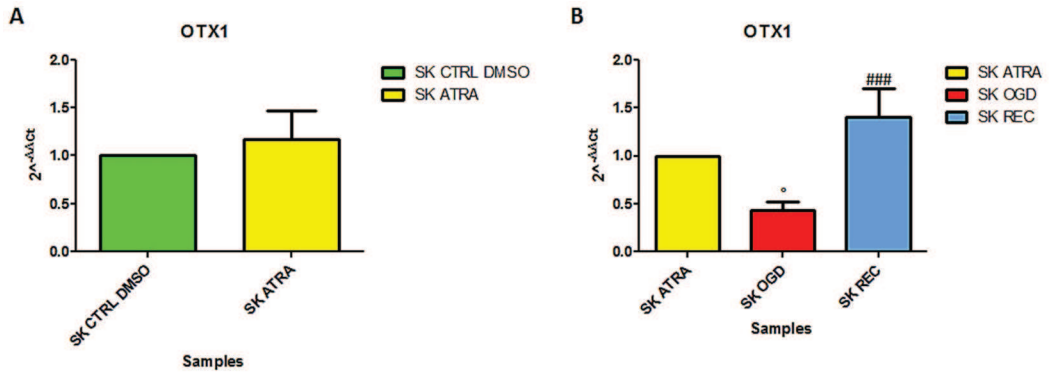

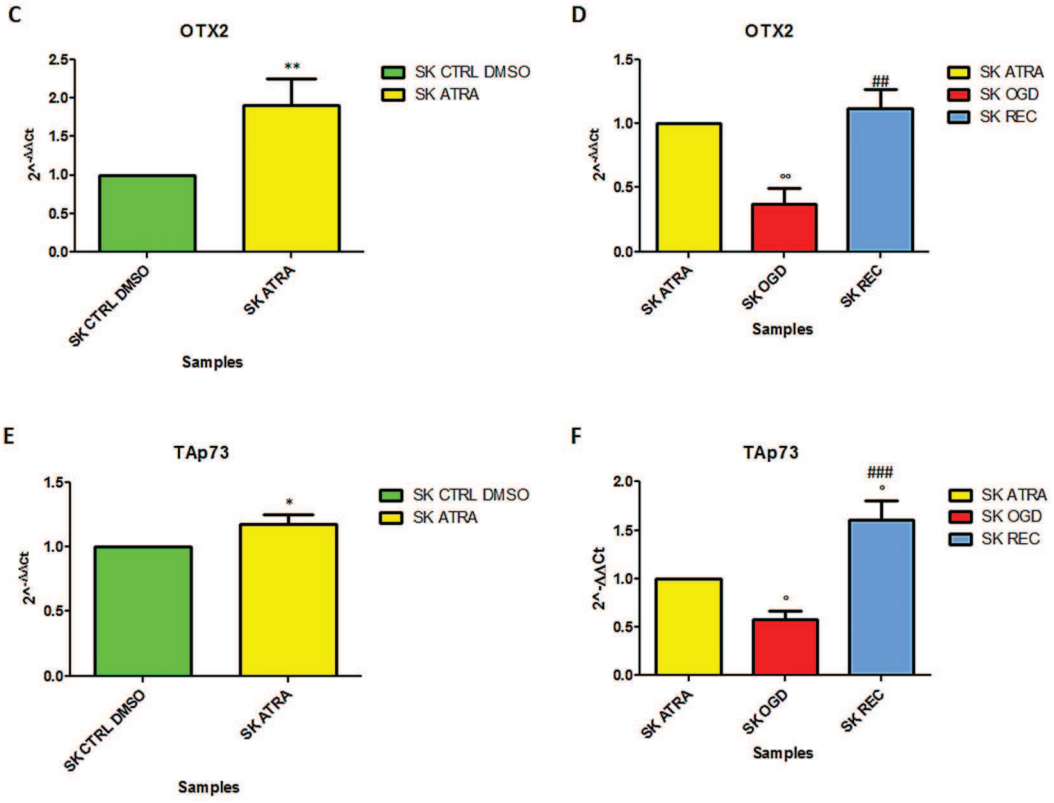

Figure 35: **qRT-PCR analyses of OTX1, OTX2 and TAp73 during the treatment with retinoic acid and the induction of an in vitro I/R damage.** (A – B) OTX1 mRNA levels, (C – D) OTX2 mRNA levels, (E – F) TAp73 mRNA levels in control cells (green bars), cells exposed to ATRA for 12 days (yellow bars), cells exposed to sodium azide for 5 minutes (red bars) and in cells after 24 hours of recovery (light blue bars). Cells exposed to DMSO were used to evaluate the effects of the treatment with retinoic acid (graphs on the left) while cells treated with ATRA were used as controls to determine the effects of the in vitro I/R damage. Values are expressed as mean ± SE of 3 independent experiments. *P < 0.05 and **P < 0.01 vs control cells; °P < 0.05 and °°P < 0.01 vs cells treated with ATRA; ##P < 0.01 and ###P < 0.001 vs cells subjected to OGD procedure by one-way ANOVA followed by Tuckey's test.

WESTERN BLOT ANALYSES ON SK-N-BE(2) CELL LINE

OTX1 specific antibody reveals one band at 37 kDa and protein levels were significantly downregulated (P < 0.01) in cells treated with retinoic acid (Figure 36A). The OGD procedure caused a further significant downregulation of protein levels (P < 0.001) while, in the subsequent recovery phase, OTX1 levels were rescued with respect to ATRA-treated cells (Figure 36B).

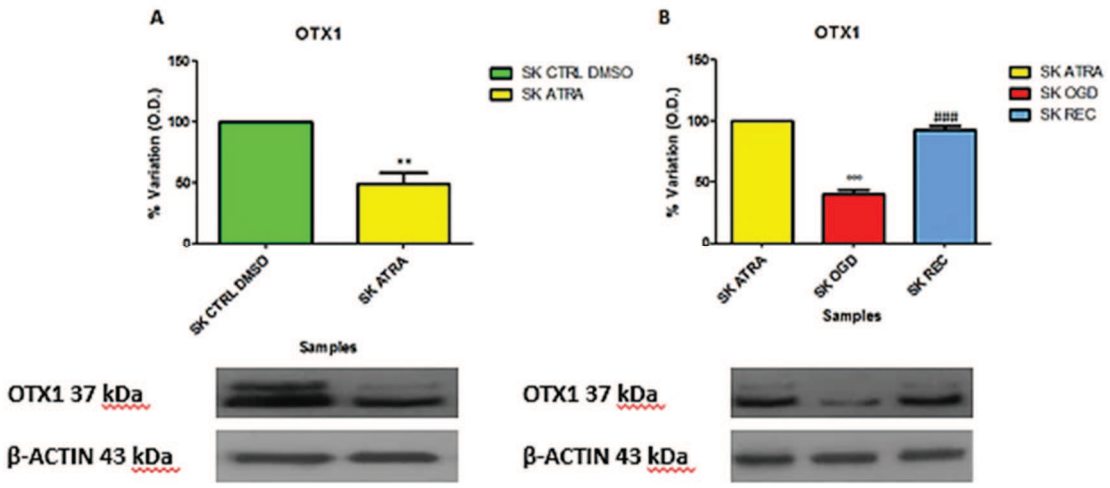

Figure 36: **Western blot analyses of OTX1 protein levels.** Protein expression levels for OTX1 were measured in total lysates from control cells (green bars), cells treated with ATRA for 12 days (yellow bars), cells subjected to OGD procedure (red bars) and in cells after 24 hours of recovery (light blue bars). Below the graphs are reported the immunoblots for OTX1 and β-actin with their molecular weights in the different experimental conditions. 200 µg of samples were electrophoresed in SDS-page 10% polyacrylamide gels and values are expressed as mean ± SE of 3 independent experiments of the percentage variation of the optical density (O. D.) with respect to values obtained from control cells exposed to DMSO and cells treated with retinoic acid. **P < 0.01 vs control cells; °°°P < 0.01 vs cells treated with ATRA; ###P < 0.001 vs cells subjected to OGD procedure by one-way ANOVA followed by Tuckey's post-hoc test.

IMMUNOFLUORESCENCE ASSAYS ON SK-N-BE(2)

Since we have observed increased mRNA levels for the microglial marker PSD95 and the radial glial marker SOX2, preliminary immunofluorescence assays have been performed on SK-N-BE(2) cells exposed to ATRA staining cells with the glial marker S100. As visible in figure 37, cells treated with ATRA showed cytoplasmic immunoreactivity for S100 and a non-uniform morphology: some cells were characterized by irregular contours with lateral lamellar projecting processes (Figure 37 I, M), other cells were characterized by the establishment of small connections with the neighbour cells (Figure 37 C, E) while, alternatively, cells presented an ovoidal shape (Figure 37 A, G). Interestingly, cells formed small aggregates (Figure 37 E, G, I, M) and transmission images revealed the presence of internal structures resembling glycogen granules (Figure 37 B, D, F, H, L, N).

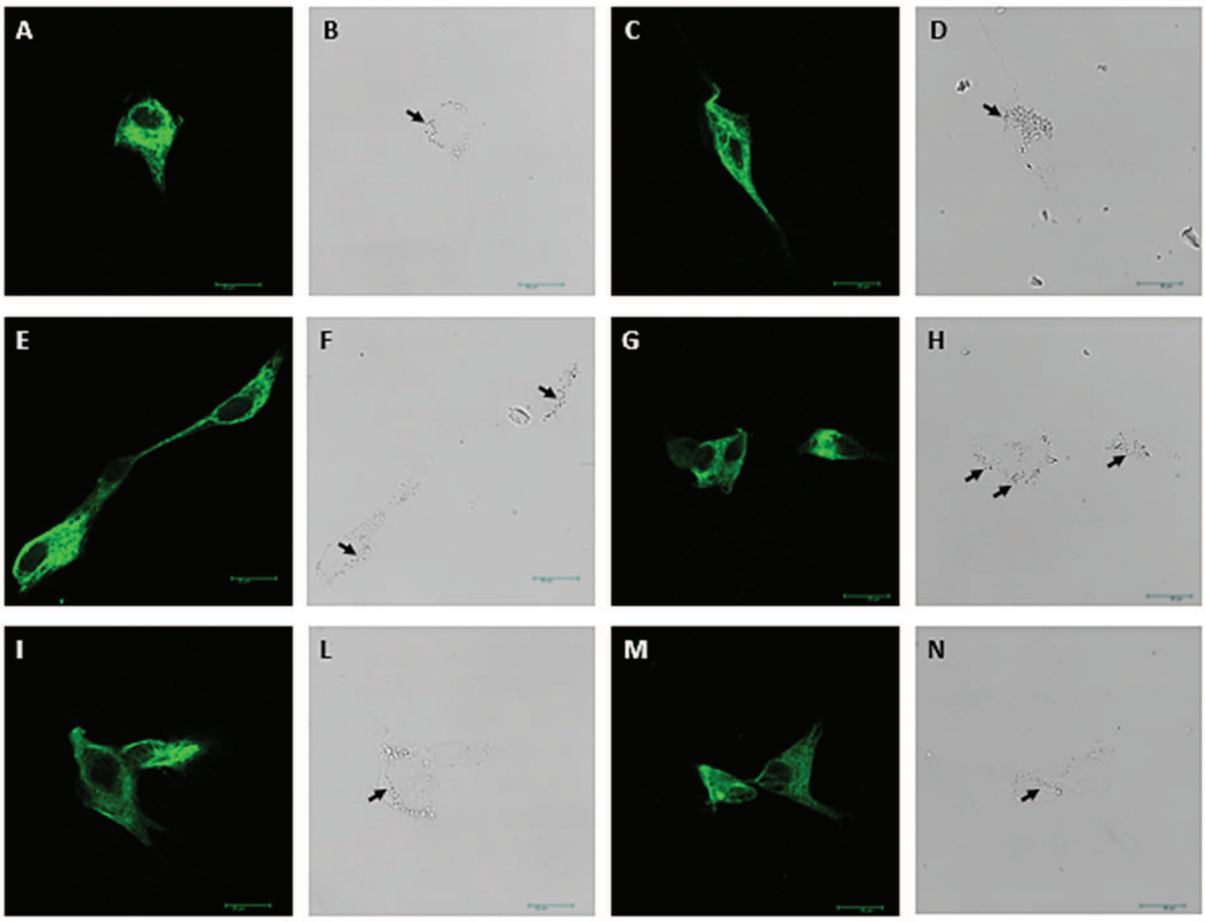

Figure 37: **Immunofluorescence assays on SK-N-BE(2).** SK-N-BE(2) cells treated with ATRA were stained with the specific antibody for the glial marker S100 and confocal images were acquired through 40X objective (bars = 20 µm). Black arrows indicate internal structures resembling glycogen granules.

DISCUSSION

The data presented in this project clearly underline that, after the induction of ischemia followed by reperfusion, myenteric neurons expressing iNOS and nNOS undergo to important changes that sustain the imbalance of motor functions [101, 141, 142]: this is evidenced, in particular, by the increase in $iNOS^+$ neurons and by the decrease of $nNOS^+$ myenteric neurons that, in physiological conditions, are fundamental for the normal intestinal propulsion. These changes may together contribute to the reduction of the intestinal transit during ischemia/reperfusion. Moreover, we show for the first time morphological and biomolecular data suggesting that iNOS/nNOS-produced NO plays a modulatory role on the expression of OTX1 and OTX2 transcription factors during I/R damage.

In our model, the reinstatement of blood flow after the occlusion of superior mesenteric artery (SMA) induces a fast infiltration of neutrophils in the external intestinal muscle layer and these cells contribute to the production of dangerous molecules like myeloperoxidase (MPO). These observations are in accordance with literature data obtained from rat, mice and humans [101, 125, 143]. The increase of neutrophils observed after I/R damage occur in the sub-mucosal and muscular layers especially at 24 hours after the SMA occlusion and, in agreement with these data, we have observed an increase in MPO activity at this time-point in mucosa-deprived intestinal segments.

Adaptive intestinal changes occur at both 60 minutes of ischemia and after 48 hours of reperfusion as demonstrated by the reduction of intestinal transit: in particular, the slow-down of transit at 60 minutes of ischemia may reflect an acute response to both the depletion of energy and hypoxic injury [144]. Analogous observations are present in literature data on mice [145] and guinea pig models [146]. In our model, the restoration of metabolic conditions causes an initial improvement of intestinal motility, but a further reduction is observed at 48 hours of reperfusion. At 72 hours of reperfusion, intestinal transit values return to control levels as observed in other studied [92]. Since 24 and 48 hours of reperfusion induce an increase in neutrophil infiltration and reduction of intestinal transit, we hypothesize that these two time-points are critical for the subsequent development of alterations in the external muscular layer and myenteric plexus as also demonstrated by the increased cellular suffering in neurons and muscular cells.

In the longitudinal muscle myenteric plexus preparations (LMMPs), mRNA for the hypoxia-inducible factor alpha (HIF-1α) significantly increased at both 24 and 48 hours after ischemia/reperfusion. HIF-1α is a key modulator of the response to hypoxia in physiological and pathological conditions since it regulates the translation of proteins necessary for cellular energy preservation and tissue oxygenation like the vascular endothelial growth factor (VEGFα). In our experimental conditions, VEGFα mRNA levels increase at both 24 and 48 hours of reperfusion and, notably, HIF-1α and VEGFα mRNA levels are also upregulated in sham-operated animals at 24 hours after the surgical procedure. This is consistent with an inflammatory process

related to the laparotomy procedure since neutrophil infiltration, HIF-1α and VEGFα levels are often upregulated in active intestinal inflammation (like inflammatory bowel diseases, IBD) [147-150].

Our immunohistochemical analyses show that in the myenteric ganglions subjected to I/R about the 22% of neurons contain nNOS with respect to the total neuronal population, this value it's similar to observations made in guinea pig and mouse [101, 149] and in accordance to these data mRNA and protein levels for nNOS are unchanged in LMMPs. Beyond these information, we have observed that myenteric neurons present morphological alterations (swollen cytoplasm, enlarged and distorted dendrites and nuclear eccentricity) supporting the knowledge that I/R selectively damages nNOS-containing myenteric neurons in the gut [151, 152]. In support to this observation, iNOS-containing control myenteric neurons represent only the 6% of the total myenteric population [141, 153, 154]. iNOS is also expressed in glial cells, an important component of the ENS, that present many similarities with astrocytes in the CNS and, like astrocytes, it has been demonstrated that glial cells of the enteric nervous system contribute to the control of the local enteric microenvironment and function through neuroligand actions [155, 156]. iNOS expressed by the enteric glia may also participate during intestinal I/R damage as does iNOS expressed by astrocytes after an ischemic brain injury [157]. The number of $iNOS^+$ neurons significantly increased at 24 and 48 hours after I/R and, in accordance to other literature data [158, 159] we have observed also increased levels for the mRNA and proteins. These results are comparable with those for HIF-1α that is also a potent modulator of iNOS transcription under I/R conditions [160].

Positive and negative feedback mechanisms have been proposed to explain the autoregulation of NO levels [161]. In our experimental model, the administration of 1400W causes iNOS mRNA modulation at both 24 and 48 hours after I/R but the treatment with the same drug attenuates the I/R-induced iNOS protein more than iNOS mRNA levels, hence suggesting the existence of a positive feedback loop that amplifies iNOS translation more than transcription.

Both 1400W and NPLA are able to reduce the enhancement of MPO activity that we have observed at 24 and 48 hours of reperfusion: this suggests that iNOS- and nNOS-derived NO may participate to the recruitment of neutrophils after an ischemic damage in the gut. Based on these data, NO produced by nNOS may contribute not only to the enteric neurotransmission but also in the development of intestinal I/R damage [162]. The administration of NPLA reduces intestinal transit both in controls and sham-operated animals, suggesting that the integrity of nNOS function is fundamental for the correct intestinal motility. In fact, the selective blockade of nNOS at 48 hours of reperfusion causes a slow-down of intestinal transit consistently with previous findings [92, 142]; on the contrary, the inhibition of iNOS restores the efficiency of intestinal transit to control values and this is consistent with the deleterious effects of iNOS-derived NO [125]. nNOS-derived nitric oxide participates to the physiological modulation of non-adrenergic and non-cholinergic motor responses performing a protective function during I/R damage; the upregulation of iNOS during these

conditions instead would enhance intestinal motor alterations. Taken together, these data indicate as nitrergic myenteric neurons might gain functional plasticity balancing NOS isoforms [141, 163].

The exacts molecular mechanisms underlying the neurodamaging and neuroprotective role of iNOS and nNOS on myenteric neurons during I/R have not been clearly elucidated. NO has been described to participate to the damage induced by I/R through different molecular and biochemical pathways like the activation of transcription factors [164]. In this project we display the capacity of NO, produced by either iNOS or nNOS during an I/R damage, to influence the expression of two homeobox transcriptions factors, OTX1 and OTX2, both necessary for brain development [163, 165].

OTX1 and OTX2 are expressed at low levels in adult brain and cellular soma but different scientific reports indicate that both transcription factors could participate in tumour growth or inflammatory injury [50, 126, 127, 166]. Our experimental model shows for the first time the involvement of both OTX1 and OTX2 in the response of myenteric ganglions during I/R injury. OTX1 is mainly expressed in the enteric glial cells while OTX2 only in neuronal cells and we have observed that both are upregulated after an I/R damage, with an increased number of OTX^+ neurons. Moreover, OTX1 transcription is increased at 24 hours and further upregulated at 48 hours of reperfusion, while OTX2 transcription is boosted at 24 hours but decreases at 48 hours of reperfusion. These observations are highly suggestive of a role of the two proteins in the modulation of the intestinal neuro-muscular functions since they are expressed in controls and undergo to changes during an I/R damage. Notably, changes in the number and functions of excitatory and inhibitory enteric neuronal pathways may occur after the deletion of genes phylogenetically related to *Otx* like *Ncx* (also known as *Hox11L.1*) [165, 167-169]. In the sham-operated group of animals we have observed increased levels of the mRNA for OTX1 and OTX2 with respect to controls and we suppose that both transcription factors may be sensitive to the inflammatory challenge associated to laparotomy procedure. In this context, different reports indicate that homeobox genes related to OTX family, like *Cdx2*, are involved in the development of inflammation in the gut [170].

In our experimental model, NPLA and 1400W reduce the enhancement of protein levels induced by I/R indicating that nitric oxide synthetized by iNOS and nNOS regulates OTX1 and OTX2 transcription and translation. Interestingly, 1400W modulates OTX1 transcription and translation more efficiently than NPLA, indicating a possible correlation between OTX1 and iNOS as also confirmed by the colocalization of the two proteins in whole mounts of LMMP samples. On the contrary, OTX2 is more sensible to NPLA treatment suggesting a relationship with nNOS as indicated by the colocalization of the two proteins' signals.

Based on these data, we hypothesize that the neurodamaging and neuroprotective roles of iNOS and nNOS during an I/R injury in the gut may involve the activation of molecular pathways downstream of OTX1 and OTX2 respectively. Moreover, these observations suggest also an interplay between myenteric nitrergic

pathways and OTX transcription factors that could sustain the development of motor alterations induced by NO after an I/R injury.

Having an appropriate *in vivo* and *in vitro* system that provide translational models for human disease is a relevant aspect in the field of neurobiology and neuroscience research [171]. Moreover, the possibility of using cells in culture provide an important platform to characterize molecular mechanisms and protein functionality at the bases of specific phenomena to understand the development of a pathological condition and to perform preliminary studies to identify therapeutic targets.

All-trans retinoic acid (ATRA) is a biologically active metabolite of vitamin A and plays a crucial role in the development, establishment and maintenance of physiological processes in adult tissues. Its function mainly relies on the induction of the differentiation through the binding to the nuclear retinoid acid receptors (RARs) and retinoid X receptors (RXRs) that are member of the steroid-thyroid hormone receptors super-family. After the binding of ATRA, these receptors form heterodimers, interact with co-activators/repressors, bind to specific retinoic acid responsive elements (RAREs) in the promoter of target genes hence activating or repressing the transcription.

In our experimental model, the increased mRNA levels of *Sox2* and *Otx2*, combined with the fact that radial glial cells are precursors during the neuronal differentiation, allow us to hypothesize that the treatment with ATRA results mainly in glial precursor cells: this is demonstrated by the immunoreactivity for the glial marker S100 and by the presence of internal structures similar to glycogen granules that are reported to be a feature of radial glial cells [172]. In support to our hypothesis of an incomplete differentiation process, we have observed increased mRNA levels for *Otx1* but downregulated levels for the protein: since OTX1 is reported to be involved during the differentiation [126], the observed decrease in protein levels might reflect the activation of protein degradation pathways (e.g. ubiquitine-proteasome pathway) that prevents the full activation of OTX1. Moreover, literature data report that TAp73 not only interacts with different miRNAs to regulate the differentiation and allow its correct progression [173] but also that this gene is induced by retinoic acid [174]. In our experimental model, *TAp73* mRNA levels are only slightly increased by ATRA and we propose that the lacking effects of ATRA on this gene are related to the undifferentiated state of the cells. Further experimental procedures, similar to that performed on SH-SY5Y human neuroblastoma cell line [175], combining ATRA with nerve growth factor (NGF), brain derived growth factor (BDNF), phorbol-esters (e.g. TPA) and/or other growth factors will be performed in order to strengthen the differentiation of SK-N-BE(2) cell line towards a mature phenotype.

Hypoxia is a condition occurring in different physiological situations (e.g. embryogenesis and stem cells modulation in terms of differentiation and/or proliferation) but also in pathological conditions like ischemia or cancer [176]. Several *in vitro* approaches have demonstrated that proliferation and differentiation are

enhanced by low oxygen concentration, creating a condition that mimics the neurogenic zone in the developing brain. In our experimental model, the OGD procedure caused generalized cellular suffering with respect to cells treated with retinoic acid. Cellular suffering is characterized primarily by a reduction of the cell number and secondly by the rounded shape and poorly adherence of the cells that display also pyknotic nuclei index of apoptosis. Along with these morphological alterations also gene and protein expression levels were downregulated with the only exception for *NeuN* that was unchanged with respect to ATRA-exposed cells. The reduction of *HIF-1α* and *Vegfα* during the induction of hypoxia might be related to the short time of exposition to sodium azide. In fact, experiments performed in our laboratory exposing cells to cobalt chloride for 24 and 48 hours after the treatment with ATRA, resulted in increased levels of both targets (data not shown) as demonstrated by Piret and co-workers in 2002 [177]. We hypothesize that the induction of hypoxia on SK-N-BE(2) cell line may constitute the attempt of stress to stimulate the proliferation and differentiation: for example, the reduction of S100B protein in precursor cells in a defined period is reported to be permissive for cell differentiation [178] and future studies regarding the analysis of S100 in our cell model after hypoxia could be useful to confirm this observation.

During the recovery phase, the downregulation of *Map2* and the unchanged levels of *NeuN* persist; interestingly we have observed downregulation for *Sox2* and upregulation the mRNA levels for *Psd95*. This might be compatible with the activation of glial cells after a hypoxic injury. The extent of cellular disfunction, injury and/or death is influenced by the magnitude and duration of the hypoxic condition. The response to a hypoxic or ischemic event is bimodal and depends on the reperfusion after this condition. In fact, despite the evident effects of the reperfusion in the reestablishment of oxygen and nutrients to support cellular metabolism, reperfusion is also liked both to exacerbation of the hypoxic/ischemic injury and to the activation of survival programs that limit the damage [179]. In this context, glial and microglial cells respond and are activated during the reperfusion to remove cellular debris and toxic products of cellular metabolism [180]. In accordance con published literature works, *HIF-1α* is induced during reperfusion [181] since it regulates the translation of proteins necessary for cellular energy preservation and induces the “reactive” morphology characterized by hypertrophic processes and stellate-shaped cell bodies [182]. Contrary to the rat model of I/R, *Vegfα* levels are downregulated during the recovery phase probably because of the activation of distinct regulatory pathways *in vivo* and *in vitro* that could exert different effects of this gene [183]. Notably, hypoxia or *HIF-1α* activation suspend the stem cells quiescence state and stimulate their proliferation: the switch from proliferation to differentiation might be due to the increased oxygen levels and/or ROS signaling during the reperfusion state [176]. As observed in the rat model of I/R, both *Otx1* and *Otx2* are involved in the recovery phase after the hypoxic event: *Otx1* is upregulated and rescued at both mRNA and protein level; *Otx2*, instead, is rescued with respect to cells treated with ATRA. Interestingly, *TAp73* mRNA levels are upregulated during the recovery phase as observed for *Otx1* even though conflicting reports show distinct roles for TAp73 in the modulation of HIF-1α and VEGFα with some authors agree in a

stimulating role on both the targets [184, 185] while others report an inhibitory effect [185, 186]. We hypothesize that homeobox genes and especially *Otx1* are activated during the reperfusion inducing the differentiation of the cells survived to the hypoxic stress into mature glial or microglial cells.

Intestinal ischemia is a rarely preventable event and most of the research in this field focused on the early identification of ischemia as well as the development of new therapeutic approaches to target the reperfusion after the ischemic insult. Moreover, one of the most promising approach is the discovery of molecular pathways underlying cell damage and the inflammatory process, which may exacerbate the I/R damage and prevent tissue repair. The development of new therapeutic approaches includes the modulation of cell death pathways and the repair process. Taken together the results showed in this project are highly suggestive of a role of the homeobox gene family *Otx* in the development of an ischemia/reperfusion damage in both mature and immature cells. Homeobox genes and their products might interact with the nitrergic pathway sustaining the development of NO-dependent alterations. Our data provide new hints on the possible sources for NO in the myenteric plexus after an I/R injury and describe new molecular pathways linked to its synthesis hence contributing to the development of novel strategies for the treatment of gastrointestinal diseases such as I/R injury.

FUTURE PERSPECTIVES

Future studies will focus on the improvement of the differentiation protocol in order to obtain mature neuronal or glial cells combining ATRA with NGF, BDNF, TPA or other factors. Once obtained, these cells will be characterized from the molecular and physiological point of view to establish the exact neuronal or glial subtype obtained. Given the role of OTX1 and OTX2 in the development, gene silencing experiments will be applied during the entire cellular differentiation to elucidate which is the leading gene involved in this process. Subsequently, as observed in the rat model of I/R, iNOS and nNOS contribution will be analyzed to confirm the correlation observed with OTX1 and OTX2: to that purpose, additional experiments will be performed using iNOS and nNOS inhibitors (1400W and NPLA) during the treatment with retinoic acid alone or in combination with other growth factors. Morphological, qRT-PCR, Western blot and immunofluorescence analyses in combination with immunoprecipitation assays, will be useful to further delineate the correlation between OTX homeobox genes and the nitrergic pathway.

BIBLIOGRAPHY

1. Lewis, M.T., *Homeobox genes in mammary gland development and neoplasia.* Breast Cancer Res, 2000. **2**(3): p. 158-69.
2. Holland, P.W., H.A. Booth, and E.A. Bruford, *Classification and nomenclature of all human homeobox genes.* BMC Biol, 2007. **5**: p. 47.
3. Boncinelli, E., *Homeobox genes and disease.* Curr Opin Genet Dev, 1997. **7**(3): p. 331-7.
4. Gehring, W.J. and Y. Hiromi, *Homeotic genes and the homeobox.* Annu Rev Genet, 1986. **20**: p. 147-73.
5. Aoki, K., et al., *Suppression of colonic polyposis by homeoprotein CDX2 through its nontranscriptional function that stabilizes p27Kip1.* Cancer Res, 2011. **71**(2): p. 593-602.
6. Pagani, I.S., et al., *The mammary gland and the homeobox gene Otx1.* Breast J, 2010. **16 Suppl 1**: p. S53-6.
7. Wilson, D., et al., *Cooperative dimerization of paired class homeo domains on DNA.* Genes Dev, 1993. **7**(11): p. 2120-34.
8. Haria, D. and H. Naora, *Homeobox Gene Deregulation: Impact on the Hallmarks of Cancer.* Cancer Hallm, 2013. **1**(2-3): p. 67-76.
9. Chang, C.P., et al., *Pbx proteins display hexapeptide-dependent cooperative DNA binding with a subset of Hox proteins.* Genes Dev, 1995. **9**(6): p. 663-74.
10. Robson, E.J., S.J. He, and M.R. Eccles, *A PANorama of PAX genes in cancer and development.* Nat Rev Cancer, 2006. **6**(1): p. 52-62.
11. Vandewalle, C., F. Van Roy, and G. Berx, *The role of the ZEB family of transcription factors in development and disease.* Cell Mol Life Sci, 2009. **66**(5): p. 773-87.
12. Chen, H. and S. Sukumar, *Role of homeobox genes in normal mammary gland development and breast tumorigenesis.* J Mammary Gland Biol Neoplasia, 2003. **8**(2): p. 159-75.
13. Boncinelli, E., *A caccia di geni*. 1996.
14. Cillo, C., et al., *Homeobox genes in normal and malignant cells.* J Cell Physiol, 2001. **188**(2): p. 161-9.
15. Abate-Shen, C., *Deregulated homeobox gene expression in cancer: cause or consequence?* Nat Rev Cancer, 2002. **2**(10): p. 777-85.
16. Imagawa, E., et al., *Severe manifestations of hand-foot-genital syndrome associated with a novel HOXA13 mutation.* Am J Med Genet A, 2014. **164A**(9): p. 2398-402.
17. Coletta, R.D., et al., *Transcriptional control of the cell cycle in mammary gland development and tumorigenesis.* J Mammary Gland Biol Neoplasia, 2004. **9**(1): p. 39-53.
18. Borrow, J., et al., *The t(7;11)(p15;p15) translocation in acute myeloid leukaemia fuses the genes for nucleoporin NUP98 and class I homeoprotein HOXA9.* Nat Genet, 1996. **12**(2): p. 159-67.

19. He, W.W., et al., *A novel human prostate-specific, androgen-regulated homeobox gene (NKX3.1) that maps to 8p21, a region frequently deleted in prostate cancer.* Genomics, 1997. **43**(1): p. 69-77.
20. Emmert-Buck, M.R., et al., *Allelic loss on chromosome 8p12-21 in microdissected prostatic intraepithelial neoplasia.* Cancer Res, 1995. **55**(14): p. 2959-62.
21. Xie, Q. and Z.A. Wang, *Transcriptional regulation of the Nkx3.1 gene in prostate luminal stem cell specification and cancer initiation via its 3' genomic region.* J Biol Chem, 2017. **292**(33): p. 13521-13530.
22. Rauch, T., et al., *Homeobox gene methylation in lung cancer studied by genome-wide analysis with a microarray-based methylated CpG island recovery assay.* Proc Natl Acad Sci U S A, 2007. **104**(13): p. 5527-32.
23. Tommasi, S., et al., *Methylation of homeobox genes is a frequent and early epigenetic event in breast cancer.* Breast Cancer Res, 2009. **11**(1): p. R14.
24. Lemons, D. and W. McGinnis, *Genomic evolution of Hox gene clusters.* Science, 2006. **313**(5795): p. 1918-22.
25. Gupta, R.A., et al., *Long non-coding RNA HOTAIR reprograms chromatin state to promote cancer metastasis.* Nature, 2010. **464**(7291): p. 1071-6.
26. Ma, L., J. Teruya-Feldstein, and R.A. Weinberg, *Tumour invasion and metastasis initiated by microRNA-10b in breast cancer.* Nature, 2007. **449**(7163): p. 682-8.
27. Imam, J.S., et al., *MicroRNA-185 suppresses tumor growth and progression by targeting the Six1 oncogene in human cancers.* Oncogene, 2010. **29**(35): p. 4971-9.
28. Klein, W.H. and X. Li, *Function and evolution of Otx proteins.* Biochem Biophys Res Commun, 1999. **258**(2): p. 229-33.
29. Bellipanni, G., T. Murakami, and E.S. Weinberg, *Molecular dissection of Otx1 functional domains in the zebrafish embryo.* J Cell Physiol, 2010. **222**(2): p. 286-93.
30. Larsen, K.B., et al., *Expression of the homeobox genes OTX2 and OTX1 in the early developing human brain.* J Histochem Cytochem, 2010. **58**(7): p. 669-78.
31. Simeone, A., E. Puelles, and D. Acampora, *The Otx family.* Curr Opin Genet Dev, 2002. **12**(4): p. 409-15.
32. Rubenstein, J.L., et al., *Regionalization of the prosencephalic neural plate.* Annu Rev Neurosci, 1998. **21**: p. 445-77.
33. Simeone, A., *Otx1 and Otx2 in the development and evolution of the mammalian brain.* EMBO J, 1998. **17**(23): p. 6790-8.
34. Zhang, Y.A., et al., *Regulated nuclear trafficking of the homeodomain protein otx1 in cortical neurons.* Mol Cell Neurosci, 2002. **19**(3): p. 430-46.

35. Zhang, Y.F., et al., *Otx1 promotes basal dendritic growth and regulates intrinsic electrophysiological and synaptic properties of layer V pyramidal neurons in mouse motor cortex.* Neuroscience, 2015. **285**: p. 139-54.
36. Acampora, D., et al., *Transient dwarfism and hypogonadism in mice lacking Otx1 reveal prepubescent stage-specific control of pituitary levels of GH, FSH and LH.* Development, 1998. **125**(7): p. 1229-39.
37. Acampora, D., et al., *Epilepsy and brain abnormalities in mice lacking the Otx1 gene.* Nat Genet, 1996. **14**(2): p. 218-22.
38. Acampora, D., P. Barone, and A. Simeone, *Otx genes in corticogenesis and brain development.* Cereb Cortex, 1999. **9**(6): p. 533-42.
39. Acampora, D., et al., *The role of Otx and Otp genes in brain development.* Int J Dev Biol, 2000. **44**(6): p. 669-77.
40. Levantini, E., et al., *Unsuspected role of the brain morphogenetic gene Otx1 in hematopoiesis.* Proc Natl Acad Sci U S A, 2003. **100**(18): p. 10299-303.
41. Acampora, D., M. Gulisano, and A. Simeone, *Genetic and molecular roles of Otx homeodomain proteins in head development.* Gene, 2000. **246**(1-2): p. 23-35.
42. Takaoka, K. and H. Hamada, *Cell fate decisions and axis determination in the early mouse embryo.* Development, 2012. **139**(1): p. 3-14.
43. Saiz, N. and B. Plusa, *Early cell fate decisions in the mouse embryo.* Reproduction, 2013. **145**(3): p. R65-80.
44. Pantò, M.R., et al., *Role of the Otx1 gene in cell differentiation of mammalian cortex.* Eur J Neurosci, 2004. **19**(10): p. 2893-902.
45. Bovolenta, P., et al., *Implication of OTX2 in pigment epithelium determination and neural retina differentiation.* J Neurosci, 1997. **17**(11): p. 4243-52.
46. Hennig, A.K., G.H. Peng, and S. Chen, *Regulation of photoreceptor gene expression by Crx-associated transcription factor network.* Brain Res, 2008. **1192**: p. 114-33.
47. Lawrence, J.M., et al., *MIO-M1 cells and similar muller glial cell lines derived from adult human retina exhibit neural stem cell characteristics.* Stem Cells, 2007. **25**(8): p. 2033-43.
48. Roger, J.E., et al., *OTX2 loss causes rod differentiation defect in CRX-associated congenital blindness.* J Clin Invest, 2014. **124**(2): p. 631-43.
49. Sugiyama, S., A. Prochiantz, and T.K. Hensch, *From brain formation to plasticity: insights on Otx2 homeoprotein.* Dev Growth Differ, 2009. **51**(3): p. 369-77.
50. Di, C., et al., *Identification of OTX2 as a medulloblastoma oncogene whose product can be targeted by all-trans retinoic acid.* Cancer Res, 2005. **65**(3): p. 919-24.
51. Lu, Y., et al., *OTX2 expression contributes to proliferation and progression in Myc-amplified medulloblastoma.* Am J Cancer Res, 2017. **7**(3): p. 647-656.

52. Kaghad, M., et al., *Monoallelically expressed gene related to p53 at 1p36, a region frequently deleted in neuroblastoma and other human cancers.* Cell, 1997. **90**(4): p. 809-19.
53. Trink, B., et al., *A new human p53 homologue.* Nat Med, 1998. **4**(7): p. 747-8.
54. Collavin, L., A. Lunardi, and G. Del Sal, *p53-family proteins and their regulators: hubs and spokes in tumor suppression.* Cell Death Differ, 2010. **17**(6): p. 901-11.
55. Melino, G., et al., *Functional regulation of p73 and p63: development and cancer.* Trends Biochem Sci, 2003. **28**(12): p. 663-70.
56. Murray-Zmijewski, F., D.P. Lane, and J.C. Bourdon, *p53/p63/p73 isoforms: an orchestra of isoforms to harmonise cell differentiation and response to stress.* Cell Death Differ, 2006. **13**(6): p. 962-72.
57. Danilova, N., K.M. Sakamoto, and S. Lin, *p53 family in development.* Mech Dev, 2008. **125**(11-12): p. 919-31.
58. Maas, A.M., et al., *Targeting p73 in cancer.* Cancer Lett, 2013. **332**(2): p. 229-36.
59. Deyoung, M.P. and L.W. Ellisen, *p63 and p73 in human cancer: defining the network.* Oncogene, 2007. **26**(36): p. 5169-83.
60. Courtois, S., C. Caron de Fromentel, and P. Hainaut, *p53 protein variants: structural and functional similarities with p63 and p73 isoforms.* Oncogene, 2004. **23**(3): p. 631-8.
61. Wei, J., E. Zaika, and A. Zaika, *p53 Family: Role of Protein Isoforms in Human Cancer.* J Nucleic Acids, 2012. **2012**: p. 687359.
62. Qin, H., et al., *Regulation of apoptosis and differentiation by p53 in human embryonic stem cells.* J Biol Chem, 2007. **282**(8): p. 5842-52.
63. Gil-Perotin, S., et al., *Loss of p53 induces changes in the behavior of subventricular zone cells: implication for the genesis of glial tumors.* J Neurosci, 2006. **26**(4): p. 1107-16.
64. Dumble, M., et al., *The impact of altered p53 dosage on hematopoietic stem cell dynamics during aging.* Blood, 2007. **109**(4): p. 1736-42.
65. Riley, T., et al., *Transcriptional control of human p53-regulated genes.* Nat Rev Mol Cell Biol, 2008. **9**(5): p. 402-12.
66. Kandoth, C., et al., *Mutational landscape and significance across 12 major cancer types.* Nature, 2013. **502**(7471): p. 333-339.
67. Muller, P.A. and K.H. Vousden, *Mutant p53 in cancer: new functions and therapeutic opportunities.* Cancer Cell, 2014. **25**(3): p. 304-17.
68. Craig, A.L., et al., *DeltaNp63 transcriptionally regulates ATM to control p53 Serine-15 phosphorylation.* Mol Cancer, 2010. **9**: p. 195.
69. Finlan, L.E. and T.R. Hupp, *p63: the phantom of the tumor suppressor.* Cell Cycle, 2007. **6**(9): p. 1062-71.

70. Suh, E.K., et al., *p63 protects the female germ line during meiotic arrest.* Nature, 2006. **444**(7119): p. 624-8.
71. Keyes, W.M., et al., *ΔNp63α is an oncogene that targets chromatin remodeler Lsh to drive skin stem cell proliferation and tumorigenesis.* Cell Stem Cell, 2011. **8**(2): p. 164-76.
72. Zaika, A.I., et al., *DeltaNp73, a dominant-negative inhibitor of wild-type p53 and TAp73, is up-regulated in human tumors.* J Exp Med, 2002. **196**(6): p. 765-80.
73. Domínguez, G., et al., *DeltaTAp73 upregulation correlates with poor prognosis in human tumors: putative in vivo network involving p73 isoforms, p53, and E2F-1.* J Clin Oncol, 2006. **24**(5): p. 805-15.
74. Furness, J.B., et al., *The enteric nervous system and gastrointestinal innervation: integrated local and central control.* Adv Exp Med Biol, 2014. **817**: p. 39-71.
75. Young, H.M., C.J. Hearn, and D.F. Newgreen, *Embryology and development of the enteric nervous system.* Gut, 2000. **47 Suppl 4**: p. iv12-4; discussion iv26.
76. Hansen, M.B., *The enteric nervous system I: organisation and classification.* Pharmacol Toxicol, 2003. **92**(3): p. 105-13.
77. Rühl, A., Y. Nasser, and K.A. Sharkey, *Enteric glia.* Neurogastroenterol Motil, 2004. **16 Suppl 1**: p. 44-9.
78. Rolle, U., L. Nemeth, and P. Puri, *Nitrergic innervation of the normal gut and in motility disorders of childhood.* J Pediatr Surg, 2002. **37**(4): p. 551-67.
79. Ekblad, E., P. Alm, and F. Sundler, *Distribution, origin and projections of nitric oxide synthase-containing neurons in gut and pancreas.* Neuroscience, 1994. **63**(1): p. 233-48.
80. Kunze, W.A., et al., *The soma and neurites of primary afferent neurons in the guinea-pig intestine respond differentially to deformation.* J Physiol, 2000. **526 Pt 2**: p. 375-85.
81. Pompolo, S. and J.B. Furness, *Quantitative analysis of inputs to somatostatin-immunoreactive descending interneurons in the myenteric plexus of the guinea-pig small intestine.* Cell Tissue Res, 1998. **294**(2): p. 219-26.
82. Shepherd, A.P., *Local control of intestinal oxygenation and blood flow.* Annu Rev Physiol, 1982. **44**: p. 13-27.
83. Parks, D.A. and E.D. Jacobson, *Physiology of the splanchnic circulation.* Arch Intern Med, 1985. **145**(7): p. 1278-81.
84. Margaritis, E.V., et al., *Effects of oral administration of (L)-arginine, (L)-NAME and allopurinol on intestinal ischemia/reperfusion injury in rats.* Life Sci, 2011. **88**(23-24): p. 1070-6.
85. Thornton, M. and M.J. Solomon, *Crohn's disease: in defense of a microvascular aetiology.* Int J Colorectal Dis, 2002. **17**(5): p. 287-97.
86. Yasuhara, H., *Acute mesenteric ischemia: the challenge of gastroenterology.* Surg Today, 2005. **35**(3): p. 185-95.

87. Massberg, S. and K. Messmer, *The nature of ischemia/reperfusion injury.* Transplant Proc, 1998. **30**(8): p. 4217-23.

88. Brookes, P.S., et al., *Calcium, ATP, and ROS: a mitochondrial love-hate triangle.* Am J Physiol Cell Physiol, 2004. **287**(4): p. C817-33.

89. McCord, J.M., *Oxygen-derived free radicals in postischemic tissue injury.* N Engl J Med, 1985. **312**(3): p. 159-63.

90. Lindeström, L.M. and E. Ekblad, *Structural and neuronal changes in rat ileum after ischemia with reperfusion.* Dig Dis Sci, 2004. **49**(7-8): p. 1212-22.

91. Ferrer-Sueta, G. and R. Radi, *Chemical biology of peroxynitrite: kinetics, diffusion, and radicals.* ACS Chem Biol, 2009. **4**(3): p. 161-77.

92. Ballabeni, V., et al., *Alterations of intestinal motor responsiveness in a model of mild mesenteric ischemia/reperfusion in rats.* Life Sci, 2002. **71**(17): p. 2025-35.

93. Attuwaybi, B.O., et al., *Heme oxygenase-1 induction by hemin protects against gut ischemia/reperfusion injury.* J Surg Res, 2004. **118**(1): p. 53-7.

94. Spehlmann, M.E. and L. Eckmann, *Nuclear factor-kappa B in intestinal protection and destruction.* Curr Opin Gastroenterol, 2009. **25**(2): p. 92-9.

95. Zou, L., B. Attuwaybi, and B.C. Kone, *Effects of NF-kappa B inhibition on mesenteric ischemia-reperfusion injury.* Am J Physiol Gastrointest Liver Physiol, 2003. **284**(4): p. G713-21.

96. Montalto, M.C., et al., *Role for complement in mediating intestinal nitric oxide synthase-2 and superoxide dismutase expression.* Am J Physiol Gastrointest Liver Physiol, 2003. **285**(1): p. G197-206.

97. Koury, J., et al., *Persistent HIF-1alpha activation in gut ischemia/reperfusion injury: potential role of bacteria and lipopolysaccharide.* Shock, 2004. **22**(3): p. 270-7.

98. Sukhotnik, I., et al., *The effect of 100% oxygen on intestinal preservation and recovery following ischemia-reperfusion injury in rats.* Crit Care Med, 2009. **37**(3): p. 1054-61.

99. Lipton, P., *Ischemic cell death in brain neurons.* Physiol Rev, 1999. **79**(4): p. 1431-568.

100. Kermer, P., N. Klöcker, and M. Bähr, *Neuronal death after brain injury. Models, mechanisms, and therapeutic strategies in vivo.* Cell Tissue Res, 1999. **298**(3): p. 383-95.

101. Rivera, L.R., et al., *The reactions of specific neuron types to intestinal ischemia in the guinea pig enteric nervous system.* Acta Neuropathol, 2009. **118**(2): p. 261-70.

102. Pontell, L., et al., *Damaging effects of ischemia/reperfusion on intestinal muscle.* Cell Tissue Res, 2011. **343**(2): p. 411-9.

103. Lundberg, J.O., E. Weitzberg, and M.T. Gladwin, *The nitrate-nitrite-nitric oxide pathway in physiology and therapeutics.* Nat Rev Drug Discov, 2008. **7**(2): p. 156-67.

104. Bentz, B.G., et al., *The yin and yang of nitric oxide: reflections on the physiology and pathophysiology of NO.* Head Neck, 2000. **22**(1): p. 71-83.

105. Steel, J.H., et al., *Increased nitric oxide synthase immunoreactivity in rat dorsal root ganglia in a neuropathic pain model.* Neurosci Lett, 1994. **169**(1-2): p. 81-4.

106. Bagetta, G., et al., *Lithium and tacrine increase the expression of nitric oxide synthase mRNA in the hippocampus of rat.* Biochem Biophys Res Commun, 1993. **197**(3): p. 1132-9.

107. Guo, Y., et al., *Regulation of cerebellar nitric oxide production in response to prolonged in vivo hypoxia.* J Neurosci Res, 1997. **49**(1): p. 89-97.

108. Calzà, L., L. Giardino, and S. Ceccatelli, *NOS mRNA in the paraventricular nucleus of young and old rats after immobilization stress.* Neuroreport, 1993. **4**(6): p. 627-30.

109. Förstermann, U. and W.C. Sessa, *Nitric oxide synthases: regulation and function.* Eur Heart J, 2012. **33**(7): p. 829-37, 837a-837d.

110. Zago, A.S. and A. Zanesco, *Nitric oxide, cardiovascular disease and physical exercise.* Arq Bras Cardiol, 2006. **87**(6): p. e264-70.

111. Shesely, E.G., et al., *Elevated blood pressures in mice lacking endothelial nitric oxide synthase.* Proc Natl Acad Sci U S A, 1996. **93**(23): p. 13176-81.

112. Marletta, M.A., *Nitric oxide synthase structure and mechanism.* J Biol Chem, 1993. **268**(17): p. 12231-4.

113. Garthwaite, J. and C.L. Boulton, *Nitric oxide signaling in the central nervous system.* Annu Rev Physiol, 1995. **57**: p. 683-706.

114. Takahashi, T., *Pathophysiological significance of neuronal nitric oxide synthase in the gastrointestinal tract.* J Gastroenterol, 2003. **38**(5): p. 421-30.

115. Sakakibara, R., et al., *Bladder, bowel, and sexual dysfunction in Parkinson's disease.* Parkinsons Dis, 2011. **2011**: p. 924605.

116. Shah, V., et al., *Nitric oxide in gastrointestinal health and disease.* Gastroenterology, 2004. **126**(3): p. 903-13.

117. Zhou, L. and D.Y. Zhu, *Neuronal nitric oxide synthase: structure, subcellular localization, regulation, and clinical implications.* Nitric Oxide, 2009. **20**(4): p. 223-30.

118. Eliasson, M.J., et al., *Neuronal nitric oxide synthase activation and peroxynitrite formation in ischemic stroke linked to neural damage.* J Neurosci, 1999. **19**(14): p. 5910-8.

119. Dawson, V.L., et al., *Resistance to neurotoxicity in cortical cultures from neuronal nitric oxide synthase-deficient mice.* J Neurosci, 1996. **16**(8): p. 2479-87.

120. Samdani, A.F., T.M. Dawson, and V.L. Dawson, *Nitric oxide synthase in models of focal ischemia.* Stroke, 1997. **28**(6): p. 1283-8.

121. Sekhon, B., et al., *N-Acetyl cysteine protects against injury in a rat model of focal cerebral ischemia.* Brain Res, 2003. **971**(1): p. 1-8.

122. Cuzzocrea, S., et al., *Role of induced nitric oxide in the initiation of the inflammatory response after postischemic injury.* Shock, 2002. **18**(2): p. 169-76.

123. Naito, Y., et al., *Suppression of intestinal ischemia-reperfusion injury by a specific peroxisome proliferator-activated receptor-gamma ligand, pioglitazone, in rats.* Redox Rep, 2002. **7**(5): p. 294-9.

124. Hassoun, H.T., et al., *Inducible nitric oxide synthase mediates gut ischemia/reperfusion-induced ileus only after severe insults.* J Surg Res, 2001. **97**(2): p. 150-4.

125. Barocelli, E., et al., *The selective inhibition of inducible nitric oxide synthase prevents intestinal ischemia-reperfusion injury in mice.* Nitric Oxide, 2006. **14**(3): p. 212-8.

126. Terrinoni, A., et al., *OTX1 expression in breast cancer is regulated by p53.* Oncogene, 2011. **30**(27): p. 3096-103.

127. Azzolini, C., et al., *Expression of VEGF-A, Otx homeobox and p53 family genes in proliferative vitreoretinopathy.* Mediators Inflamm, 2013. **2013**: p. 857380.

128. Pirrone, C., et al., *OTX1 and OTX2 as possible molecular markers of sinonasal carcinomas and olfactory neuroblastomas.* Eur J Histochem, 2017. **61**(1): p. 2730.

129. Hedrera, M.I., et al., *Soybean meal induces intestinal inflammation in zebrafish larvae.* PLoS One, 2013. **8**(7): p. e69983.

130. Zhang, H.Q., et al., *Potent and selective inhibition of neuronal nitric oxide synthase by N omega-propyl-L-arginine.* J Med Chem, 1997. **40**(24): p. 3869-70.

131. Kankuri, E., et al., *Suppression of acute experimental colitis by a highly selective inducible nitric-oxide synthase inhibitor, N-[3-(aminomethyl)benzyl]acetamidine.* J Pharmacol Exp Ther, 2001. **298**(3): p. 1128-32.

132. Kato, S., et al., *Aggravation of cold-restraint stress-induced gastric lesions in adjuvant arthritic rats: pathogenic role of inducible and endothelial nitric oxide.* J Pharmacol Sci, 2009. **111**(3): p. 244-52.

133. Garvey, E.P., et al., *1400W is a slow, tight binding, and highly selective inhibitor of inducible nitric-oxide synthase in vitro and in vivo.* J Biol Chem, 1997. **272**(8): p. 4959-63.

134. Puig, M.M., W. Warner, and O. Pol, *Intestinal inflammation and morphine tolerance alter the interaction between morphine and clonidine on gastrointestinal transit in mice.* Anesthesiology, 2000. **93**(1): p. 219-30.

135. Bradley, P.P., et al., *Measurement of cutaneous inflammation: estimation of neutrophil content with an enzyme marker.* J Invest Dermatol, 1982. **78**(3): p. 206-9.

136. Livak, K.J. and T.D. Schmittgen, *Analysis of relative gene expression data using real-time quantitative PCR and the 2(-Delta Delta C(T)) Method.* Methods, 2001. **25**(4): p. 402-8.

137. Giaroni, C., et al., *Protein kinase C modulates NMDA receptors in the myenteric plexus of the guinea pig ileum during in vitro ischemia and reperfusion.* Neurogastroenterol Motil, 2011. **23**(2): p. e91-103.

138. Giaroni, C., et al., *Involvement of Ca2+-dependent PKCs in the adaptive changes of mu-opioid pathways to sympathetic denervation in the guinea pig colon.* Biochem Pharmacol, 2009. **78**(9): p. 1233-41.

139. Limb, G.A., et al., *In vitro characterization of a spontaneously immortalized human Müller cell line (MIO-M1).* Invest Ophthalmol Vis Sci, 2002. **43**(3): p. 864-9.

140. Lisowski, P., et al., *Stress susceptibility-specific phenotype associated with different hippocampal transcriptomic responses to chronic tricyclic antidepressant treatment in mice.* BMC Neurosci, 2013. **14**: p. 144.

141. Giaroni, C., et al., *Role of neuronal and inducible nitric oxide synthases in the guinea pig ileum myenteric plexus during in vitro ischemia and reperfusion.* Neurogastroenterol Motil, 2013. **25**(2): p. e114-26.

142. Rivera, L.R., et al., *Knock out of neuronal nitric oxide synthase exacerbates intestinal ischemia/reperfusion injury in mice.* Cell Tissue Res, 2012. **349**(2): p. 565-76.

143. Türler, A., et al., *Molecular and functional observations on the donor intestinal muscularis during human small bowel transplantation.* Gastroenterology, 2002. **122**(7): p. 1886-97.

144. Walus, K.M. and E.D. Jacobson, *Relation between small intestinal motility and circulation.* Am J Physiol, 1981. **241**(1): p. G1-15.

145. Bielefeldt, K. and J.L. Conklin, *Intestinal motility during hypoxia and reoxygenation in vitro.* Dig Dis Sci, 1997. **42**(5): p. 878-84.

146. Rodriguez, R., et al., *Altered responsiveness of the guinea-pig isolated ileum to smooth muscle stimulants and to electrical stimulation after in situ ischemia.* Br J Pharmacol, 2006. **147**(4): p. 371-8.

147. Aulí, M., et al., *Neuromuscular changes in a rat model of colitis.* Auton Neurosci, 2008. **141**(1-2): p. 10-21.

148. Bakirtzi, K., et al., *The neurotensin-HIF-1α-VEGFα axis orchestrates hypoxia, colonic inflammation, and intestinal angiogenesis.* Am J Pathol, 2014. **184**(12): p. 3405-14.

149. Feinman, R., et al., *HIF-1 mediates pathogenic inflammatory responses to intestinal ischemia-reperfusion injury.* Am J Physiol Gastrointest Liver Physiol, 2010. **299**(4): p. G833-43.

150. Giatromanolaki, A., et al., *Hypoxia inducible factor 1alpha and 2alpha overexpression in inflammatory bowel disease.* J Clin Pathol, 2003. **56**(3): p. 209-13.

151. Rivera, L.R., et al., *The involvement of nitric oxide synthase neurons in enteric neuropathies.* Neurogastroenterol Motil, 2011. **23**(11): p. 980-8.

152. Silva, M.A., L.R. de Meirelles, and J.M. Bustorff-Silva, *Changes in intestinal motility and in the myenteric plexus in a rat model of intestinal ischemia-reperfusion.* J Pediatr Surg, 2007. **42**(6): p. 1062-5.

153. Green, C.L., et al., *Dextran sodium sulfate-induced colitis reveals nicotinic modulation of ion transport via iNOS-derived NO.* Am J Physiol Gastrointest Liver Physiol, 2004. **287**(3): p. G706-14.

154. Miampamba, M. and K.A. Sharkey, *Temporal distribution of neuronal and inducible nitric oxide synthase and nitrotyrosine during colitis in rats.* Neurogastroenterol Motil, 1999. **11**(3): p. 193-206.

155. Gulbransen, B.D. and K.A. Sharkey, *Novel functional roles for enteric glia in the gastrointestinal tract.* Nat Rev Gastroenterol Hepatol, 2012. **9**(11): p. 625-32.

156. Sarosi, G.A., et al., *Capacitative Ca2+ entry in enteric glia induced by thapsigargin and extracellular ATP.* Am J Physiol, 1998. **275**(3 Pt 1): p. G550-5.

157. Askalan, R., et al., *Astrocytic-inducible nitric oxide synthase in the ischemic developing human brain.* Pediatr Res, 2006. **60**(6): p. 687-92.

158. Moro, M.A., et al., *Neuronal expression of inducible nitric oxide synthase after oxygen and glucose deprivation in rat forebrain slices.* Eur J Neurosci, 1998. **10**(2): p. 445-56.

159. Zheng, L., et al., *Effects and Mechanism of Action of Inducible Nitric Oxide Synthase on Apoptosis in a Rat Model of Cerebral Ischemia-Reperfusion Injury.* Anat Rec (Hoboken), 2016. **299**(2): p. 246-55.

160. Kannan, K.B., et al., *Hypoxia-inducible factor plays a gut-injurious role in intestinal ischemia reperfusion injury.* Am J Physiol Gastrointest Liver Physiol, 2011. **300**(5): p. G853-61.

161. Aktan, F., *iNOS-mediated nitric oxide production and its regulation.* Life Sci, 2004. **75**(6): p. 639-53.

162. Duma, D., et al., *NOS-1-derived NO is an essential triggering signal for the development of systemic inflammatory responses.* Eur J Pharmacol, 2011. **668**(1-2): p. 285-92.

163. Spatazza, J., et al., *Homeoprotein signaling in development, health, and disease: a shaking of dogmas offers challenges and promises from bench to bed.* Pharmacol Rev, 2013. **65**(1): p. 90-104.

164. Mallick, I.H., et al., *Ischemia-reperfusion injury of the intestine and protective strategies against injury.* Dig Dis Sci, 2004. **49**(9): p. 1359-77.

165. Nam, J. and M. Nei, *Evolutionary change of the numbers of homeobox genes in bilateral animals.* Mol Biol Evol, 2005. **22**(12): p. 2386-94.

166. Yu, K., et al., *OTX1 promotes colorectal cancer progression through epithelial-mesenchymal transition.* Biochem Biophys Res Commun, 2014. **444**(1): p. 1-5.

167. Aoki, T., et al., *Ncx (Enx, Hox11L.1) is required for neuronal cell death in enteric ganglia of mice.* J Pediatr Surg, 2007. **42**(6): p. 1081-8.

168. Kobayashi, H., et al., *The mechanism of intestinal motility in homozygous mutant Ncx/Hox11L.1-deficient mice--a model for intestinal neuronal dysplasia.* J Pediatr Surg, 2007. **42**(12): p. 2062-6.

169. Yanai, T., et al., *Acetylcholine-related bowel dysmotility in homozygous mutant NCX/HOX11L.1-deficient (NCX-/-) mice-evidence that acetylcholine is implicated in causing intestinal neuronal dysplasia.* J Pediatr Surg, 2004. **39**(6): p. 927-30.

170. Coskun, M., J.T. Troelsen, and O.H. Nielsen, *The role of CDX2 in intestinal homeostasis and inflammation.* Biochim Biophys Acta, 2011. **1812**(3): p. 283-9.

171. Shipley, M.M., C.A. Mangold, and M.L. Szpara, *Differentiation of the SH-SY5Y Human Neuroblastoma Cell Line.* J Vis Exp, 2016(108): p. 53193.

172. Götz, M. and Y.A. Barde, *Radial glial cells defined and major intermediates between embryonic stem cells and CNS neurons.* Neuron, 2005. **46**(3): p. 369-72.

173. Agostini, M., et al., *Neuronal differentiation by TAp73 is mediated by microRNA-34a regulation of synaptic protein targets.* Proc Natl Acad Sci U S A, 2011. **108**(52): p. 21093-8.

174. Mody, M., et al., *Genome-wide gene expression profiles of the developing mouse hippocampus.* Proc Natl Acad Sci U S A, 2001. **98**(15): p. 8862-7.

175. Kovalevich, J. and D. Langford, *Considerations for the use of SH-SY5Y neuroblastoma cells in neurobiology.* Methods Mol Biol, 2013. **1078**: p. 9-21.

176. Vieira, H.L., P.M. Alves, and A. Vercelli, *Modulation of neuronal stem cell differentiation by hypoxia and reactive oxygen species.* Prog Neurobiol, 2011. **93**(3): p. 444-55.

177. Piret, J.P., et al., *CoCl2, a chemical inducer of hypoxia-inducible factor-1, and hypoxia reduce apoptotic cell death in hepatoma cell line HepG2.* Ann N Y Acad Sci, 2002. **973**: p. 443-7.

178. Donato, R., et al., *Functions of S100 proteins.* Curr Mol Med, 2013. **13**(1): p. 24-57.

179. Kalogeris, T., et al., *Cell biology of ischemia/reperfusion injury.* Int Rev Cell Mol Biol, 2012. **298**: p. 229-317.

180. Kaur, C., V. Sivakumar, and W.S. Foulds, *Early response of neurons and glial cells to hypoxia in the retina.* Invest Ophthalmol Vis Sci, 2006. **47**(3): p. 1126-41.

181. Conde, E., et al., *Hypoxia inducible factor 1-alpha (HIF-1 alpha) is induced during reperfusion after renal ischemia and is critical for proximal tubule cell survival.* PLoS One, 2012. **7**(3): p. e33258.

182. Du, F., et al., *Hyperthermic preconditioning protects astrocytes from ischemia/reperfusion injury by up-regulation of HIF-1 alpha expression and binding activity.* Biochim Biophys Acta, 2010. **1802**(11): p. 1048-53.

183. Basile, D.P., et al., *Renal ischemia reperfusion inhibits VEGF expression and induces ADAMTS-1, a novel VEGF inhibitor.* Am J Physiol Renal Physiol, 2008. **294**(4): p. F928-36.

184. Dulloo, I., et al., *Hypoxia-inducible TAp73 supports tumorigenesis by regulating the angiogenic transcriptome.* Nat Cell Biol, 2015. **17**(4): p. 511-23.

185. Sabapathy, K., *p73: a Positive or Negative Regulator of Angiogenesis, or Both?* Mol Cell Biol, 2015. **36**(6): p. 848-54.

186. Amelio, I., et al., *TAp73 opposes tumor angiogenesis by promoting hypoxia-inducible factor 1α degradation.* Proc Natl Acad Sci U S A, 2015. **112**(1): p. 226-31.

OTHER PUBLICATIONS

Author of the following video-article

- Conti, A., et al., *Identification of OTX1 and OTX2 as Two Possible Molecular Markers for Sinonasal Carcinomas and Olfactory Neuroblastomas.* JoVe, 2017, In-Press.

Co-author of the following papers

- Filpa, V., et al., *Nitric oxide regulates homeoprotein OTX1 and OTX2 expression in the rat myenteric plexus after intestinal ischemia-reperfusion injury.* Am J Physiol Gastrointest Liver Physiol, 2017. **312**(4): p. G374-G389.
- Pirrone, C., et al., *OTX1 and OTX2 as possible molecular markers of sinonasal carcinomas and olfactory neuroblastomas.* Eur J Histochem, 2017. **61**(1): p. 2730.

Author of the poster presented at the XIX National Convention SIGU "**OTX1 homeobox gene as potential target of HIF1α during early retinal hypoxic events**".

Author of the poster presented at the XVIII National Convention SIGU "**Evaluation of OTX homeobox genes expression levels in MIO-M1 cell line following all-trans retinoic acid treatment**".

Co-author of the posters presented at the XVIII National Convention SIGU

- "**OTX1 and OTX2 expression in human normal, inflammatory and neoplastic nasal mucosa**"
- "**Evaluation of BCR-ABL1 DNA and RNA levels in K562 cell line treated with imatinib and nilotinib**"
- "**Identificazione di marcatori pazienti specifici basati sul DNA per l'individuazione di mosaicismi misti post-trapianto di midollo osseo nelle malattie ematologiche**"

RINGRAZIAMENTI

Giunto al termine di questo importante percorso, mi sembra assolutamente doveroso ringraziare tutti coloro che mi hanno accompagnato nel raggiungimento di questo obiettivo così importante.

Devo ringraziare i miei genitori perché, tramite i sacrifici che hanno compiuto, mi hanno permesso di raggiungere questa importantissima tappa della mia formazione. Avevo deciso di intraprendere la strada del dottorato perché lo vedevo come un modo per ringraziarli di tutto ciò che hanno fatto. L'aver concluso questo cammino mi sembra il modo più bello per mostrare loro quanto i loro sacrifici non siano stati vani.

Un grazie va anche a Claudia che mi ha accompagnato a sostenere il colloquio di ammissione al dottorato e che durante questi tre lunghi anni mi è sempre stata accanto, supportandomi e sopportandomi anche nei momenti più complicati, aiutandomi anche quando le cose sembravano impossibili. Ha sempre trovato il modo di spronarmi a proseguire nonostante le difficoltà che ho incontrato e quindi davvero un grazie alla mia Wonder Woman.

Ringrazio il prof. Giovanni Porta per avermi permesso di svolgere il percorso di dottorato nel suo laboratorio.

Un doveroso ringraziamento va anche alla dott.ssa Cristina Giaroni perché non solo ha permesso la realizzazione di questo lavoro di tesi ma anche perché, grazie ai suoi consigli, mi ha fatto crescere dal punto di vista professionale. Molto di quello che ho imparato lo devo a ciò che mi ha trasmesso non solo durante le riunioni formali ma anche semplicemente quando "bazzicavo" nel suo laboratorio (ovvero tutti i giorni) e la trovavo lì a lavorare insieme alle sue colleghe. A lei va la tutta la mia più profonda stima e rispetto.

Un ringraziamento va anche ai miei colleghi di laboratorio con cui ho condiviso tutti i momenti della giornata lavorativa e con cui ho portato avanti i numerosi progetti. Ci siamo supportati e abbiamo fatto gioco di squadra, perché alla fine questo è quello che siamo…una squadra. Grazie quindi ad Alessia, che è stata mia collega dal primo anno, e a Giovanni, collega di questo ultimo anno; grazie poi anche a Cristina per averci accolto in laboratorio e avviato all'attività che avremmo poi svolto in autonomia. Grazie infine a Manuel per tutte le risate che ci siamo fatte in laboratorio e a Giorgia.

Un ringraziamento non può che andare anche a tutti coloro con cui ho stretto legami professionali e di amicizia nel corso di questi anni. Grazie a Paola per ogni prezioso consiglio che ha saputo darmi anche quando ponevo domande "bizzarre" e a Giuseppe per i suoi consigli e per le sue canzoni cantate a squarciagola che rendevano la giornata di lavoro meno pesante. Grazie poi anche a Roberto e Annalisa, al prof. Pasquali e alla prof. Maserati per ogni prezioso consiglio o dettaglio che mi hanno trasmesso. E poi un grazie al resto della banda, ovvero ai miei colleghi che hanno già finito o stanno proseguendo il dottorato: Viviana e Michela, Ilaria, Elena ed Eleonora. Se ho imparato qualcosa durante il dottorato lo devo anche a voi. Grazie per ogni bel momento passato insieme.

L'ultimo ringraziamento va infine a me stesso per non aver mai ceduto, per aver trovato il modo di rialzarmi e andare avanti (il più delle volte con modalità poco ortodosse) sempre e comunque.